

Microstructure Evolution and Optimization of the Tempering Heat Treatment of a Medium-Carbon Low-Alloy Steel

by

Seyyed Hesamodin TALEBI

MANUSCRIPT-BASED THESIS PRESENTED TO
ÉCOLE DE TECHNOLOGIE SUPÉRIEURE IN PARTIAL FULFILLMENT
FOR A MASTER'S DEGREE WITH THESIS IN MECHANICAL
ENGINEERING
M.A.Sc.

MONTREAL, August 20, 2018

ÉCOLE DE TECHNOLOGIE SUPÉRIEURE
UNIVERSITÉ DU QUÉBEC



Seyyed Hesamodin Talebi, 2018



This Creative Commons licence allows readers to download this work and share it with others as long as the author is credited. The content of this work can't be modified in any way or used commercially.

BOARD OF EXAMINERS

THIS THESIS HAS BEEN EVALUATED

BY THE FOLLOWING BOARD OF EXAMINERS

Prof. Mohammad Jahazi, Thesis Supervisor

Mechanical Engineering Department at École de technologie supérieure

Prof. Vladimir Brailovski, President of the Board of Examiners

Mechanical Engineering Department at École de technologie supérieure

Prof. Vincent Demers, Member of the jury

Mechanical Engineering Department at École de technologie supérieure

THIS THESIS WAS PRESENTED AND DEFENDED

IN THE PRESENCE OF A BOARD OF EXAMINERS AND PUBLIC

IN AUGUST 15, 2018

AT ÉCOLE DE TECHNOLOGIE SUPÉRIEURE

ACKNOWLEDGMENT

The author would like to thank his supervisor, Professor Mohammad Jahazi, for his guidance, support and expertise during the degree, without which none of this would have been possible. It was an excellent opportunity for working with him during this master journey.

Grateful thanks are given to our Industrial Partner, Finkl Steel, for their help in sample preparation, accessing Sorel Forge data base, and their collaboration in this project.

Gratitude is also expressed for all CM2P members for their cooperation during the entire diploma.

ÉVALUATION DE LA MICROSTRUCTURE ET OPTIMISATION DU TRAITEMENT DE REVENU DES ACIERS FAIBLEMENT ALLIÉS

Seyyed Hesamodin Talebi

RESUME

Dans ce travail de recherche, l'influence des différents paramètres sur les phénomènes qui se produisent durant le revenu des aciers faiblement alliés, ont été investiguées. Grâce à un dilatomètre à haute résolution, les échantillons ont été refroidis suivant les trois vitesses de refroidissement suivantes 4.8, 18 et 180 °C/min afin de former respectivement la martensite, la matensite-bainite et la bainite. Ces microstructures correspondent à des zones spécifiques dans un lingot forgé de grande taille après trempé.

Par la suite, des cycles de revenus non-isothermes jusqu'à 600 °C ont été réalisés avec différents vitesses de chauffe pour étudier les différents stades du revenu ainsi que les transformations de phases qui y interviennent, notamment la bainite.

Les résultats ont indiqué que le comportement durant du revenu varie de manière remarquable depuis la microstructure primaire, et à travers tous les stades du revenue. En particulier, il a été observé que la décomposition de l'austénite résiduelle et la précipitation des carbures se produit durant le revenu d'une microstructure bainitique.

Ensuite, des revenus isothermes à 350, 550 and 600 °C et différents temps de maintien ont été réalisés afin d'étudier la décomposition de l'austénite résiduelle et l'évolution des carbures durant le revenu d'échantillons bainitiques. Les résultats ont montré que la décomposition complète de l'austénite résiduelle se produit seulement à 600 °C. Même, après 16 h de revenu à 600 °C, les carbures ont tendance à être riche en chrome, les carbures Cr_7C_3 et $Cr_{23}C_6$ ont surtout été identifié. Une augmentation de la dureté a été observée lors de la précipitation des carbures, suivi d'une diminution qui indique le début de la croissance des carbures.

Mots clés: Revenu, Bainite, Transformation de phase, Dilatométrie, Austénite résiduelle, Carbures.

Microstructure Evolution and Optimization of the Tempering Heat Treatment of a Medium-Carbon Low-Alloy Steel

Seyyed Hesamodin TALEBI

ABSTRACT

In this research, the effects of processing parameters on different phenomena occurring during tempering of a medium-carbon low-alloy steel were investigated. Conducting high-resolution dilatometry machine, samples were cooled with three cooling rates of 4.8, 18 and 180 °C/min, to produce martensite, martensite mixed with bainite and bainite, respectively. These microstructures correspond to different locations of a large-size forged ingot after quenching.

Subsequently, non-isothermal tempering up to 600 °C with different heating rates was carried out to study various tempering stages and phase transformations occurring during tempering especially for bainite. Results indicated that tempering behaviour differed remarkably with the primary microstructure, and among all the tempering stages, only retained austenite decomposition and carbide precipitation have occurred during tempering of a bainitic microstructure.

Furthermore, isothermal tempering for three temperatures of 350, 550 and 600 °C with different holding times up to 16 h was performed to study retained austenite decomposition and carbides evolution during tempering of a bainitic specimen containing retained austenite. Results showed that full decomposition of retained austenite occurred only at 600 °C. Also, after 16 h of tempering at 600 °C, carbides tend to be rich in chromium and mostly Cr₇C₃ and Cr₂₃C₆ carbides were identified. Hardness increase was observed during carbides precipitation, while it decreased when carbide coarsening started.

Keywords: Tempering, Bainite, Phase transformation, Dilatometry, Retained austenite, Carbides.

TABLE OF CONTENTS

	Page
INTRODUCTION	1
CHAPTER 1 LITERATURE REVIEW	3
1.1 Medium-Carbon Low-Alloy Steels.....	3
1.1.1 AISI P20.....	3
1.2 Phase transformations	4
1.2.1 Austenite to Pearlite	4
1.2.2 Austenite to Martensite	6
1.2.3 Austenite to Bainite.....	6
1.3 Effect of Alloying Elements	6
1.3.1 Effect of Alloying Elements on Phase Transformation	7
1.3.2 Effect of Alloying Elements on Mechanical Properties	8
1.4 Bainitic Transformation	10
1.4.1 Mechanisms of Bainite Formation.....	11
1.4.2 Definition of T_0 Curve.....	13
1.4.3 Morphology of Bainite.....	15
1.4.4 Effects of Alloying Elements on Bainite Start Temperature	17
1.5 Tempering of Bainite	18
1.5.1 Hollomon – Jaffe Parameter	20
1.5.2 Precipitation of Transition Carbides	21
1.5.3 Retained Austenite Decomposition During Tempering.....	22
1.5.4 Double Tempering of Steels	23
1.5.5 Precipitation of Carbides During Tempering.....	23
1.5.5.1 Tempering of Bainite Containing Vanadium.....	24
1.5.5.2 Tempering of Bainite Containing Chromium	24
1.5.5.3 Tempering of Bainite Containing Molybdenum.....	25
1.5.6 Effect of Tempering on Cementite Coarsening	26

1.5.7	Secondary Hardening.....	27
1.5.8	Effects of Tempering on Mechanical Properties	28
1.6	Summary.....	29

CHAPTER 2 INFLUENCE OF STARTING MICROSTRUCTURE ON
DILATATION BEHAVIOR DURING TEMPERING OF A HIGH
STRENGTH STEEL.....31

2.1	Introduction.....	32
2.2	Materials and methods	33
2.3	Results and Discussion	33
2.3.1	Cooling dilatometric curves.....	33
2.3.2	Tempering dilatometric curves	35
2.3.3	Length changes during tempering.....	36
2.3.4	Microstructure evolution.....	37
2.4	Summary.....	40

CHAPTER 3 IN SITU STUDY OF PHASE TRANSFORMATION DURING
NON-ISOTHERMAL TEMPERING OF BAINITIC AND
MARTENSITIC MICROSTRUCTURES41

3.1	Introduction.....	42
3.2	Materials and Methods.....	44
3.3	Results and Discussion	47
3.3.1	Segregation and Clustering of Carbon Atoms	50
3.3.2	Precipitation of the ϵ/η Transition Carbides	52
3.3.3	Retained Austenite Decomposition.....	53
3.3.4	Cementite Precipitation.....	55
3.3.5	Microstructural Evolution during Tempering.....	58
3.4	Conclusions.....	61

CHAPTER 4 RETAINED AUSTENITE DECOMPOSITION AND CARBIDES
IDENTIFICATION DURING ISOTHERMAL TEMPERING OF
A MEDIUM-CARBON LOW-ALLOY BAINITIC STEEL.....63

4.1	Introduction.....	63
-----	-------------------	----

4.2	Materials and Methods.....	65
4.3	Results and Discussion	67
4.3.1	Retained austenite decomposition.....	67
4.3.2	Product of retained austenite decomposition	71
4.3.3	Carbides precipitation and hardness evolution	72
4.3.4	Characterization and identification of carbides	74
4.4	Conclusions.....	79
CHAPTER 5 Optimization of Industrial Tempering Heat Treatment Process.....		81
5.1	Introduction.....	81
5.2	Tempering temperature.....	82
5.3	Tempering time.....	82
5.3.1	Non-isothermal tempering time of a large-size slab.....	83
5.3.2	Isothermal tempering time of a large-size slab.....	84
5.4	Proposed tempering cycle.....	85
CONCLUSIONS		87
RECOMMENDATIONS.....		89
LIST OF BIBLIOGRAPHICAL REFERENCES.....		90

LIST OF TABLES

	Page
Table 1-1 Chemical Composition of AISI P20 (wt.%) (A.M. Bayer, 1990).....	4
Table 1-2 Alloying elements impact on steel phase transformation.....	8
Table 1-3 Different tempering stages and their temperatures in martensite based on 1-hour treatment (Dhua, Ray, & Sarma, 2001).....	18
Table 2-1 Total length change during tempering from 25 °C to 600 °C and specific length change due to tempering phenomena.....	37
Table 3-1 Lattice parameters and carbon contents of the as-received microstructure, bainitic ferrite, and martensite, before and after non- isothermal tempering with a heating rate of 5 °C/min, determined using X-ray diffraction.....	51
Table 3-2 Temperature interval of retained austenite decomposition and percentage of relative length change for maximum and minimum heating rates in both investigated microstructure.....	55
Table 4-1 Chemical composition of the investigated steel (wt.%).....	65
Table 4-2 Crystal structure, morphology and size of identified carbides in the tempered medium-carbon low-alloy bainite.....	79
Table 5-1 Hardness changes during isothermal tempering with different holding times at 600 °C.....	85

LIST OF FIGURES

	Page
Figure 1-1 Part of Fe-C phase diagram associated with steel phase transformations, up to 2.0 wt.% of C (Smallman & Ngan, 2011).	5
Figure 1-2 Influence of different manganese contents on the A1 and A3 lines (Roberts et al., 1998).....	7
Figure 1-3 Effect of chromium percentage on the γ -field phase in a steel containing chromium (Roberts et al., 1998).	8
Figure 1-4 Jominy curves of effect of different amount (a) manganese, and (b) nickel on the hardness of steel (Hashmi, 2014; George E Totten et al., 2004).	9
Figure 1-5 Image taken by atomic force microscope showing the displacements as a result of formation of bainite on a polished surface of austenite (Swallow & Bhadeshia, 1996).	12
Figure 1-6 Schematic evolution of free energy as a function of carbon concentration showing the T ₀ curve (H. Bhadeshia, 2001).	13
Figure 1-7 Schematic of an incomplete bainitic transformation. After diffusionless formation of bainite plate, the excess carbon escape into the retained austenite and oncoming plate forms from carbon enriched austenite. The phenomenon stops at T ₀ curve because thermodynamically, diffusionless transformation cannot occur when austenite composition reaches T ₀ line (H. Bhadeshia, 2001).	14
Figure 1-8 Schematic illustration of transformation of austenite to lower and upper bainite (Takahashi & Bhadeshia, 1990).	15
Figure 1-9 Upper bainite in Fe–0.095C–1.63Si–2Mn–2Cr wt.% steel transformed isothermally at 400 °C (H. Bhadeshia & Honeycombe, 2011).	16
Figure 1-10 lower bainite microstructure of Fe–0.3C–4Cr (H. Bhadeshia & Honeycombe, 2011).	17
Figure 1-11 Hardness changes for two bainitic steels consisting different percentages of carbon, as a function of Hollomon-Jaffe parameter (Irvine, Pickering, Met, & Heselwood, 1957).	21

Figure 1-12 (a) lath type and blocky retained austenite in as-quenched sample, (b) martensite formation after 5 hours of tempering at 230 °C (Yan et al., 2017).	22
Figure 1-13 (a) retained austenite in as-quenched sample, (b) lower bainite after 1 hour of tempering at 400 °C (Yan et al., 2017).	23
Figure 1-14 Influence of various amounts of chromium on hardness during tempering of a steel containing 0.35 wt.% carbon (Bain & Paxton, 1966).	25
Figure 1-15 Size variation of cementite versus tempering time at 700 °C for a Fe-0.45C-0.22Si-0.62Mn wt.% steel. The upper bound on each shaded region is for average size of cementite located at the lath boundaries and the lower bound is for Intra-lath cementite (Nam, 1999).	27
Figure 1-16 Secondary hardening peak for a bainitic steel containing 0.3 wt.% vanadium (Irvine & Pickering, 1957).	28
Figure 1-17 Change in different mechanical properties during 1 h tempering as a function of tempering temperature for 1.5Ni-1Cr-0.25Mo-0.4C wt.% steel (Thelning, 1975)	29
Figure 2-1(a) Dilatometric cooling curves of studied steel. Derivatives of relative length changes during cooling at cooling rates of (b) 0.08 °C/s, (c) 0.3 °C/s, and (d) 3 °C/s.	34
Figure 2-2. (a) Relative length changes, and (b) derivatives of relative length changes during non-isothermal tempering of bainitic, martensitic and mixture specimens with a heating rate of 10 °C/min.	35
Figure 2-3. Microstructure of different samples: (a) bainite plus retained austenite (RA) after cooling rate of 0.08 °C/s (b) tempered bainite, (c) bainite plus martensite after cooling rate of 0.3 °C/s (d) sheaves of tempered bainite and carbides between them, (e) plate of tempered martensite with carbides inside, (f) full martensite after cooling rate of 3 °C/s, and (g) tempered martensite	39
Figure 3-1 SEM image illustrating as-received microstructure composed of bainite and retained austenite (RA).	45
Figure 3-2 As-cooled microstructures obtained for different cooling rates: (a) Martensitic microstructure, 180 °C/min and (b) bainitic microstructure, 4.8 °C/min.	46
Figure 3-3(a) Relative length change diagram during non-isothermal tempering of bainitic specimen at heating rates of 5 °C/min and 30 °C/min, and (b)	

the first derivative curve of the relative length change corresponding to these heating rates.....	48
Figure 3-4 (a) Relative length change diagram during non-isothermal tempering of the martensitic specimen at the heating rates of 5 °C/min and 30 °C/min, and (b) the first derivative curve of relative length change corresponding to these heating rates.....	49
Figure 3-5 Two XRD (X-ray diffraction) peaks of bainite and martensite: (a) (110) peak and (b) (200) peak.....	51
Figure 3-6 Relative length variations near the inflection point.....	54
Figure 3-7 XRD spectra of bainite and non-isothermal tempered bainite at heating rate of 5 °C/min.....	56
Figure 3-8 XRD spectra of martensite and non-isothermal tempered martensite at heating rate of 5 °C/min.....	56
Figure 3-9 Relative length change and its derivation during the cooling cycle (from 600 °C to ambient temperature at a cooling rate of 600 °C/min) after tempering of: (a) The bainitic specimen non-isothermally tempered at a heating rate of 5 °C/min; (b) the bainitic specimen non-isothermally tempered at a heating rate of 30 °C/min; (c) the martensitic specimen non-isothermally tempered at a heating rate of 5 °C/min and (d) the martensitic specimen non-isothermally tempered at a heating rate of 30 °C/min.....	58
Figure 3-10 SEM images of microstructure evolution in the bainitic sample during non-isothermal tempering at heating rate of 5 °C/min: (a) The microstructure after tempering; (b) blocks of retained austenite (RA) prior to tempering and (c) blocks of decomposed retained austenite after tempering.....	60
Figure 3-11 SEM images after non-isothermal tempering at heating rate of 30 °C/min: (a) Plates of tempered martensite with fine needle-like carbides within the plate and (b) tempered bainite with coarser rod-shape carbides.....	61
Figure 4-1 Primary microstructure of bainite with retained austenite before tempering.....	66
Figure 4-2 Dilatometry curves during isothermal tempering for 16 h at (a) 350 °C, (b) 550 °C, and (c) 600 °C.....	68
Figure 4-3 dilatometry curves of cooling cycle with cooling rate of 600 °C/min after isothermal tempering for 16 h at (a) 550 °C, and (b) 600 °C.....	69

Figure 4-4 XRD (110) peak of retained austenite.....	70
Figure 4-5 Change in carbon content of retained austenite during tempering at 550 °C.	71
Figure 4-6 SEM images of (a) blocks of partially decomposed retained austenite after 16 h of tempering at 350 °C, (b) fresh martensite formed during cooling after 16 h of tempering at 550 °C, and (c) fully decomposed retained austenite and tempered microstructure blocks after 16 h of tempering at 600 °C.	72
Figure 4-7 Bainite hardness as a function of tempering time for tempering temperatures of 350 °C, 550 °C and 600 °C.	74
Figure 4-8 SEM images bainitic specimens after tempering for 16 h at (a) 350 °C, (b) 550 °C, and (c) 600 °C.	75
Figure 4-9 Bright-field TEM image and corresponding selected area electron diffraction (SAED) pattern of (a) Fe ₃ C carbide after 1 h of tempering at 550 °C, (b) Cr ₇ C ₃ carbide after 16 h of tempering at 600 °C, (c) and (d) Cr ₂₃ C ₆ carbides after 16 h of tempering at 600 °C.	77
Figure 5-1 Schematic of double tempering process for a medium-carbon low-alloy steel.	81
Figure 5-2 Real temperature versus time curve during non-isothermal tempering of a large-size slab.....	84
Figure 5-3 Proposed tempering cycle for a large-size slab.....	86

LIST OF ABBREVIATIONS

B: Bainite
bct: Body Centered Tetragonal
B_f: Bainite finish temperature
B_s: Bainite start temperature
CCT: Continuous Cooling Transformation
FCC: Face Centered Cubic
HRC: Hardness Rockwell C
ICDD: International Centre for Diffraction Data
M: Martensite
M_f: Martensite finish temperature
M_s: Martensite start temperature
PDF: Powder Diffraction Files
RA: Retained Austenite
SAED: Selected Area Electron Diffraction
SEM: Scanning Electron Microscopy
TEM: Transmission Electron microscope
TM: Tempered Martensite
TTT: Time Temperature Transformation diagrams
XRD: X-Ray Diffraction

LIST OF SYMBOLS

$^{\circ}\text{C}$: Degree Celsius

μm : Micrometer

α : Ferrite

γ : Austenite

η : Transition carbide

Δl : Length change

L_0 : Initial length

K: Kelvin

wt.%: Weight percent

MN m^{-2} : Mega Newton per square metre

INTRODUCTION

Tempering is a thermal treatment process in steels often carried out after the quench. The aim of the tempering operation is to modify the microstructure and achieve the desired mechanical properties such as hardness and toughness. Different phenomena occur during tempering of steels, including segregation of carbides, precipitation of transition carbides, retained austenite decomposition, carbide precipitation and carbide coarsening. Depending on chemical composition of steel, primary microstructure and heating rate, each phenomenon occurs during a specific temperature interval and time. Therefore, appropriate tempering holding time and temperature need to be determined based on the above mentioned tempering phenomena.

Nevertheless, tempering of large-size slabs has been always a controversial process. Since in real conditions, a large-size slab contains different microstructures, from martensite on the surface to bainite and retained austenite in the center of slab, therefore, the response of each location of the slab during tempering is different.

Choosing the proper tempering temperature and holding time has always been an open question because it is completely dependable on the size of the slab. In the industry, tempering holding time is considered 1 or 2 hours for every inch of thickness, but in the case of large-size slabs, sometimes tempering takes 4-5 days at 500 to 600 °C and usually more than one tempering is applied. Therefore, there is a clear need for a more fundamental understanding of the metallurgical phenomena occurring during the tempering process. The present project has been defined with the view to increase the existing knowledge of the tempering process, specifically for bainitic and martensitic microstructures which are the dominant phase in large-size ingots.

In order to achieve this objective, the following topics have been studied in this research by experimentally simulating the industrial heat treatment conditions using dilatometry machine:

- Influence of primary microstructure on tempering behaviour of medium-carbon low-alloy steel.
- Detailed phase transformation study during non-isothermal tempering of martensite and bainite.
- Investigate phase transformations during isothermal tempering of bainite.

Chapter 1 of this thesis starts with a literature review about bainitic transformation and tempering of bainite. Then, different phase transformations during tempering and effect of alloying elements on the carbide precipitation during tempering are described.

In chapter 2, three different cooling rates (from 0.08 to 3 °C/s) representative of different regions from the surface to the core of the slab were experimentally simulated, and then non-isothermal tempering was carried out for each starting microstructure to determine the effect of non-isothermal tempering on microstructure evolution in large-size slabs

In chapter 3, different tempering stages and phase transformations during non-isothermal tempering of bainitic and martensitic microstructures obtained after quenching of a medium-carbon low-alloy steel was studied.

In chapter 4, the effect of isothermal tempering on different tempering stages such as retained austenite decomposition and carbide precipitation is investigated for a bainitic steel

In chapter 5, based on the findings of this research, tempering process of a large-size slab is studied and an optimized tempering cycle based on the industrial requirements is proposed.

CHAPTER 1

LITERATURE REVIEW

1.1 Medium-Carbon Low-Alloy Steels

Medium-Carbon steels contain 0.30 to 0.60 wt.% of carbon and 0.60 to 1.65 wt.% of manganese. Increasing the carbon content to almost 0.5%, with an increase in manganese, permit medium-carbon steels to improve their mechanical properties by quenching and tempering treatment. Applications of this category of steels is wide and include shafts, couplings, crankshafts, axles, gears, and forgings (Davis, 1994; Philip & Mccaffrey, 1990).

On the other hand, low-alloy steels include a group of ferrous materials consisting of alloying elements such as nickel, chromium, vanadium, manganese and molybdenum, leading to higher mechanical properties than plain carbon steels. The total proportion of alloying elements can range from 2.07 wt.% until that of stainless steels, which contain a minimum of 10 wt.% of chromium. The main role of alloying elements in low-alloy steels is to improve hardenability and toughness after heat treatment. The mechanisms that improve mechanical properties for this type of steel include: (i) solid solution strengthening, (ii) carbide forming elements which cause the austenite boundaries to be pinned by second-phase particles, (iii) grain refinement hardening and (iv) phase transformation hardening during heat treatment and deformation (Demeri, 2001; Handbook, 1990).

In the following sections, AISI P20, which is a Medium-carbon low-alloy steel, is discussed.

1.1.1 AISI P20

AISI P20 mold steel is a medium-carbon low-alloy tool steel that is characterized by its good toughness at moderate strength levels. This steel is commonly used for low-temperature applications such as plastic injection molds, casting dies and also for die casting of alloys with melting temperatures lower than 200 °C (R.A. Mesquita, 2014).

Table 1-1 shows the alloying elements of AISI P20. It can be seen that this steel contains 0.6-1.0 wt.% of manganese, 1.4-2.0 wt.% of chromium, 0.30-0.55 wt.% of molybdenum and 0.2-0.8 wt.% of silicon with negligible amount of phosphorus and sulphur (A.M. Bayer, 1990).

AISI P20 is normally heat-treated to achieve the hardness range of 30 to 36 HRC; this hardness makes it desirable to be machined into large, complicated dies and molds. When P20 is used for plastic injection molding or die casting of low-melting alloys, usually it is used in prehardened condition. However, when used for compression molds, after machining, it is subjected to carburizing and hardening treatment to increase the surface hardness to the required amount depending on the materials (R.A. Mesquita, 2014).

Table 1-1 Chemical Composition of AISI P20 (wt.%) (A.M. Bayer, 1990)

Carbon		Manganese		Phosphorus	Sulphur	Silicon		Chromium		Molybdenum	
Min	Max	Min	Max	Max	Max	Min	Max	Min	Max	Min	Max
0.28	0.40	0.60	1.00	0.030	0.030	0.20	0.80	1.40	2.00	0.30	0.55

1.2 Phase Transformations

Heat-treated medium-carbon steel comprises different phases such as martensite, bainite and retained austenite. In this section, a brief introduction will be provided to different phase transformations of austenite including pearlite, martensite and bainite. In the present research, the focus has been placed on bainite, therefore, in section 1.4, bainitic transformation will be comprehensively discussed.

1.2.1 Austenite to Pearlite

Austenite (γ -iron) in comparison with ferrite (α -iron) has much higher carbon solubility with a maximum value of around 2 wt.% at 1147 °C. However, the α -iron maximum solubility of

carbon is 0.02 wt.% at 723 °C (Figure 1-1). Pearlite reaction starts due to the significant difference in carbon solubility in austenite and ferrite which causes carbon rejection and formation of carbides at the boundaries of austenite. During the cooling of austenite containing 0.78 wt.% of carbon between 720 °C and 550 °C, transformation of austenite to pearlite occurs by an eutectoid reaction. By cooling of austenite with less than 0.78 wt.% of carbon, hypo-eutectoid ferrite forms at A_3 line before the eutectoid reaction which occurs at A_1 line. In the higher amount of carbon, first, cementite forms at A_{cm} line to reduce the carbon amount of austenite to 0.78 wt.%, and then eutectoid reaction occurs. In homogeneous austenite, the nucleation of pearlite due to regions of high energy occurs at grain boundaries. (Porter & Easterling, 1992; Smallman & Ngan, 2011).

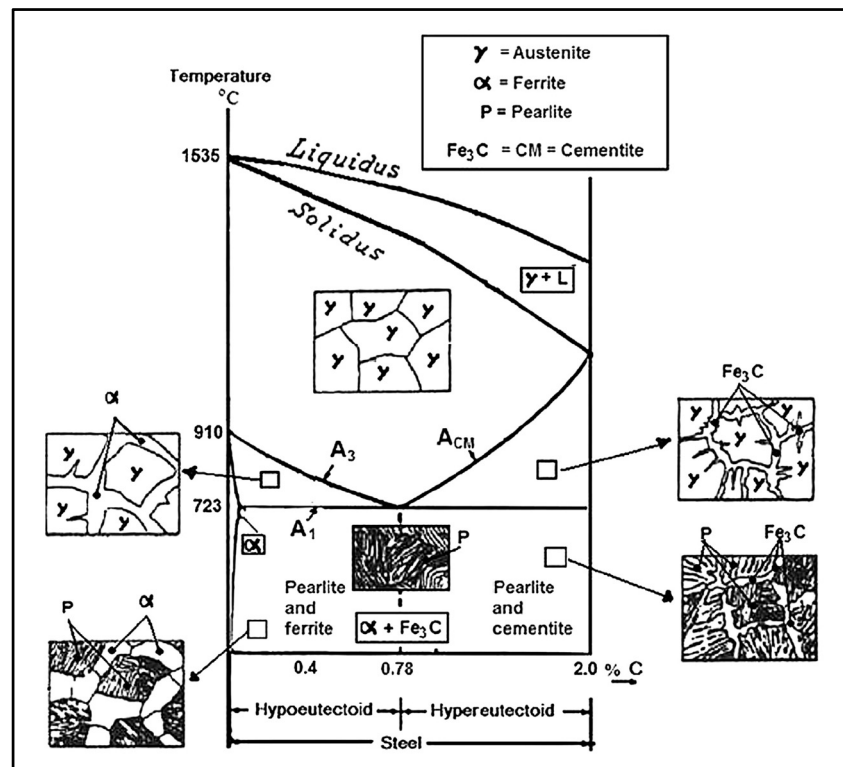


Figure 1-1 Part of Fe-C phase diagram associated with steel phase transformations, up to 2.0 wt.% of C (Smallman & Ngan, 2011).

1.2.2 Austenite to Martensite

Solid solution of austenite by rapid cooling to temperatures below about 200 °C forms a supersaturated solid solution called martensite (α'). Martensite is the hardest constituent in quenched steel. Rapid cooling or quenching of steels to the ambient temperature causes carbon atoms of austenite trap in the octahedral sites of the face centered cubic (FCC) austenite during martensite formation and then lead to the formation of a tetragonal (bct) structure. The morphology of martensite, depending on the carbon content of austenite, can be plate or lath or mixed (Krauss, 1999).

In contrast to ferrite or pearlite, martensitic transformation is diffusionless and occurs with deformation of austenite's lattice. Martensitic transformation occurs athermally and starts when the temperature drops below the martensite start (M_s) temperature and finishes at martensite finish (M_f) temperature. By adding more carbon to steel, M_s and M_f decrease. (H. Bhadeshia & Honeycombe, 2011).

1.2.3 Austenite to Bainite

The bainitic transformation has many similarities to martensite and pearlite reaction. The martensitic transformation occurs with structural change without diffusion and pearlite forms by redistribution and diffusion of carbon atoms. However, the bainite transformation starts with a structure change followed by diffusion of carbon atoms which precipitate as carbides in the matrix. In section 1.4, bainitic phase transformation will be discussed with detail.

1.3 Effect of Alloying Elements

Steel chemical composition plays a significant role in the final microstructures and mechanical properties achieved after the heat treatment process. The effects of alloying elements can be discussed from two points of view: (i) their effects on phase transformation; and (ii) their effects on mechanical properties.

1.3.1 Effect of Alloying Elements on Phase Transformation

Alloying elements can influence phase transformations in steels in the two following ways:

Austenite Stabilizer

Elements such as nickel, cobalt and manganese stabilize the austenite phase by expanding the γ -field. Figure 1-2 shows changes in the γ -field by adding manganese as an austenite stabilizer element (H. Bhadeshia & Honeycombe, 2011; Roberts, Kennedy, & Krauss, 1998).

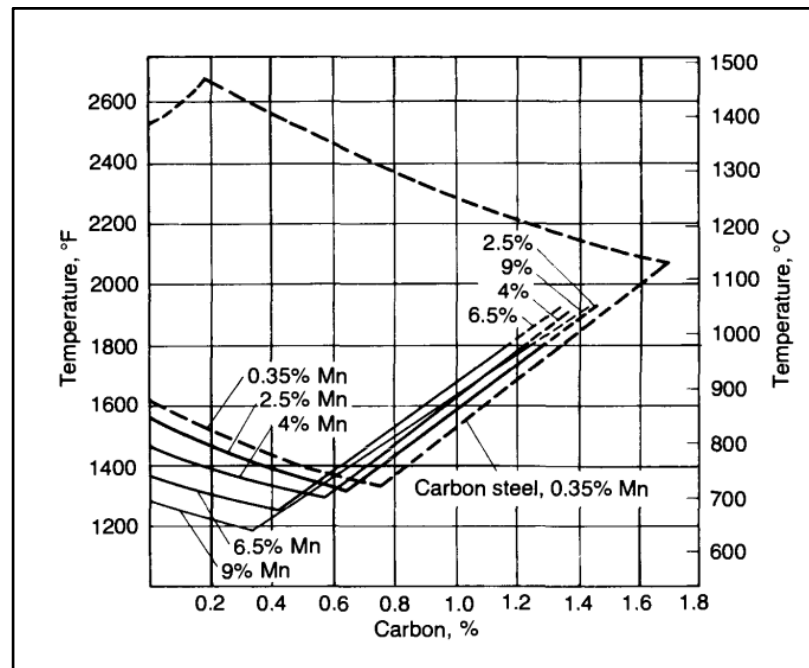


Figure 1-2 Influence of different manganese contents on the A1 and A3 lines (Roberts et al., 1998).

Ferrite Stabilizers

Ferrite stabilizers (α -stabilizers) contract the γ -field and boost ferrite formation over wider temperature range. Figure 1-3 illustrates how increasing the percentage of chromium affects the γ -field; it can be seen that by raising the chromium content up to 19%, the austenite phase tends to disappear (H. Bhadeshia & Honeycombe, 2011). Table 1-2 shows the alloying elements in two groups of austenite or ferrite stabilizers.

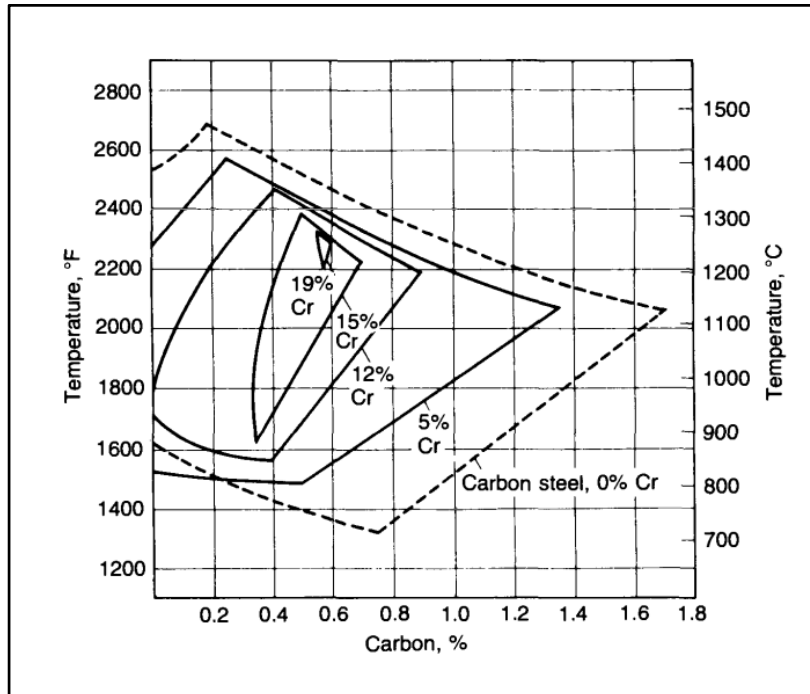


Figure 1-3 Effect of chromium percentage on the γ -field phase in a steel containing chromium (Roberts et al., 1998).

Table 1-2 Alloying elements impact on steel phase transformation.

	Elements
Austenite stabilizer	Mn, Ni, Co, Cu, Zn, C, N
Ferrite stabilizer	Cr, Si, Mo, V, Ti, Al, Sn, W, P, Nb, B, S, Ta, Zr

1.3.2 Effect of Alloying Elements on Mechanical Properties

Besides the effect of alloying elements on austenite and ferrite, their impact on mechanical properties is the primary reason for industries to include them in steels. In the following, the alloying elements that exist in the studied steel with their exclusive effects on mechanical properties are discussed.

Manganese (Mn): Manganese has been added to steel to help the deoxidation by forming MnO. Manganese refines the grain size, therefore decreases the ductile to brittle transition temperature, increases the tensile and yield strength. Manganese remarkably increases the hardness and hardenability in comparison with nickel (Figure 1-4). It interacts with carbon and forms Mn_7C_3 carbides. However, Mn decreases the transformation temperature range. Typical range of manganese in steels is from 0.3 to 2 wt.% (Hashmi, 2014; George E Totten, Funatani, & Xie, 2004).

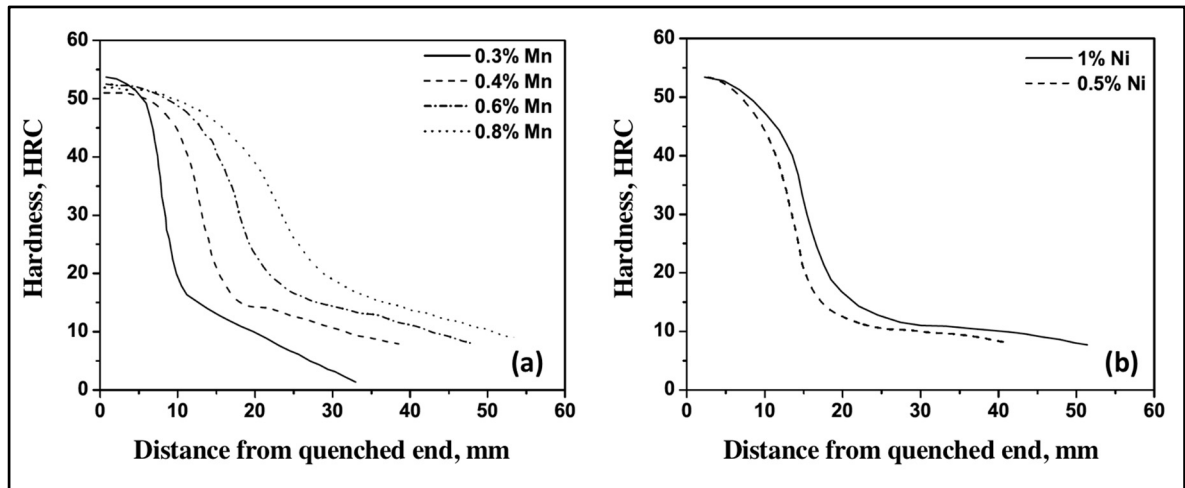


Figure 1-4 Jominy curves of effect of different amount (a) manganese, and (b) nickel on the hardness of steel (Hashmi, 2014; George E Totten et al., 2004).

Nickel (Ni): Nickel is added to steels to enhance the toughness, tensile and yield strength. Nickel increases the hardness of steel but not as much as manganese (Figure 1-4). Nickel lowers the austenite to ferrite transformation temperature range, retards the austenite decomposition and improves fatigue resistance. Typical range of nickel in steels is from 0.3 to 5 wt.% (Hashmi, 2014; George E Totten et al., 2004).

Chromium (Cr): Chromium improves strength, hardness, hardenability, hot strength and forms wear resistant carbides. Chromium enhances remarkably the austenite to ferrite transformation temperature when the percentage exceeds 12 wt.%. Typical range of

chromium in steels is between 0.3 and 12 wt.% (Hashmi, 2014; George E Totten et al., 2004).

Molybdenum (Mo): Molybdenum increases creep and corrosion resistance, high-temperature strength and hardenability by refining the grains. Also, reduces susceptibility to temper embrittlement. The typical range of molybdenum for low-alloy steels is between 0.1 to 0.5 wt.%, and in stainless steels is from 2 to 4 wt.% (Hashmi, 2014; George E Totten et al., 2004).

Vanadium (V): Adding vanadium causes grain refinement. Hence, increases the hardenability and allows the production of prehardened blocks with a cross section larger than the same alloy without vanadium. Vanadium is a strong carbide forming element; increases wear and temper resistance in steels. Addition of vanadium also increases the impact toughness up to 120%, raises the yield strength up to 17% and improves hardness after tempering by 24%. The typical range for low-alloy steel is between 0.1 and 0.3 wt.% and for tool steels is around 2 wt.%. (Hashmi, 2014; George E Totten et al., 2004)

Copper (Cu): Copper provides strength without endangering toughness during tempering heat treatment and raises atmospheric corrosion resistance. Typical range of copper in steels is from 0.2 to 0.5 wt.% (Hashmi, 2014; George E Totten et al., 2004).

Silicon (Si): Silicon picks up hardenability and reduces toughness, throughout the tempering heat treatment process, enhances the transformation temperature from epsilon carbide ($\text{Fe}_{2.4}\text{C}$) to cementite (Fe_3C). Silicon also strengthens ferrite and raises the transformation temperatures. Typical range of silicon in steels is between 0.2 and 2.5 wt.% (Hashmi, 2014; George E Totten et al., 2004).

1.4 Bainitic Transformation

In 1930, bainite was discovered by Davenport and Bain, when they did isothermal transformation of austenite at temperatures just above martensitic transformation (Davenport,

Bain, Paxton, & Westbrook, 1930). Generally, bainite is made of fine aggregates of ferrite plates with cementite particles. Bainitic transformation occurs during cooling from austenite to the temperatures below pearlite formation, but higher than martensite start temperature. Bainite can be produced either by isothermal transformation or continuous cooling with cooling rates which are neither fast to form martensite nor slow to form pearlite (H. Bhadeshia, 2001; Davenport et al., 1930).

1.4.1 Mechanisms of Bainite Formation

Extensive research has been performed on the mechanisms of bainite formation. Some researchers believe that this transformation is displacive and diffusionless, whereas others hold the view that the transformation is controlled by diffusion. According to Bhadeshia, bainitic transformation leads to a deformation with a shear component of 0.26 and dilatation strain of 0.03 which is compatible with displacive transformation mechanism. This deformation occurs at higher temperatures in comparison with martensitic transformation and causes plastic deformation, as shown in Figure 1-5. However, the transformation is diffusionless, but carbon escapes from bainitic ferrite to the retained austenite or precipitates as carbide, after formation of bainite sheaves (HKDH Bhadeshia, 1981; Sandvik, 1982).

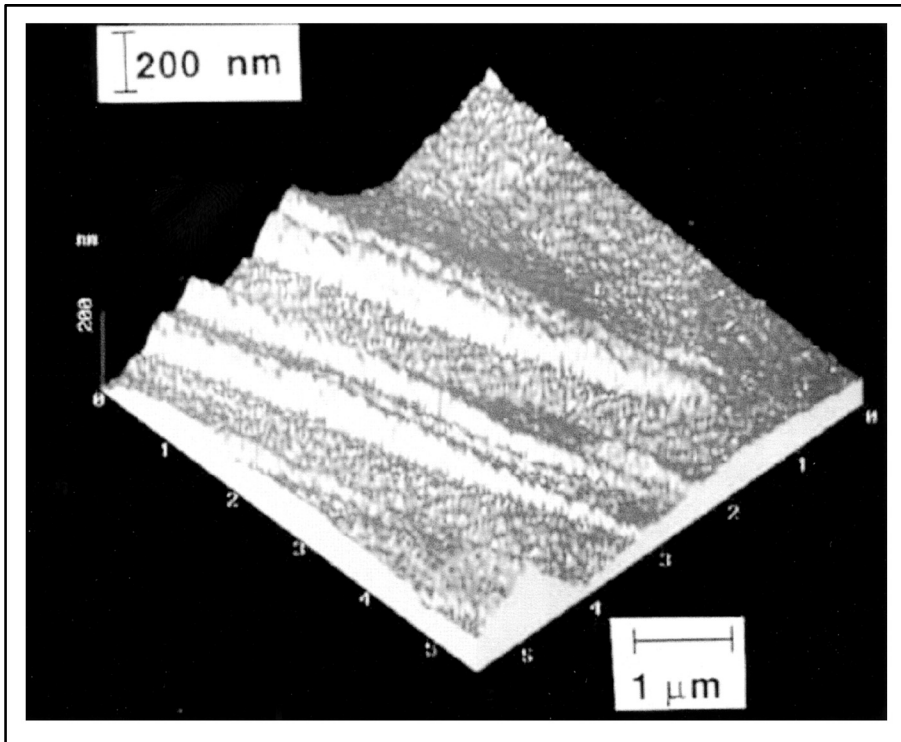


Figure 1-5 Image taken by atomic force microscope showing the displacements as a result of formation of bainite on a polished surface of austenite (Swallow & Bhadeshia, 1996).

Substitutional alloying elements do not partition during bainitic transformation. Their principal influence is on stabilizing austenite and ferrite phases. The ratio of iron to substitutional atoms stay constant during transformation which supports the view on diffusionless nature of bainite and small diffusivity of substitutional atoms at the temperatures related to bainitic transformation (Podder, 2011).

In contrast to substitutional elements, interstitial alloying elements such as C and N can partition into the austenite. In comparison with martensite, carbon has the ability to escape into another plate after formation of bainitic ferrite since bainite forms at higher temperatures (Podder, 2011).

1.4.2 Definition of T_0 Curve

Thermodynamically, diffusionless transformation can only occur at temperatures below a critical temperature, T_0 , where bainite has lower free energy than austenite with the same composition (Figure 1-6). The T_0 curve is obtained from T_0 temperatures for different carbon concentrations. Figure 1-6 is an example of T_0 curve plotted for Fe-C phase diagram. For example, in Figure 1-6, at T_1 , if the carbon concentration of austenite is less than the amount specified by T_0 curve, diffusionless transformation of austenite to bainite can occur (H. Bhadeshia, 2001).

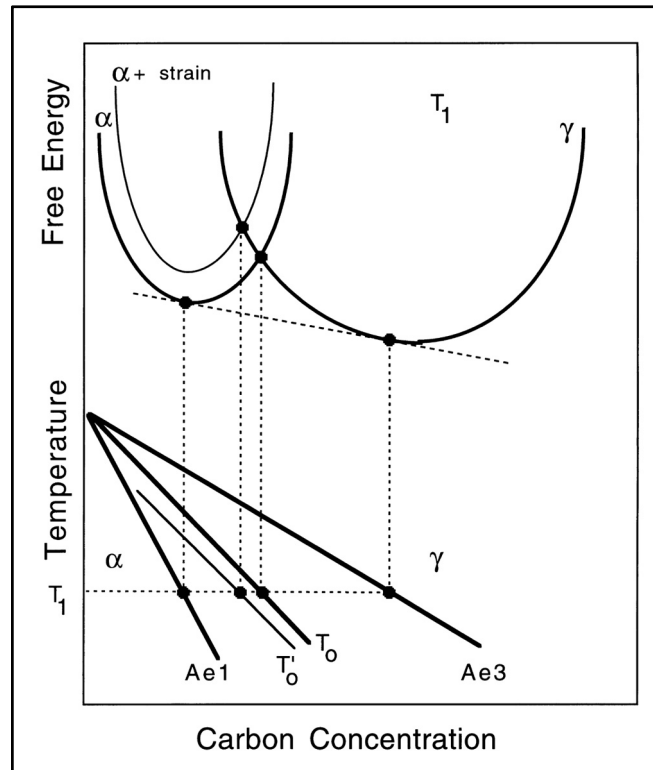


Figure 1-6 Schematic evolution of free energy as a function of carbon concentration showing the T_0 curve (H. Bhadeshia, 2001).

Considering diffusionless transformation of bainite, after formation of bainite plate (sheave), the surplus amount of carbon is rejected into the retained austenite. Hence, the subsequent plate of bainite has to form from a carbon enriched austenite (Figure 1-7). This process

continues until the amount of carbon in austenite meets the T_0 curve because at higher amount of carbon than the amount specified by T_0 curve, diffusionless transformation of austenite to bainite cannot occur. Experimental investigations also show that austenite to bainite transformation process comes to an end when the amount of carbon in austenite reaches the T_0 curve instead of equilibrium A_3 curve. Therefore, the reaction is incomplete because the austenite has not reached the equilibrium composition. Since the bainitic transformation is an “incomplete-reaction phenomenon”, a bainite finish temperature B_f does not have any fundamental definition (H. Bhadeshia, 2001).

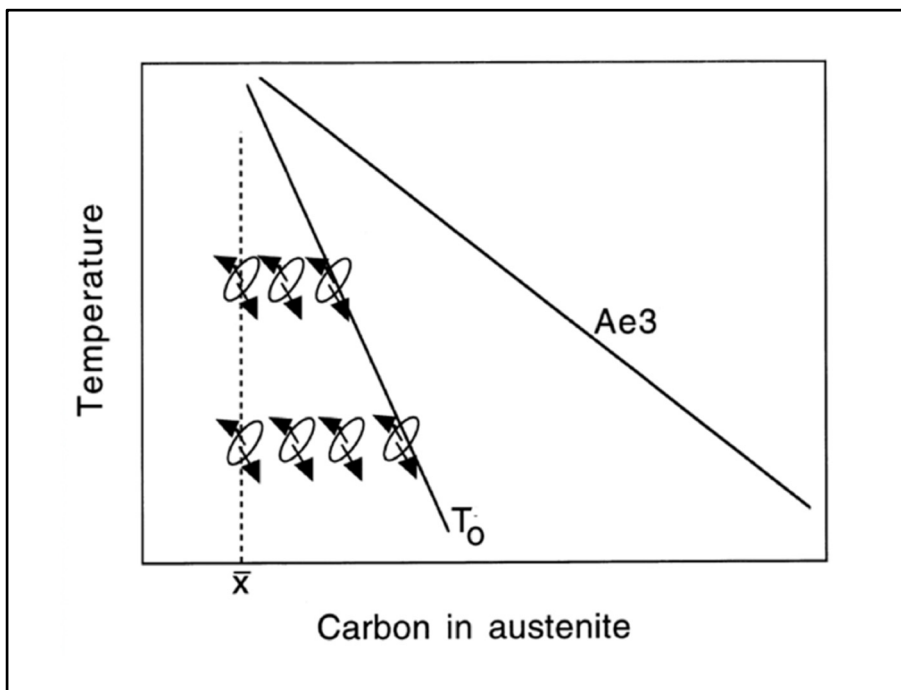


Figure 1-7 Schematic of an incomplete bainitic transformation. After diffusionless formation of bainite plate, the excess carbon escape into the retained austenite and oncoming plate forms from carbon enriched austenite. The phenomenon stops at T_0 curve because thermodynamically, diffusionless transformation cannot occur when austenite composition reaches T_0 line (H. Bhadeshia, 2001).

By decreasing the temperature, bainite has the ability to form from austenite with higher amount of supersaturated carbon, therefore, as the temperature drops, more bainite forms and less amount of retained austenite remains.

1.4.3 Morphology of Bainite

Bainite includes aggregates of fine ferritic plates which are detached by regions of remaining phases. These regions can be retained austenite or carbides. The fine plates of ferrite are about $0.2\mu\text{m}$ thick and $10\mu\text{m}$ long and their combination is called sheave. The thickness of the plates decreases by reducing the transformation temperature, therefore the density of plates inside the sheaves increases. Bainite structure changes with temperature and two types of bainite can be formed depending on the temperature at which bainite forms and have been classified as: (i) upper bainite, and (ii) lower bainite (Figure 1-8) (H. Bhadeshia, 2001).

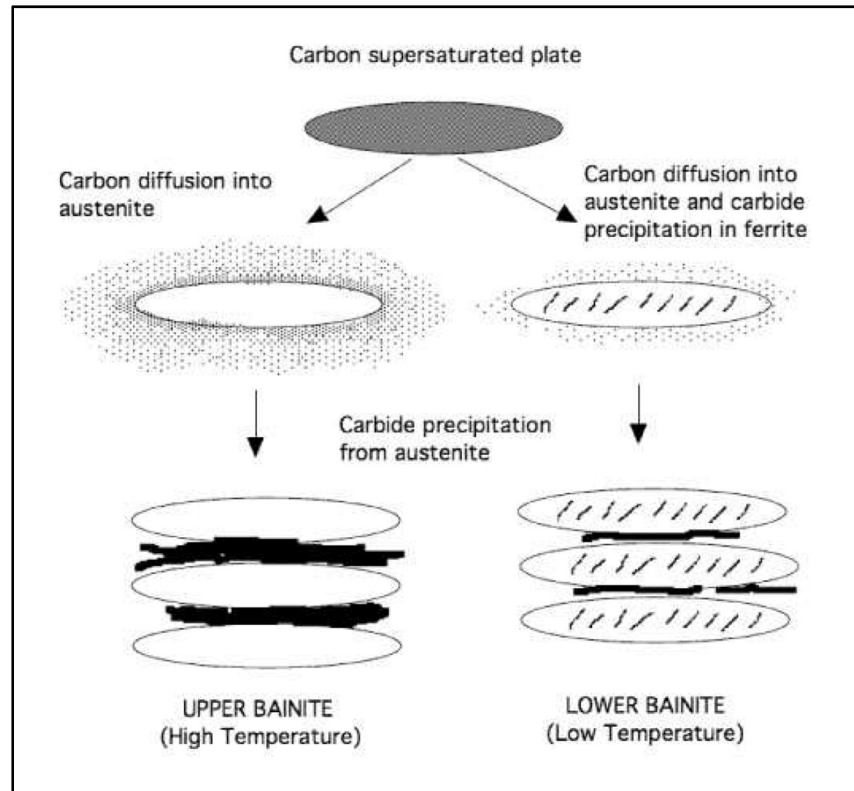


Figure 1-8 Schematic illustration of transformation of austenite to lower and upper bainite (Takahashi & Bhadeshia, 1990).

Upper Bainite: Figure 1-8 schematically shows the upper bainite formation, which is comprised of fine plates of ferrite (with thickness of $0.2\mu\text{m}$) and carbides precipitation from austenite among the ferritic plates. Formation of upper bainite occurs in the temperature

range between 400 °C and 550 °C. Ferrite in upper bainite is free from precipitations of carbide (Figure 1-9) (H. Bhadeshia, 2001).

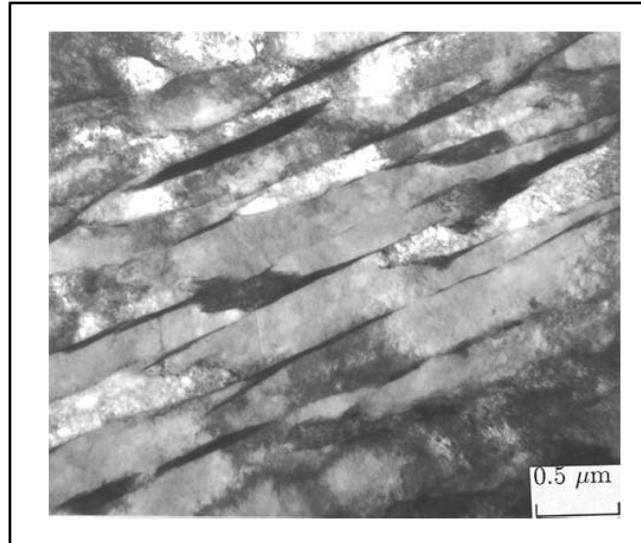


Figure 1-9 Upper bainite in Fe-0.095C-1.63Si-2Mn-2Cr wt.% steel transformed isothermally at 400 °C (H. Bhadeshia & Honeycombe, 2011).

Lower Bainite: Lower bainite forms at temperatures higher than M_s , approximately from 250 °C to 400 °C. The microstructure is similar to upper bainite, but carbides also precipitate inside the plates. In lower bainite, there are two types of cementite precipitations, one type forms from carbon enriched austenite and precipitate between the plates of ferrite, and the second type, which forms from supersaturated plates of ferrite, and precipitate inside the plates (Figure 1-10) (H. Bhadeshia & Honeycombe, 2011).

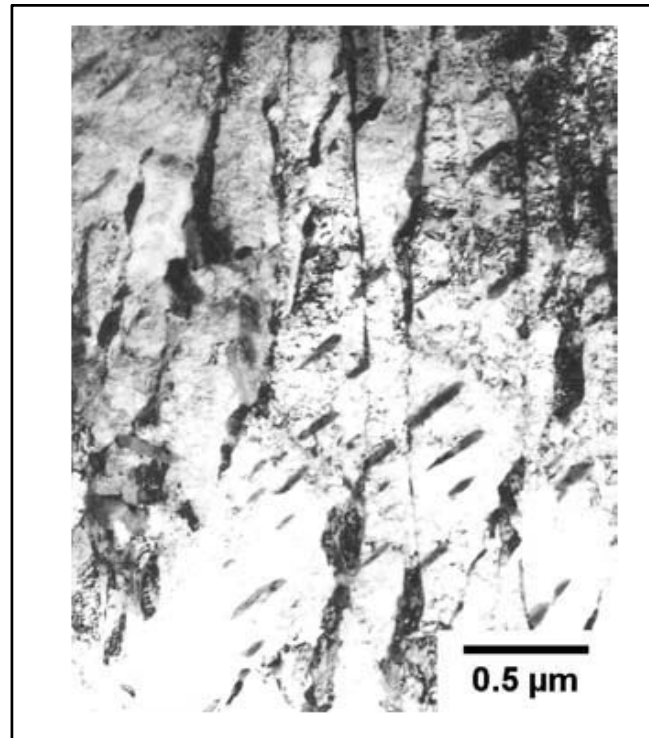


Figure 1-10 lower bainite microstructure of Fe–0.3C–4Cr (H. Bhadeshia & Honeycombe, 2011).

1.4.4 Effects of Alloying Elements on Bainite Start Temperature

Carbon has a significant role in the formation of bainite. The effect of carbon on the start temperature of bainite is shown in the Equation 1.1. As indicated in this equation, other elements such as manganese, nickel, chromium and molybdenum can postpone the bainite formation to lower temperatures (H. Bhadeshia & Honeycombe, 2011).

$$B_s (\text{°C}) = 830 - 270 w_C - 90w_{Mn} - 37w_{Ni} - 70w_{Cr} - 83w_{Mo} \quad (1.1)$$

Where, w_i is the weight percent of alloying elements.

1.5 Tempering of Bainite

Medium-carbon low-alloy steels (Cr-Mo-Ni-V) have wide applications in pressure vessels, automotive applications and plastic dies. Ductility is a limiting factor for application of these steels since the as-quenched steel is hard and brittle. Tempering is a heat treatment of as-quenched martensite and bainite to modify the microstructure and obtain the desired mechanical properties such as toughness, ductility and dimensional stability by holding the steel below the lower critical temperature (A_1) which austenite begins to form.

Tempering in martensitic and bainitic steels comprises different phenomena which occur during tempering. Different tempering phenomena in martensite can be classified as shown in the Table 1-3.

Table 1-3 Different tempering stages and their temperatures in martensite based on 1-hour treatment (Dhua, Ray, & Sarma, 2001)

Stage	Temperature range (°C)	Phenomenon
I	25 to 80	Diffusion of carbon, segregation and carbon clustering
II	100 to 200	Precipitation of transition carbides
III	200 to 350	Decomposition of retained austenite
IV	250 to 450	Dissolution of transition carbides and precipitation of cementite
V	500 to 650	Recovery of dislocations
VI	500 to 700	Precipitation of alloying elements
VII	600 to 700	Carbide coarsening
VIII	650 to 700	Recrystallization into equiaxed structure

Generally, the change in microstructures and properties during tempering depends on the primary microstructure; therefore, the bainite reaction during tempering is different from that of martensite (Fonstein, 2015).

In contrast with martensite, bainite has lower carbon in solid solution. Since carbon has a significant solid solution effect, during the tempering of martensite, mechanical properties drop remarkably as carbon diffuses out of the bcc lattice and forms carbides. On the other hand, tempering has much milder effect on bainite because carbides have already been formed during the formation of bainite; therefore, mostly carbide coarsening occurs during the tempering, which decreases the strength (Woodhead & Quarrell, 1965).

The tempering stages of Table 1-3 are idealized and many of them may not occur during the formation of martensite and bainite, particularly when the M_s is high. Bainitic transformation occurs at higher temperatures in comparison with martensite. It means that many stages of tempering occur during the formation of bainite. Hence, carbon diffusion, carbon clustering and precipitation of transition carbides occur during bainitic transformation due to a phenomenon called *autotempering*. Autotempering is inevitable for bainite and its influence is greater in bainite than martensite.

In comparison with martensite, bainite forms at higher temperatures and the microstructure also experiences some extent of recovery during bainite formation. Hardness and strength of lower bainite throughout tempering declines more than upper bainite. This reduction is also more considerable for high strength steels (Irvine & Pickering, 1957).

Microstructure evolution during bainite tempering could be summarized as following: (H. Bhadeshia & Honeycombe, 2011):

- I. Considerable changes in strength during the coarsening of bainite plate and recrystallization into equiaxed ferrite grains.
- II. Insignificant changes in strength during cementite particle coarsening and recovery of the dislocations in the substructure.

1.5.1 Hollomon – Jaffe Parameter

Tempering temperature and time are both the controlling parameters during tempering heat treatment. Both variables were combined in a parameter named Hollomon-Jaffe to describe the changes in hardness of steel during tempering (George E Totten et al., 2004). The Hollomon-Jaffe parameter can be calculated according to Equation 1.2 (Janjusevic, Gulisija, Mihailovic, & Pataric, 2009):

$$P = T(C + \log(t)) \quad (1.2)$$

Where P is the Hollomon-Jaffe parameter, C is the Hollomon-Jaffe constant, T is temperature in Kelvin (K), and t is time in hour (h).

At the beginning, Hollomon-Jaffe constant (C) of 20 was considered appropriate for all kind of steels. Later, Sinha's works showed that the constant C depends on carbon content of the steel (Sinha, 1989). Therefore, Hollomon-Jaffe constant can be calculated according to Equation 1.3 (George E Totten et al., 2004):

$$C = 21.3 - (5.8 \times \% \text{ Carbon}) \quad (1.3)$$

Figure 1-11 depicts the relation between Hollomon-Jaffe parameter and hardness during tempering of two bainitic steels with different amounts of carbon. It can be seen in Figure 1-11 that minor changes in the amount of carbon (0.06-0.14 wt.%) in bainitic steels causes small effect on the hardness.

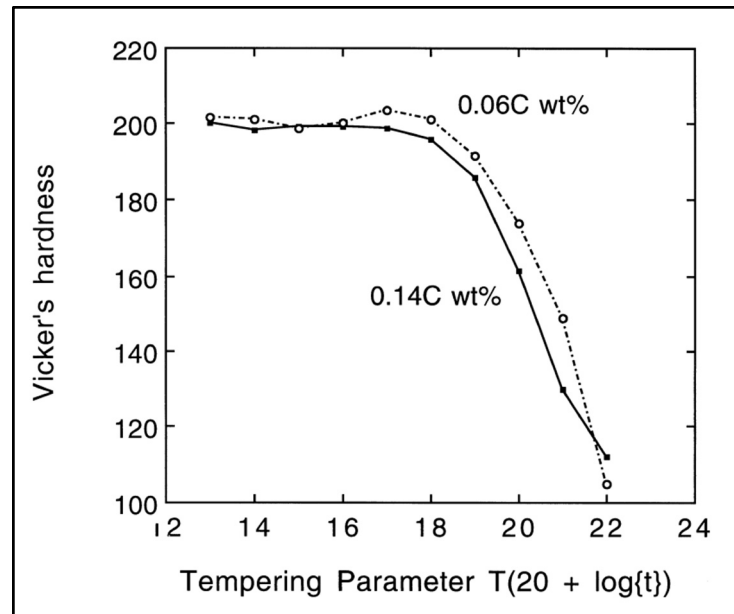


Figure 1-11 Hardness changes for two bainitic steels consisting different percentages of carbon, as a function of Hollomon-Jaffe parameter (Irvine, Pickering, Met, & Heselwood, 1957)

1.5.2 Precipitation of Transition Carbides

Transition carbides form during first stages of tempering as the precursor for the formation of cementite. During tempering of bainite, precipitation of transition carbides is unlikely because of the nature of bainite, which already consists of cementite and also due to the autotempering effect during formation of bainite. However, in general for steels, at tempering temperatures of 100 °C to 200 °C, the first carbide that precipitate in the matrix of low-carbon steels is orthorhombic η -carbide (Fe_2C). Hexagonal ϵ -carbide (Fe_2C) precipitates in steels with more than 0.2 wt.% of carbon. In steels with higher amounts of carbon, another transition carbide with stoichiometric composition of Fe_5C_2 forms before cementite and is called Hägg carbide (H. Bhadeshia, 2001; Morra, Böttger, & Mittemeijer, 2001; Naraghi, Selleby, & Ågren, 2014).

1.5.3 Retained Austenite Decomposition During Tempering

Residual austenite decomposition occurs during the third stage of tempering. The decomposition starts at about 200 °C and ends at about 350 °C. The behaviour of retained austenite decomposition throughout tempering differs as a function of chemical composition of steel. The decomposition product generally is a mixture of ferrite and cementite. However, formation of martensite has also been reported by Podder et al. and Yan et al. during the decomposition of retained austenite (Figure 1-12). In addition, Yan et al. investigations have shown the transformation of retained austenite to lower bainite, as well (Figure 1-13) (Saha Podder & Bhadeshia, 2010; Yan, Han, Li, Luo, & Gu, 2017)

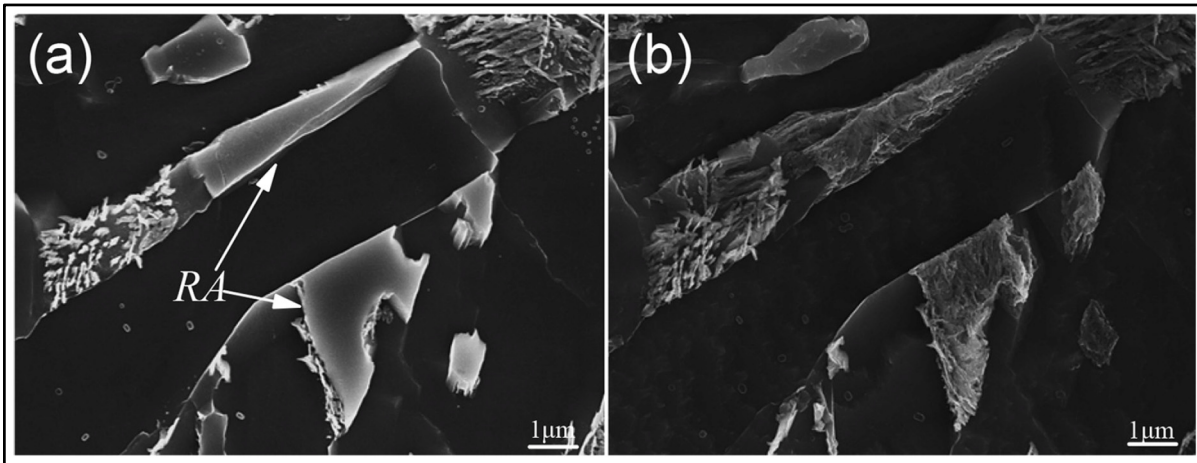


Figure 1-12 (a) lath type and blocky retained austenite in as-quenched sample, (b) martensite formation after 5 hours of tempering at 230 °C (Yan et al., 2017).

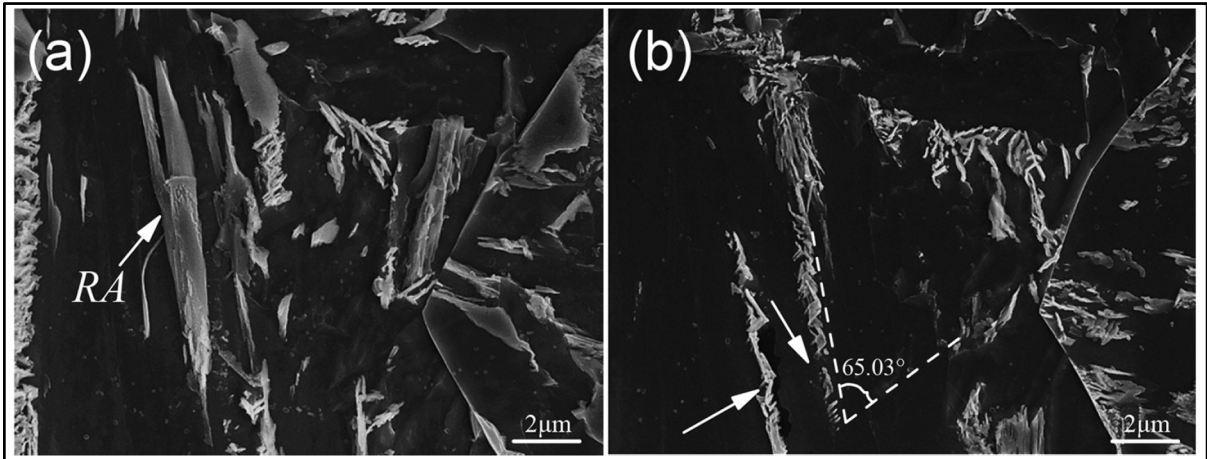


Figure 1-13 (a) retained austenite in as-quenched sample, (b) lower bainite after 1 hour of tempering at 400 °C (Yan et al., 2017).

1.5.4 Double Tempering of Steels

During tempering, retained austenite transforms over the temperature range of 200-350 °C. Alloying elements such as chromium and silicon hinder this transformation and postpone it to higher temperatures. Retained austenite decomposition during tempering of alloy steels is mostly not completed at the end of tempering. For example, in high-alloy steels containing 10 wt.% of chromium, even a long holding time cannot decompose the retained austenite. By tempering between 500 °C and 550 °C, part of this retained austenite transforms to martensite during cooling cycle after tempering and produces fresh martensite. Therefore, to acquire a full transformation of retained austenite as well as tempering the fresh martensite, double tempering is often applied for alloyed steels (G.E. Totten & Howes, 1997).

1.5.5 Precipitation of Carbides During Tempering

In bainitic steels, understanding the carbides precipitation and carbides evolution throughout tempering is important. Thermodynamically, Mo, Cr, Ti, V and W carbides are more stable than cementite and can form carbides in steels. Therefore, it is anticipated that if the amounts of alloying elements are sufficiently high in steels, these carbides can form prior to

cementite. Nevertheless, because these substitutional elements cannot diffuse sufficiently at lower temperatures, alloy carbides do not form until about 500 °C (H. Bhadeshia & Honeycombe, 2011).

Five types of carbides, M_3C , M_7C_3 , M_2C , $M_{23}C_6$ and M_6C , can be found during tempering which vary as a function of tempering time and temperature. However, three types of carbides, M_3C , M_7C_3 and $M_{23}C_6$ have been widely reported among researchers. The type and size of carbides are very important because they affect the mechanical properties of the steel (Inoue & Masumoto, 1980).

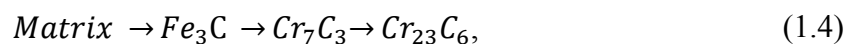
During tempering, stable M_3C carbide is the first one that forms in the matrix followed by M_7C_3 which is a metastable carbide. Further tempering causes replacement of metastable carbides with $M_{23}C_6$ which is an equilibrium carbide (Dépinoy et al., 2017).

1.5.5.1 Tempering of Bainite Containing Vanadium

Vanadium is among the elements with strong carbide formation tendency. Even in steels with 0.1 wt.% of vanadium, VC carbide with FCC structure can form. V_4C_3 is another type of vanadium carbide that can form alongside with VC. VC or V_4C_3 can be replaced with cementite at higher temperatures during tempering (Honeycombe & Mehl, 1976).

1.5.5.2 Tempering of Bainite Containing Chromium

In comparison to vanadium, chromium carbides are less stable. In bainitic steels, two types of chromium carbides, Cr_7C_3 and $Cr_{23}C_6$, frequently form during tempering. The common sequence of formation for these chromium carbides is (H. Bhadeshia & Honeycombe, 2011):



At least 1.0 wt.% of chromium and 0.2 wt.% of carbon in the steel should exist for the formation of Cr_7C_3 . Diffusion of chromium is faster than other substitutional atoms, therefore, Cr_7C_3 carbides can form at lower temperatures of approximately 500 °C. Also, chromium carbides coarsen faster than vanadium carbides. Figure 1-14 depicts the impact of chromium percentage on hardness. It is evident that, secondary hardening effect during tempering occurs in steels with chromium amounts higher than 12 wt.% (Honeycombe & Mehl, 1976).

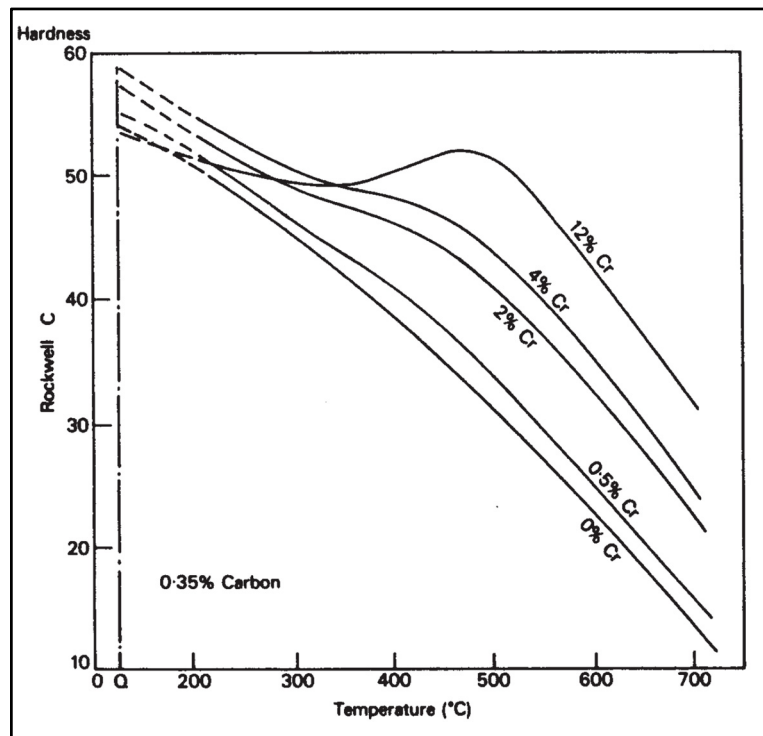


Figure 1-14 Influence of various amounts of chromium on hardness during tempering of a steel containing 0.35 wt.% carbon (Bain & Paxton, 1966).

1.5.5.3 Tempering of Bainite Containing Molybdenum

Molybdenum is another carbide forming element during tempering. Two types of carbides, Mo_2C and Mo_6C , are observed after tempering. For molybdenum contents between 4 to 6 wt.%, the formation sequence is:



Between these two types of carbides, hexagonal Mo_2C is the carbide responsible for secondary hardening during tempering. Secondary hardening related to Mo_2C precipitation generally occurs after 25 h of tempering at 550 °C (H. Bhadeshia & Honeycombe, 2011).

Mo_2C carbides nucleate at primary austenite grain boundaries and ferrite lath boundaries. For steels containing vanadium, Mo_2C carbides nucleate at cementite-ferrite interface and on dislocation in the ferrite (H. Bhadeshia & Honeycombe, 2011).

1.5.6 Effect of Tempering on Cementite Coarsening

Coarsening of cementite results in lowering the interface energy between the cementite and matrix that has been stored in the specimen. Cementite particles in the tempered martensite and bainite microstructure are generally located at the lath boundaries or distributed inside the laths. However, cementite exists only at lath boundaries of upper bainite (Greenwood, 1956).

Cementite coarsening during the tempering of a medium-carbon steel is shown in Figure 1-15. The upper line of each region illustrates the lath boundary cementite and the lower line shows the intra-lath cementite. In the beginning, cementite in bainite is coarser than martensite because cementite already exists in bainite and also because of the autotempering effect during the bainitic transformation. While bainite shows high degree of stability to tempering, martensite experiences higher rate of coarsening. Therefore, bainitic microstructures remains finer than martensite over a longer time of tempering (Nam, 1999).

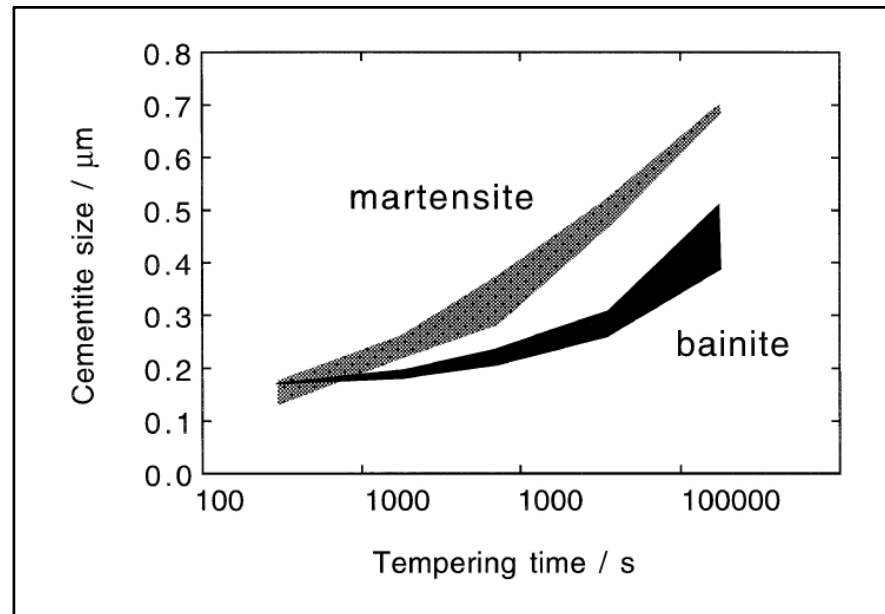


Figure 1-15 Size variation of cementite versus tempering time at 700 °C for a Fe-0.45C-0.22Si-0.62Mn wt.% steel. The upper bound on each shaded region is for average size of cementite located at the lath boundaries and the lower bound is for Intra-lath cementite (Nam, 1999).

1.5.7 Secondary Hardening

Secondary hardening occurs during tempering in martensitic and bainitic steels containing strong carbide formers such as Cr, V, Mo and Nb. The alloying carbide precipitation with these elements require diffusion of substitutional atoms; therefore, their precipitation is slow and can only occur at higher temperatures (>500 °C). At the beginning of tempering (mainly in martensite), the hardness decreases as cementite precipitation takes place and replaces the carbon in solid solution. Hardness begins to rise again when the alloy carbides form (Baker & Nutting, 1959; Irvine & Pickering, 1957).

The secondary hardening effect in bainite is less than martensite because the cementite in bainite is coarser. Figure 1-16 shows secondary hardening peak in bainitic steel containing vanadium. Huang et al. works on the effect of molybdenum in low carbon bainitic steels has shown that by adding 0.3 wt.% molybdenum, the steel gains dramatic benefits from

secondary hardening. Saha et al. found that secondary hardening took place during tempering at 500 °C due to the formation of M_4C_3 and M_2C carbides (Huang et al., 2014; Saha, Nayak, Biro, Gerlich, & Zhou, 2014).

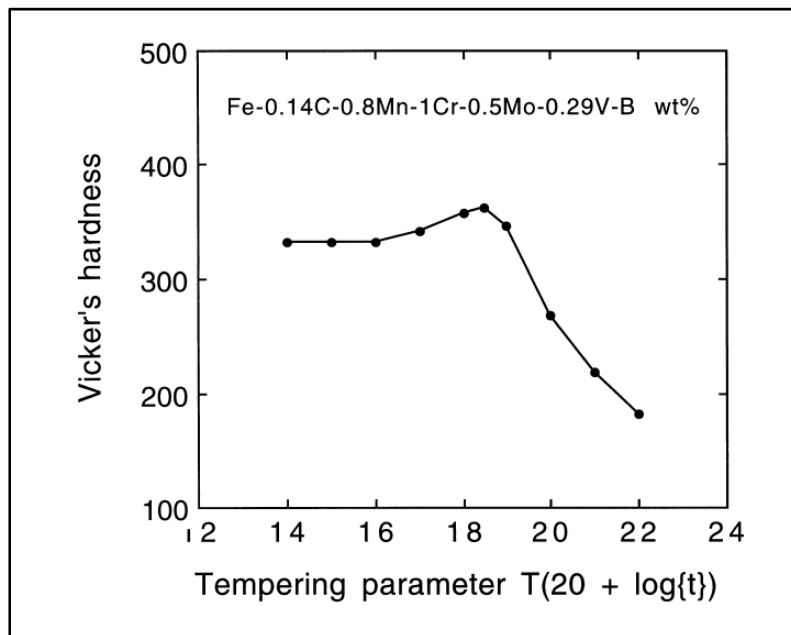


Figure 1-16 Secondary hardening peak for a bainitic steel containing 0.3 wt.% vanadium (Irvine & Pickering, 1957).

1.5.8 Effects of Tempering on Mechanical Properties

An extensive range of mechanical properties can be obtained during tempering of alloyed steel from 200 °C to 700 °C. In Figure 1-17 Changes in different mechanical properties during 1 h tempering as a function of tempering temperature for 1.5Ni-1Cr-0.25Mo-0.4C wt.% steel is shown. Specifically, tensile strength changes from 1800 to 900 $MN m^{-2}$, when the tempering temperature is increased from 200 °C to 700 °C. In the case of ductility, it increases as the tensile strength falls by increasing the tempering temperature; however, there is a minimum ductility around 300 °C which corresponds to retained austenite decomposition and formation of cementite films at the boundaries (H. Bhadeshia & Honeycombe, 2011).

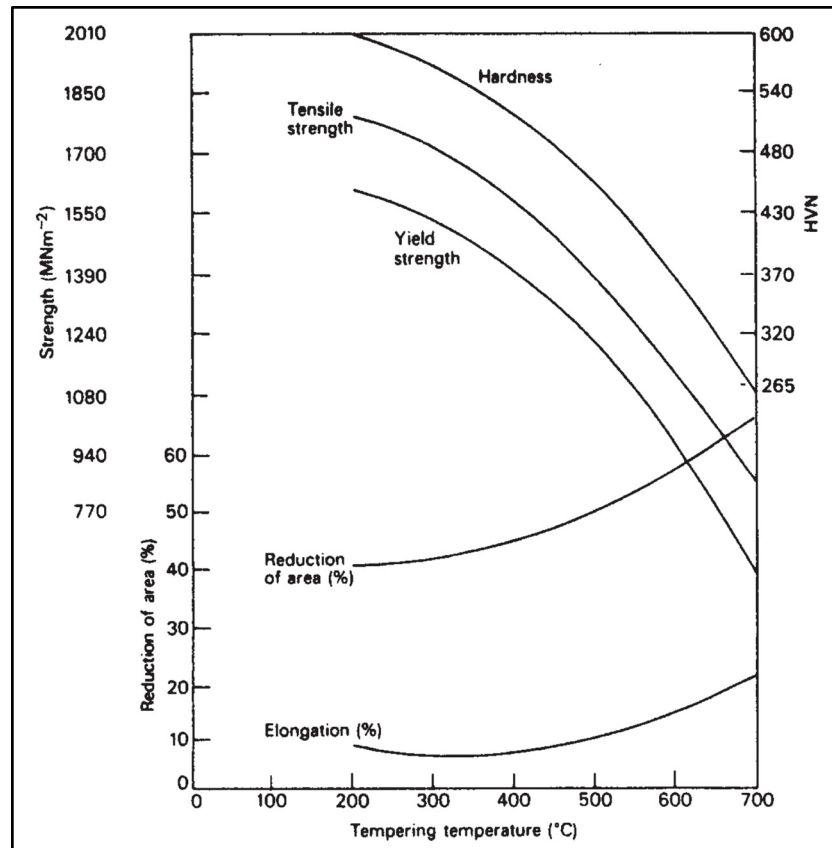


Figure 1-17 Change in different mechanical properties during 1 h tempering as a function of tempering temperature for 1.5Ni-1Cr-0.25Mo-0.4C wt.% steel (Thelning, 1975)

1.6 Summary

In this chapter, bainite formation and effect of tempering on bainite were discussed. In the field of bainite tempering, there is a lack of study for medium-carbon low-alloy steels, especially concerning phase transformations and tempering parameters regarding industrial tempering of large-size slabs. In addition, tempering cycle, chemical composition, and sample size vary from one research to another, which make tempering process difficult to be analysed. For instance, the tempering temperature in which full retained austenite decomposition occurs is not clear for the studied steel. In this research, by methodical design of experiments, tempering parameters are investigated to fill this gap and strengthen the knowledge of tempering.

CHAPTER 2

INFLUENCE OF STARTING MICROSTRUCTURE ON DILATATION BEHAVIOR DURING TEMPERING OF A HIGH STRENGTH STEEL

S. Hesamodin Talebi¹, Hadi Ghasemi Nanesa¹, Mohammad Jahazi¹ and Haikouhi Melkonyan²

¹ École de Technologie Supérieure, Département de Génie Mécanique, Montréal, Québec, Canada.

² Finkl Steel Inc., 100 McCarthy, Saint-Joseph-de-Sorel, QC J3R 3M8, Canada.

This article has been accepted for presentation in the conference of THERMEC2018.
This article has been also selected to be published in the Journal of Materials Science Forum
(Accepted: 19 November 2017)

Abstract

The aim of this study was to determine the effect of non-isothermal tempering on microstructure evolution in large-size slabs. Using high-resolution dilatometry, three different cooling rates (from 0.08 to 3 °C/s) representative of different regions from the surface to the core of the slab were experimentally simulated, and then tempering was carried out for each starting microstructure. A combination of light and electron microscopy and X-ray diffraction analyses were employed to accurately analyze different phenomena occurring during the tempering process, specially, the identification of different microstructures (bainite, martensite and retained austenite), and the determination of the percentage of retained austenite for each experimental condition were considered. Experimental results revealed that the microstructure after the cooling rate of 0.08 °C/s consisted of bainite and some retained austenite. For the cooling rate of 0.3 °C/s, martensite plus bainite was detected, and when the cooling rate was increased to 3 °C/s, a martensitic microstructure was obtained. Analysis of dilatometry curves indicated that tempering behavior varied significantly with the starting microstructure. Martensite tempering was accompanied with a length decrease due to the decomposition of medium-carbon martensite to low-carbon

martensite plus carbides. Tempering of bainite and retained austenite resulted in a remarkable length increase.

2.1 Introduction

Large-size high strength steels with chromium and nickel are used as dies to form automotive components due to their excellent mechanical properties and good machinability. The manufacturing process of these steels consists of ingot casting, followed by open die forging. The slabs are then quenched and tempered to achieve the desired mechanical properties (Chentouf et al., 2014; Liu et al., 1998; Wu et al., 2017).

The mechanical properties after quenching are strictly depending on the transformation of austenite to different phases including martensite and bainite. Afterwards, tempering of the produced microstructure leads to a more ductile material (Chentouf et al., 2014; Speich et Leslie, 1972). Changes during tempering of martensite and bainite can be classified into four stages. 1) Segregation of carbon atoms and clustering into solid solution which occur below 80 °C; 2) Precipitation of transition carbides in the matrix between 100 °C and 200 °C; 3) Decomposition of retained austenite from 200 °C to 350 °C. Retained austenite decomposes to ferrite/cementite, martensite or bainite depending on steel composition, and 4) conversion of formed transition carbides to more stable cementite in the tempering range of 250 °C to 450 °C. It is worth noting that stages three and four could overlap over a vast range of temperatures (Cheng et al., 1988; Miller, Beaven et Smith, 1981; Morra, Böttger et Mittemeijer, 2001; Nagakura et al., 1983; Primig et Leitner, 2011; Yan et al., 2017).

Large-size slab cools with different cooling rates, and therefore various microstructures form in each region of the slab. The purpose of the present work is to investigate the influence of the starting microstructure and its evolution during tempering.

2.2 Materials and methods

The chemical composition of the high strength steel studied in this study was (wt.%) C 0.35–V 0.15–Mn 0.99–Si 0.41–Ni 0.5–Cr 1.86–Mo 0.53–Cu 0.16. Cylindrical samples 10 mm in length and 4 mm diameter were cut from a large-size forged slab. The primary microstructure of the studied sample consisted of bainite and retained austenite.

Cooling and tempering were simulated using a high-resolution TA DIL 805A/D dilatometer (TA instruments, New Castle, DE, USA). To reach a fully austenitic microstructure, first, the specimens were heated up to 870 °C and hold at this temperature for 10 min before cooling at rates of 0.08, 0.3 and 3 °C/s in order to produce a fully bainitic, a mixed microstructure of bainite and martensite, and a fully martensitic one. Then, non-isothermal tempering with a heating rate of 10 °C/min was performed to investigate different phase transformations as a function of the starting microstructure.

Phase identifications after cooling were made using X-ray diffraction (XRD). The details of the XRD analysis and obtained results have already been reported in a previous publication and will not be reported here (Talebi et al., 2017). Volume fraction of martensite and bainite were calculated using optical micrographs and MIP image analysis software.

2.3 Results and Discussion

2.3.1 Cooling dilatometric curves

Figure 2-1(a) illustrates the dilatation curve versus temperature for the cooling section from austenitization temperature to room temperature for the three investigated cooling rates of 0.08 °C/s, 0.3 °C/s and 3 °C/s. ΔL and L_0 represent length change and initial length of the samples, respectively. The influence of cooling rate on transformation points is also illustrated in Figure 2-1(b), (c), and (d), where the derivatives of relative length changes are presented. For example, in Figure 2-1(c) a clear transition around 295 °C is observed for the cooling rate of 0.3 °C/s. Similarly, as can be seen in Figure 2-1(d) this transition is near the

martensite start temperature, therefore indicating the formation of martensite with this cooling rate. The results clearly show that three different transformations have taken place.

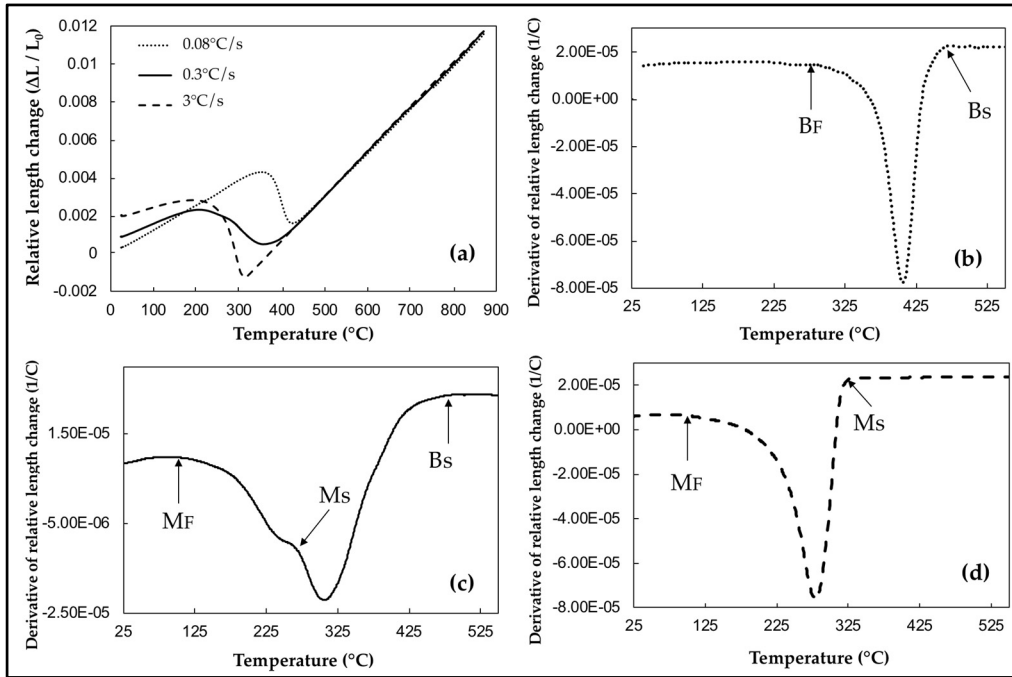


Figure 2-1(a) Dilatometric cooling curves of studied steel. Derivatives of relative length changes during cooling at cooling rates of (b) 0.08 °C/s, (c) 0.3 °C/s, and (d) 3 °C/s.

In Figure 2-1(a), for the cooling rate of 0.08 °C/s, the specimen contains 23% (phase fraction) of retained austenite and the rest is bainite. Using Figure 2-1(b), the bainite start (B_s) and the bainite finish (B_f) temperatures were calculated to be 472 °C and 283 °C, respectively. For the cooling rate of 3 °C/s, martensitic transformation starts (M_s) at 316 °C and finishes (M_f) at 122 °C. This specimen is considered to be fully martensitic as no retained austenite was detected in the XRD analysis (Talebi et al., 2017). In the case of mixed microstructure, the transformation starts with bainite formation at 468 °C and ends with martensite at 116 °C. The microstructure at this cooling rate contains 77% of bainite, 11% of martensite and 12% of retained austenite.

2.3.2 Tempering dilatometric curves

Non-isothermal tempering of the quenched samples was carried out with a heating rate of 10 °C/min until 600 °C for all starting microstructures. Different behaviors were observed in the dilatation curves depending on the starting microstructure as shown in Figure 2-2(a) and (b).

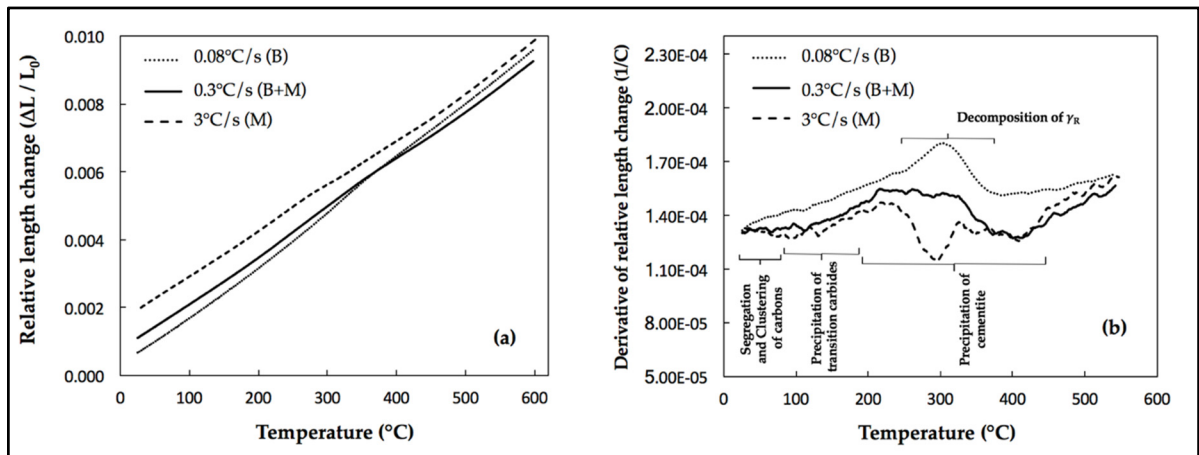


Figure 2-2. (a) Relative length changes, and (b) derivatives of relative length changes during non-isothermal tempering of bainitic, martensitic and mixture specimens with a heating rate of 10 °C/min.

Carbon segregation, formation of transition carbides and precipitation of cementite were not identified with high-resolution dilatometry for tempered bainite. This is probably due to the small carbon content of bainite (0.19 wt.%) and auto-tempering effect of the microstructure during non-isothermal tempering (Talebi et al., 2017). The only revealed peak in the bainitic specimen is related to the retained austenite decomposition at 303 °C (stage 3 of the tempering process).

The pattern is reversed when it comes to the martensitic case. Since martensite contains 0.29 wt.% of carbon (Talebi et al., 2017), all the four stages of tempering mentioned in Introduction are normally expected to take place. Specifically, minor contraction due to carbon segregation, followed by another decrease due to precipitation of transition carbides ending below 215 °C were observed. Subsequently, a wide peak for cementite precipitation

was observed in the temperature range 240 °C to 450 °C. Finally, a small peak at 327 °C was observed in the cementite precipitation zone which probably corresponds to retained austenite decomposition.

In the specimen with mixed bainite and martensite microstructure, a linear behavior was observed between 215 °C and 325 °C. This length stability is assumed to be due to addition of two phenomena: (1) Contraction due to cementite formation in martensite, and (2) Expansion due to the decomposition of retained austenite which in this study is blocky shape and exists at the bainitic ferrite boundaries (Figure 2-3 (a)). Further temperature increase caused a length decrease from 326 °C. At this temperature, retained austenite decomposition is not finished yet; therefore, cementite precipitation (in the martensite) is probably the dominant phase transformation mechanism.

2.3.3 Length changes during tempering

As shown in Figure 2-2(a), independently of the heating rate employed, as the temperature increases a positive length change is observed. However, the length increase is not linear, and its amount varies with the starting microstructure. Table 2-1 summarizes the different length changes as a function of the starting microstructure. For example, it can be seen that during tempering of the bainitic specimen, specimen's length increased by 12.4%. This increase is in fact the sum of thermal expansion of the material, due to temperature increase and decomposition of retained austenite during tempering. Considering that retained austenite decomposition is the only phenomenon occurring for bainitic specimens; if one assumes that all the retained austenite is decomposed during tempering, then its decomposition has resulted in +3.7% increase in total length. Further detailed analysis is required to confirm the above findings.

On the other hand, the tempering effect on martensitic specimen, which is the precipitation of carbides, has reduced the length by 6.5%. Adding this reduction to thermal expansion, total length increase of martensitic microstructure during non-isothermal tempering is 3.8%.

In the case of mixed microstructure, excluding the thermal expansion, the reduction of tempered martensite has overcome the increase of retained austenite (12%) decomposition, which finally leads to a length reduction of 3.1% that could be associated to the tempering process. The above findings are further confirmed by the analysis presented in Figure 2-2(b), where a clear slope change can be seen after 326 °C, due to cementite precipitation.

Table 2-1 Total length change during tempering from 25 °C to 600 °C and specific length change due to tempering phenomena

Specimen	Total length change from 25 °C to 600 °C (%)	Length change due to tempering phenomena (%)
Bainitic (B=77%, RA=23%)	+12.4	+3.7
Bainite/Martensite (B=74%, M=14%, RA=12%)	+7.1	-3.1
Martensitic (less than 5% RA)	+3.8	-6.5

2.3.4 Microstructure evolution

The different microstructures obtained before and after non-isothermal tempering are depicted in Figure 2-3 which confirm the observations made on dilatometric curves. Figures 2-3 (a), (c), and (f) show that the microstructures obtained after applying cooling rates of 0.08 °C/s, 0.3 °C/s and 3 °C/s are bainite, mixed bainite/martensite, and full martensite, respectively. The retained austenite at the grain boundaries of the bainitic ferrite shown in Figure 2-3(a), decomposes to fresh bainite during non-isothermal tempering, as shown in Figure 2-3(b); thereby confirming that the peak observed in Figure 2-2(b) corresponds to austenite decomposition in a bainitic structure. This finding is also in agreement with those reported by Morra (Morra, Böttger et Mittemeijer, 2001). With an increase of the cooling rate to 0.3 °C/s, martensite forms alongside the bainite as shown in Figure 2-3(c).

After tempering of the mixed microstructure, carbides were observed in the martensitic region while bainitic sheaves became wider. In order to better illustrate the microstructural changes, SEM analysis was carried out at higher magnifications and examples are shown in Figure 2-3(d) for the bainitic zones and Figure 2-3(e) for the martensitic zones. It is interesting to note that, while dilatometric curve of tempered bainite did not show precipitation of carbides, they are clearly present in the tempered condition. One possibility could be that carbide coarsening has occurred during non-isothermal tempering. However, in order to confirm this finding, further work is required that is out of the scope of the present investigation.

Finally, SEM micrographs of Figure 2-3 (f) and (g) confirm that by increasing the cooling rate to 3 °C/s, martensite is the only phase present in the microstructure. Upon heating up to 600 °C martensite plates grow and carbides are formed within them. The above behavior was also detected in the dilatometric curves and is in agreement with observations in the literature (Liu et al., 2016; Morra, Böttger et Mittemeijer, 2001).

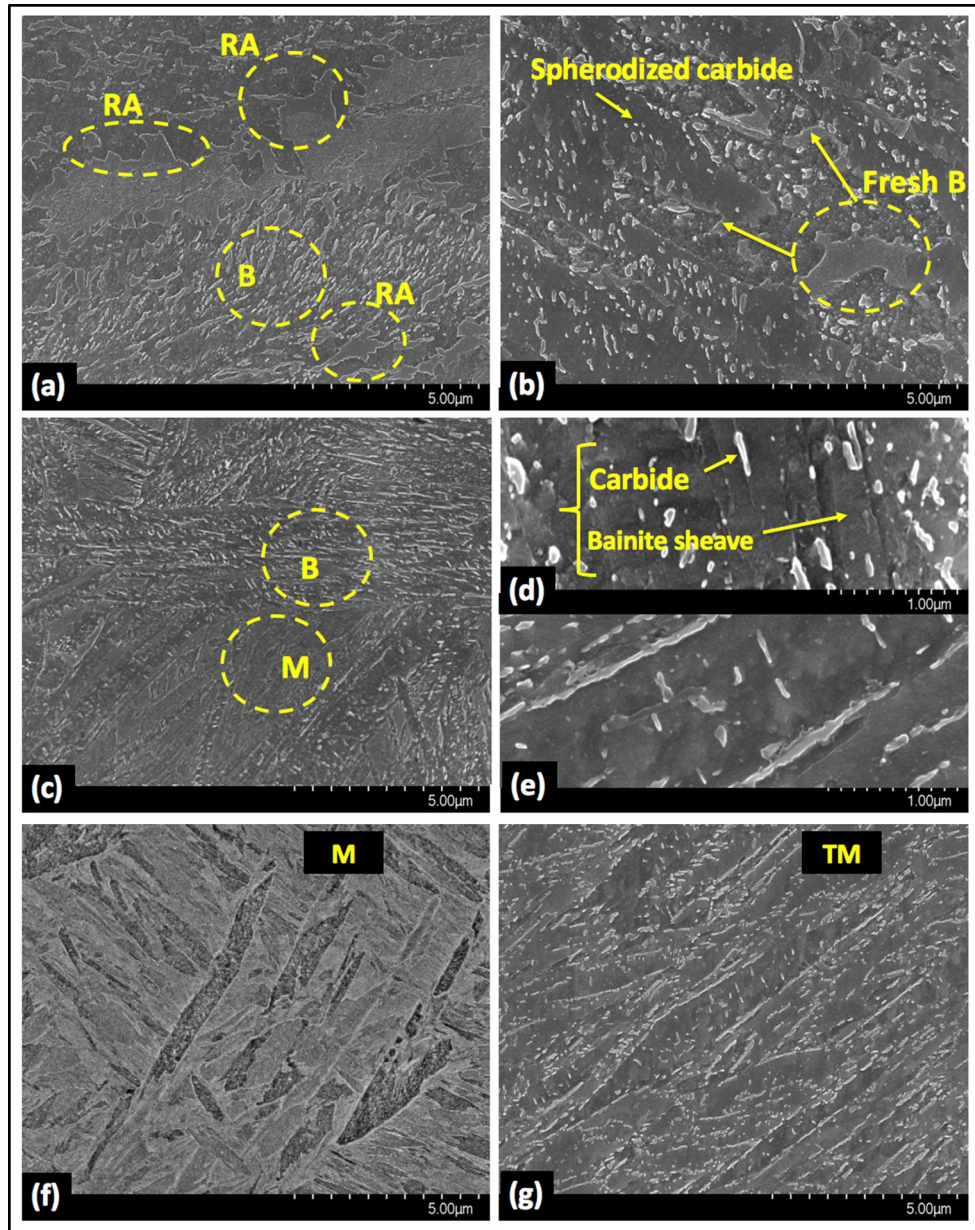


Figure 2-3. Microstructure of different samples: (a) bainite plus retained austenite (RA) after cooling rate of 0.08 °C/s (b) tempered bainite, (c) bainite plus martensite after cooling rate of 0.3 °C/s (d) sheaves of tempered bainite and carbides between them, (e) plate of tempered martensite with carbides inside, (f) full martensite after cooling rate of 3 °C/s, and (g) tempered martensite.

2.4 Summary

Dilatometry tests were carried out on three microstructures representing different regions of a large slab of a medium carbon low alloy steel. Clear differences were observed in the dilatometric behaviors as a function of the starting microstructure. While all the four stages of phase transformation can be seen during tempering of martensite, just retained austenite decomposition was observed during tempering of bainite. This variation in tempering behavior affects the length change for mixed microstructure indicating that length changes due to tempering phenomena are dependent on the starting microstructure.

CHAPTER 3

IN SITU STUDY OF PHASE TRANSFORMATION DURING NON-ISOTHERMAL TEMPERING OF BAINITIC AND MARTENSITIC MICROSTRUCTURES

S. Hesamodin Talebi ¹, Hadi Ghasemi-Nanesa ¹, Mohammad Jahazi ¹ and Haikouhi Melkonyan ²

¹ Département de Génie Mécanique, École de Technologie Supérieure, Montréal, QC H3C 1K3, Canada;

² Finkl Steel Inc., 100 McCarthy, Saint-Joseph-de-Sorel, QC J3R 3M8, Canada;

This article has been published in the Journal of Metals, vol. 7 (2017), p.346.
DOI: 10.3390/met7090346 (Published: 4 September 2017)

Abstract

Phase transformations during non-isothermal tempering of bainitic or martensitic microstructures obtained after quenching of a medium-carbon low-alloy steel was studied. The microstructures correspond to different locations of an as-quenched large-sized forged ingot used as a die material in the automotive industry. High-resolution dilatometry experiments were conducted to simulate the heat treatment process, as well as to investigate different phenomena occurring during non-isothermal tempering. The microstructures were characterized using optical and scanning electron microscopy. Dilatometry analyses demonstrated that tempering behavior varied significantly from bainitic to martensitic microstructures. Retained austenite, which exists between bainitic ferrite sheaves, decomposes to lower bainite causing a remarkable volume increase. It was found that this decomposition finishes below 386 °C. By contrast, martensite tempering was accompanied with a volume decrease due to the decomposition of medium-carbon martensite to low carbon martensite and carbides.

3.1 Introduction

Automotive industries' high demands for large size plastic components, such as bumpers and dashboards, have resulted in the production of ever larger-sized die steels. Consistent and uniform mechanical properties throughout the volume of the die material are required by industry (Firrao et al., 2013). The die materials are generally made of medium-carbon low-alloy steels and their manufacturing process consists of ingot casting, open die forging, quenching, tempering, and final machining (Firrao et al., 2007; Firrao et al., 2013). The heat treatment usually includes austenitizing in the 840–880 °C temperature range, quenching and double-tempering between 550 °C and 600 °C.

The as-quenched microstructure is comprised of bainite, martensite, plus some retained austenite (Biss et Cryderman, 1971; Chentouf et al., 2014; Morra, Böttger et Mittemeijer, 2001). The transformation of austenite to bainite and martensite during quenching is dependent on the cooling rate, chemical composition of the steel and prior austenite grain size and can be predicted by continuous cooling transformation (CCT) diagrams diagrams (Chentouf et al., 2014; Gojić, Sućeska et Rajić, 2004; Rodrigues, Pereloma et Santos, 2000). The as-quenched microstructure will then rely on the mutual influences of the above factors. However, due to the large size of the forged block, significant temperature variations are generated between the surface and the center during quenching. Therefore, as it is difficult to improve the quenched microstructure, the material properties are optimized by modification of tempering parameters (Yan et al., 2017). Hence, systematic study of phase transformations and microstructure evolution of the die steel during non-isothermal tempering is highly desired.

Phase transformation during non-isothermal tempering with a constant heating rate can be divided into the following stages:

Stage 1 (occurring below 80 °C): The stress fields of dislocations, lattice defects, and cell walls in the martensite, particularly interstitial lattice sites close to these defects provide

lower energy sites for carbon. Stage 1 of tempering consists of segregation of carbon atoms to these lower energy sites and pre-precipitation clustering in the iron matrix (Cheng et al., 1988; Miller, Beaven et Smith, 1981; Morra, Böttger et Mittemeijer, 2001; Nagakura et al., 1983; Primig et Leitner, 2011; Speich et Leslie, 1972).

Stage 2 (100–200 °C): In steels containing more than 0.2 wt.% C, at temperatures between 100 °C and 200 °C, ϵ -carbide is the first carbide precipitating in the matrix. Some authors also reported η -carbide formation in low carbon steel at this temperature range (Olson et Cohen, 1983; Speich et Leslie, 1972; Taylor et al., 1989).

Stage 3 (200–350 °C): Retained austenite, if present, decomposes at tempering temperatures of 200 °C to 350 °C. The behavior of retained austenite during tempering significantly varies as a function of steel composition. It generally consists of transformation into ferrite and cementite (Fe_3C) (Cheng et al., 1988; Mittemeher et al., 1988; Morra, Böttger et Mittemeijer, 2001; Primig et Leitner, 2011). However, transformation into lower bainite has been reported by Yan et al. (Yan et al., 2017). Additionally, Podder and Bhadeshia's investigations on retained austenite in bainitic steels revealed that retained austenite transformed into martensite in the cooling process after tempering (Saha Podder et Bhadeshia, 2010).

Stage 4 (250–450 °C): This stage commonly referred to as the final stage of tempering consists in the transformation of the metastable ϵ -carbide to cementite in the temperature range of 250 °C to 450 °C. The preliminary morphology of cementite is needle-like which nucleates from martensite lath boundaries or ferrite grain boundaries. This phase transformation causes a remarkable length decrease and can be clearly detected during the dilatometry test (Cheng et al., 1988; Ghasemi Nanesa et Jahazi, 2015; Morra, Böttger et Mittemeijer, 2001; Primig et Leitner, 2011).

It is worth mentioning that the above temperature ranges are approximate values and can differ depending on steel composition, microstructure and heating rate (Cheng et al., 1988; Morra, Böttger et Mittemeijer, 2001; Nagakura et al., 1983; Primig et Leitner, 2011; Speich

et Leslie, 1972). Time temperature transformation diagrams (TTT) are also used to determine the phase transformation of quenching and tempering process in non-equilibrium conditions but they are not capable to predict different stages during non-isothermal tempering either retained austenite decomposition. Despite many research studies dealing with martensitic phase transformation during tempering (Cheng et al., 1988; Jung, Lee et Lee, 2009; Leiva et al., 2009; Miller, Beaven et Smith, 1981; Mittemeher et al., 1988; Nagakura et al., 1983; Olson et Cohen, 1983; Primig et Leitner, 2011; Saha Podder et Bhadeshia, 2010; Speich et Leslie, 1972; Taylor et al., 1989), little data is available on the evolution of bainitic microstructure during tempering of medium-carbon low alloy steels particularly, during non-isothermal heating (Peet et al., 2017). The present study seeks to contribute to this aspect by considering phase transformation in a bainitic microstructure during non-isothermal tempering with different heating rates and provides a clear understanding of different phase transformations including retained austenite decomposition during tempering of bainite. For comparison purposes, a martensitic microstructure of the same steel is taken as reference. A combination of high-resolution dilatometry and microstructure observations were used to carry out this investigation. The obtained results are critically analyzed in terms of the evolution of carbon concentration of primary microstructure and correlated with microstructural features as a result of phase transformation.

3.2 Materials and Methods

The chemical composition of the steel used in the investigation was (wt.%) C 0.35–V 0.15–Mn 0.99–Si 0.41–Ni 0.5–Cr 1.86–Mo 0.53–Cu 0.16. The material, provided by Finkl Steel Inc. (Sorel, QC, Canada) was from an as-forged block with initial dimensions of 6000 mm × 1200 mm × 800 mm. From the as-received steel, samples were cut into 10 mm length and 4 mm diameter cylinders. Figure 3-1 shows the microstructure of the as-received steel consisting in bainite and 12.1% of retained austenite.

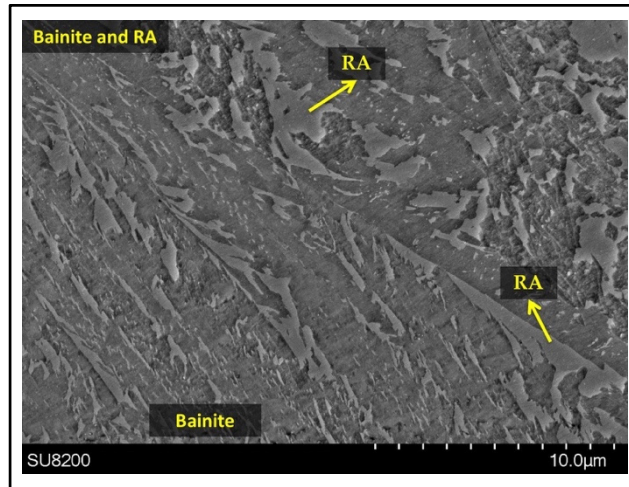


Figure 3-1 SEM image illustrating as-received microstructure composed of bainite and retained austenite (RA).

A high-resolution TA DIL 805A/D dilatometer (TA instruments, New Castle, DE, USA) with a 50-nm resolution was used to perform the heat treatment process and the dilatometry tests. Primarily, the specimens were austenitized at 870 °C for 10 min under vacuum, followed by cooling to room temperature with cooling rates of 4.8 and 180 °C/min in order to reach bainitic and a fully martensitic microstructure, respectively. To determine the optimum cooling rates, several tests using cooling rates from 2.5 °C/min to 1800 °C/min were initially carried out. Figure 3-2 illustrates the as-cooled martensite with M_s (Martensite start temperature) of 316 °C and bainite with B_s (Bainite start temperature) of 472 °C containing less than 5% and 23.2% of retained austenite, respectively. All the retained austenite measurements were carried out according to ASTM E975.

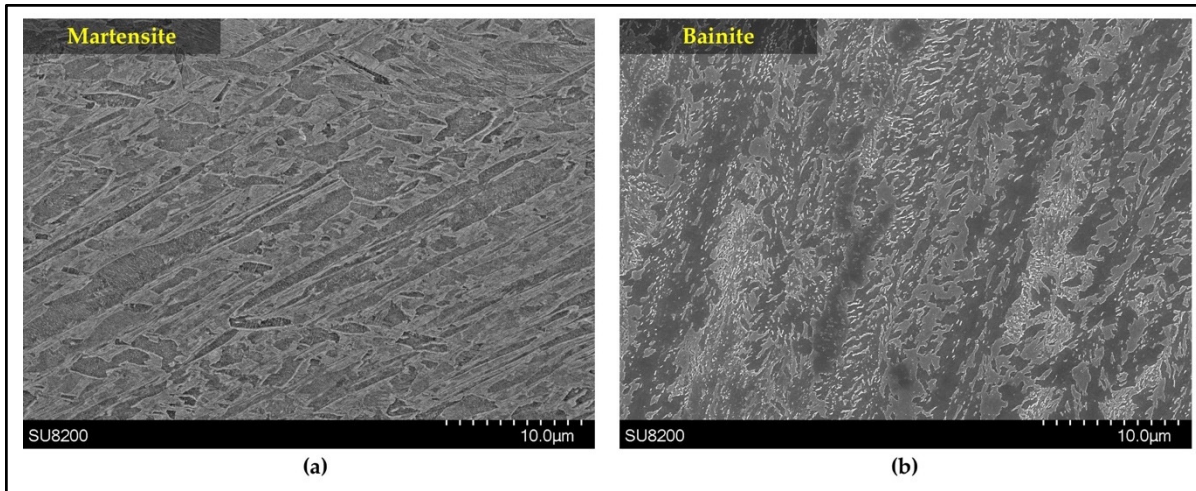


Figure 3-2 As-cooled microstructures obtained for different cooling rates: (a) Martensitic microstructure, 180 °C/min and (b) bainitic microstructure, 4.8 °C/min.

Subsequently, non-isothermal tempering up to 600 °C with heating rates of 5 and 30 °C/min were performed immediately after cooling to avoid possible segregation due to room temperature aging. To avoid any oxidation and decarburization, the non-isothermal tempering was conducted in the vacuum environment. After non-isothermal tempering, the samples were cooled down with a cooling rate of 600 °C/min. The relevant etchant was Vilella solution and Hitachi-SU8200 field emission gun SEM (scanning electron microscope; Hitachi, Tokyo, Japan) was used for microstructural studies. X-ray diffraction (XRD) with Co K α radiation in standard θ -2 θ mode was performed for phase identification using a Bruker Discover D8-2D diffractometer (Bruker, Madison, WI, USA). All the peaks' positions recorded by XRD were identified with the powder diffraction files (PDF) of the International Centre for Diffraction Data (ICDD) using the software Diffrac.Eva (version 4.0, Bruker AXS, Karlsruhe, Germany). Further analysis of the dilatometry results, using the first derivative of the dilatometry data, allowed for a more precise determination of the different stages of tempering. MIP image analysis software (MIP4, Nahamin Pardazan Asia, Mashhad, Iran) was used for calculating the orientation angle of the carbides within bainitic ferrite subunits.

3.3 Results and Discussion

Figure 3-3(a) and Figure 3-4(a) illustrate the dilatation curves versus temperature during non-isothermal tempering related to the bainitic and martensitic specimens and Figure 3-3b and Figure 3-4b their corresponding first derivatives. Where ΔL and L_0 are the length change and initial length of the specimen, respectively. In the following sections, dilatometry results are analyzed for each of the four stages of tempering according to the temperature range suggested for each stage.

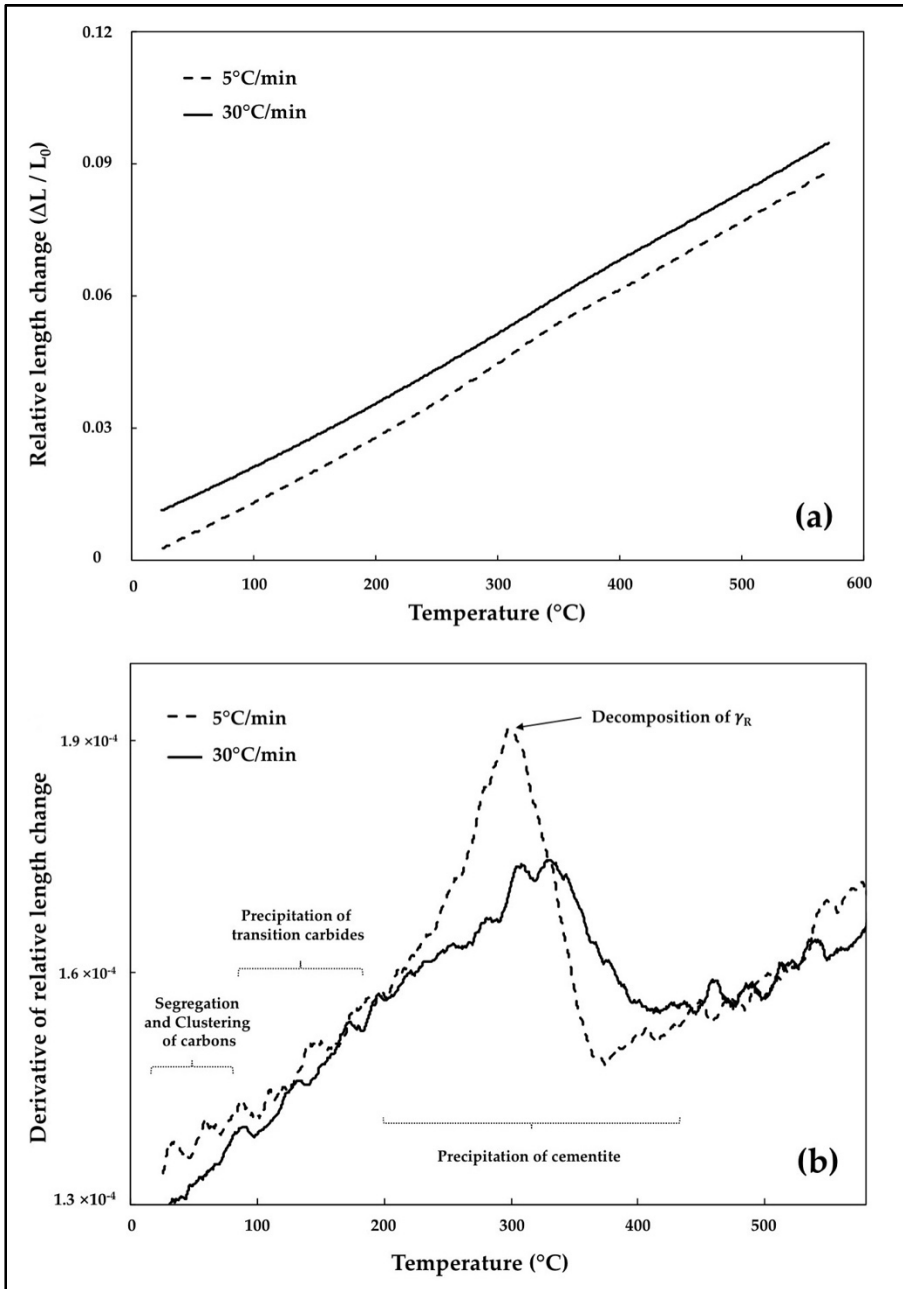


Figure 3-3(a) Relative length change diagram during non-isothermal tempering of bainitic specimen at heating rates of 5 °C/min and 30 °C/min, and (b) the first derivative curve of the relative length change corresponding to these heating rates.

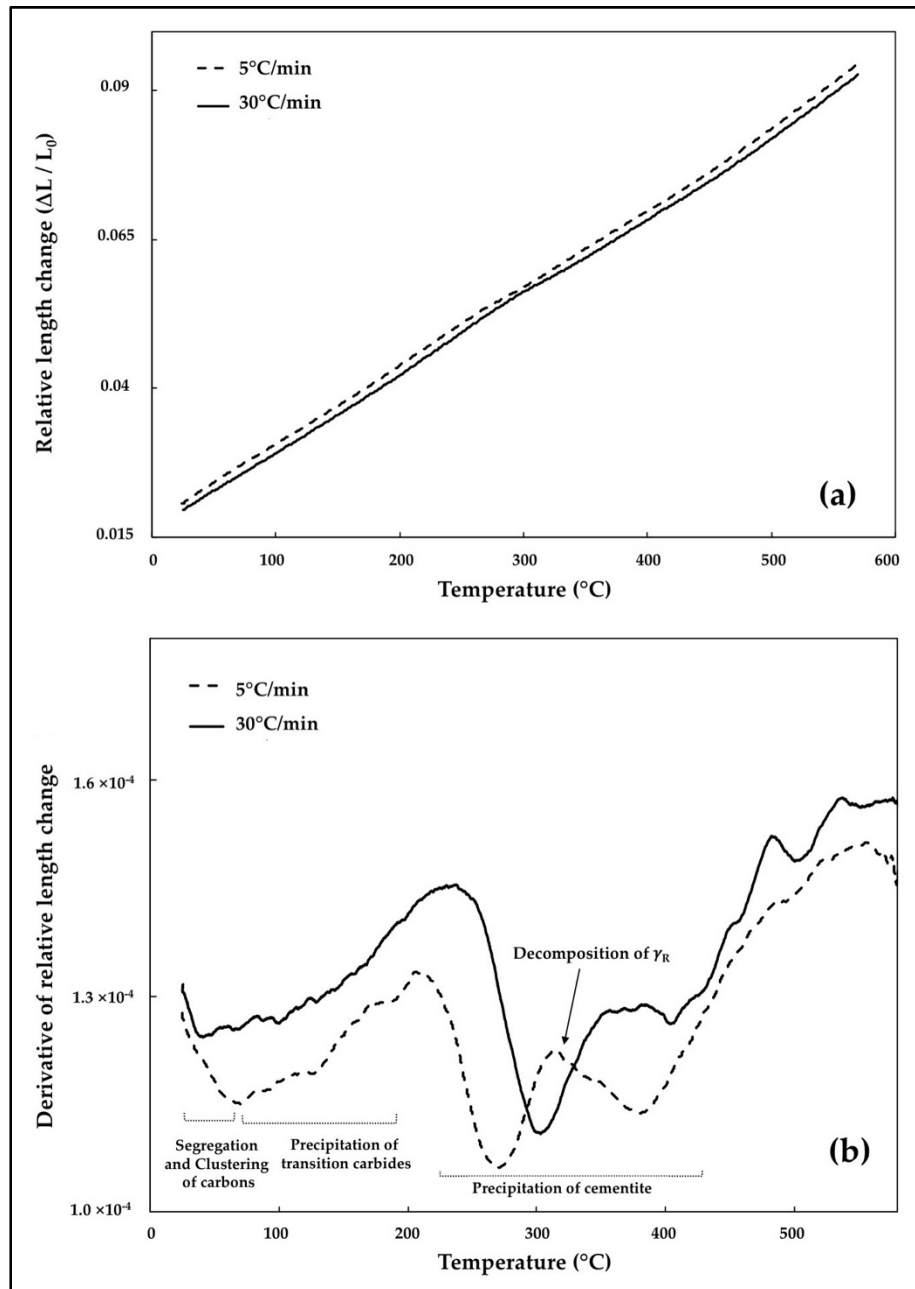


Figure 3-4 (a) Relative length change diagram during non-isothermal tempering of the martensitic specimen at the heating rates of 5 $^{\circ}\text{C}/\text{min}$ and 30 $^{\circ}\text{C}/\text{min}$, and (b) the first derivative curve of relative length change corresponding to these heating rates.

3.3.1 Segregation and Clustering of Carbon Atoms

The first stage of tempering causes carbon atom redistribution through the BCC (Body Centered Cubic) iron with carbon segregation to the lattice defects and clustering in the matrix (Krauss, 2017). Examination of the derivative curve in Figure 3-3 (b) did not reveal any clear indication of length changes for the two heating rates at temperatures below 80 °C. Therefore, carbon segregation and clustering within the solid solution in bainite, which should be accompanied with contractions, were not detected by dilatometry in this investigation. This could probably be related to the small carbon content of bainitic ferrite as discussed below.

In medium-carbon steels, the carbon content of martensite and bainitic ferrite (before non-isothermal tempering) can be calculated by determining the lattice parameters c and a from (110) and (200) peaks using the following equations (Kang et al., 2009):

$$c = \frac{\lambda}{\sqrt{2} \sin \theta_{[110]}}; a = \frac{\lambda}{\sin \theta_{[200]}} \quad (3.1)$$

where λ is the wavelength of the electron beam. Therefore, the carbon content could be defined according to Equation 3.2 and Equation 3.3 (Kang et al., 2009), where a_0 is the lattice parameter of BCC iron and $a_{0.30}$ is the lattice parameter at exactly 0.30 wt.% C:

$$c = a_0 + (0.020 \pm 0.002)[C] \quad ([C] < 0.56 \text{ wt.}\%, \text{ when } [C] < 0.30 \text{ wt.}\%, c = a) \quad (3.2)$$

$$a = a_{0.30} - (0.014 \pm 0.002)[C] \quad (0.30 \text{ wt.}\% < [C] < 0.56 \text{ wt.}\%). \quad (3.3)$$

Figure 3-5 illustrates XRD patterns obtained from bainitic and martensitic specimens for (110) and (200) peaks. From these peaks, lattice parameters were calculated. The lattice

parameters and their related carbon contents are listed in Table 3-1, where [C]c and [C]a are the carbon contents based on Equation 3.2 and Equation 3.3, respectively. According to these equations the accuracy of carbon content is ± 0.02 wt.%.

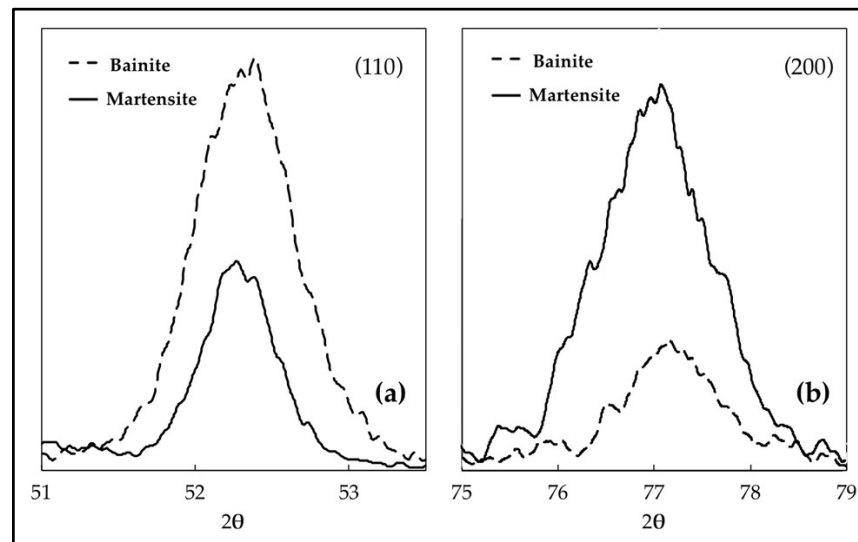


Figure 3-5 Two XRD (X-ray diffraction) peaks of bainite and martensite: (a) (110) peak and (b) (200) peak.

Table 3-1 Lattice parameters and carbon contents of the as-received microstructure, bainitic ferrite, and martensite, before and after non-isothermal tempering with a heating rate of 5 °C/min, determined using X-ray diffraction.

Microstructure	$c(\text{\AA})$	$a(\text{\AA})$	[C]c (wt.%)	[C]a (wt.%)	[C] (wt.%)
As-received (Bainite)	2.8712	2.8668	0.24	0.30	0.26
Bainite	2.8718	2.8650	0.26	0.11	0.19
Tempered Bainite (5 °C/min)	2.8713	2.8634	0.24	0.22	0.23
Martensite	2.8724	2.8702	0.30	0.27	0.29
Tempered Martensite (5 °C/min)	2.8708	2.8689	0.21	0.17	0.19

The calculated carbon content for bainitic ferrite is 0.19 wt.% before tempering and 0.23 wt.% after tempering while, in martensite, this amount before and after non-isothermal tempering is 0.29 wt.% and 0.19 wt.%, respectively. These results are in agreement with those reported by Bhadeshia et al. (Bhadeshia, 2001) restating that during cooling, most of the available carbon in bainite participated in the formation of cementite particles and a small amount remained in solid solution. The low amount of carbon probably is not enough to show detectable contraction when segregation and clustering take place.

In contrast with the bainitic case, a significant contraction of martensite occurred immediately after starting the tempering (Figure 3-4). This behavior clearly indicates the occurrence of carbon segregation and clustering below the 80 °C temperature range in a martensitic microstructure. The higher concentration of carbon in martensite, compared to bainite, is probably the main cause for such observation and detection of the contraction by the high-resolution dilatometer during this stage of tempering.

3.3.2 Precipitation of the ϵ/η Transition Carbides

The high-resolution dilatometry results presented above (Figure 3-3), do not demonstrate any length decrement corresponding to ϵ -carbide precipitation during tempering of bainite. The amount of carbides in bainite and, therefore, carbon content of supersaturated bainitic ferrite, depends on steel composition, for instance, high silicon content delays carbide precipitation and leads to supersaturated bainitic ferrite (Caballero et al., 2007). The ϵ -carbide precipitation during tempering of bainite has been reported by Caballero et al. for a steel containing 1.46 wt.% Si using atom probe field ion microscopy (Caballero et al., 2008). However, in the present case, the bainitic ferrite of the investigated steel is not supersaturated in carbon (0.19 wt.% C) and, therefore, the precipitation of transition carbides is not expected. Speich (Speich et Leslie, 1972) reported that during the bainitic reaction there is a brief period for carbon redistribution and carbide precipitation called auto-tempering. Thus, the precipitation of transition carbides could presumably occur in the present steel during the formation of bainite and auto-tempering.

Contrary to tempered bainite, this stage is observed during tempering of martensite (Figure 3-4) because of the higher carbon amount (0.29 wt.% C) in martensite. As reported in Figure 3-4, the start of phase transformation (length reduction) corresponding to the transition carbides overlap with the preceding phase transformation. It can also be seen that, when the higher heating rate of 30 °C/min is applied, the finish temperature is increased by 47 °C, reaching 217 °C. Jack (Jack, 1951) and Nakamura et al.'s (Nakamura et Nagakura, 1986) characterizations of the transition carbides demonstrated that tempering of martensite leads to the precipitation of ϵ and η transition carbides in the primarily martensitic phase.

3.3.3 Retained Austenite Decomposition

The decomposition of retained austenite occurs with an increase in length. Based on XRD measurements, the bainitic specimen contains 23.2% of retained austenite. Dilatometry results revealed a broad peak related to the decomposition of retained austenite that spans from 255 °C to approximately 355 °C for the heating rate of 5 °C/min. For the martensitic structure, this peak falls completely within the cementite precipitation zone and occurs in the range of 269 °C to 401 °C. It is worth noting that the XRD patterns did not show any austenite peaks in the martensitic sample, indicating the absence or a presence of less than 5% (detection limit of XRD) of retained austenite. Comparison between Figure 3-3 and Figure 3-4 shows a clear shift of the decomposition peaks to higher temperatures, respectively 21 °C and 31 °C for bainite and martensite.

Table 3-2 summarizes the temperature range and relative length changes corresponding to the high and low heating rates. The degree of relative length increase is associated with the cooling rate and retained austenite percentage. These relative length changes during non-isothermal tempering are determined near the inflection points of dilatometry curves using Equation 3.4 (Leiva et al., 2009):

$$\text{Relative length change} = \frac{(\Delta l(T)/l)_{\text{end}} - (\Delta l(T)/l)_0}{(\Delta l(T)/l)_0} \quad (3.4)$$

where $(\Delta l(T)/l)_{\text{end}}$ and $(\Delta l(T)/l)_0$ are the increase for relative length of the end and start points at temperature T , as it is represented schematically in Figure 3-6.

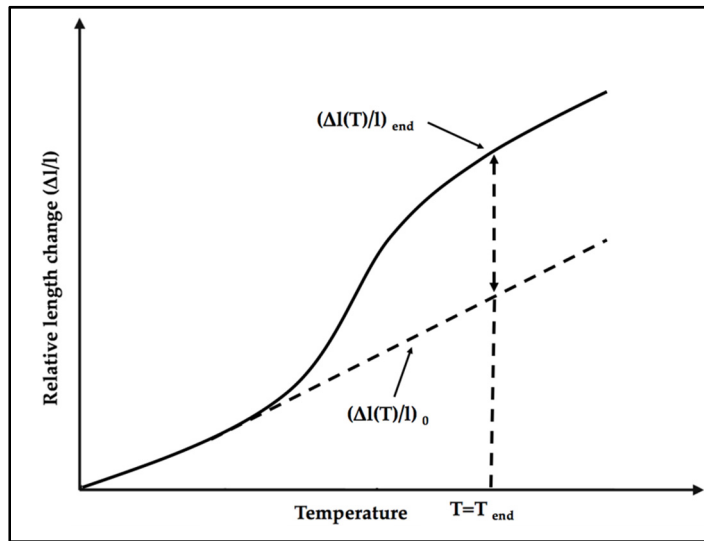


Figure 3-6 Relative length variations near the inflection point.

It can be seen from the data that the extent of decomposed retained austenite is associated with the heating rate. The relative volume increase corresponding to the bainitic specimen is 3.74% and 2.21% after non-isothermal tempering at the heating rate of 5 °C/min and 30 °C/min, respectively. On the other hand, the relative volume change is approximately constant in the martensitic specimen for both heating rates. These results point out that since the bainitic specimen contains a large amount of retained austenite, the portion of decomposed retained austenite has been influenced by the heating rate; therefore, after tempering at the heating rate of 30 °C/min still some non-decomposed retained austenite remains in the microstructure. In contrast, because the amount of retained austenite is very low in the martensitic structure, decomposition is almost finished even at the heating rate of 30 °C/min and no impact is observed on the relative length change value.

Table 3-2 Temperature interval of retained austenite decomposition and percentage of relative length change for maximum and minimum heating rates in both investigated microstructure.

Specimen	Heating Rate (°C/min)	Temperature Range (°C)	Relative Length Change (%)
Bainite	5	255–359	+3.74
	30	276–386	+2.21
Martensite	5	269–370	+0.67
	30	300–401	+0.63

3.3.4 Cementite Precipitation

The shape of the peak at temperature range related to the cementite precipitation varies with the microstructure. In Figure 3-3, there is no contraction between about 250 °C and 450 °C. Therefore, cementite precipitation was not observed for bainite. On the other hand, at the same temperature range, an intense contraction was observed in martensite associated with cementite precipitation (Figure 3-4). This phenomenon overlapped with retained austenite decomposition peak.

Good agreement was found with XRD results presented in Figure 3-7 and Figure 3-8. In Figure 3-7, the presence of chromium carbide (Cr_7C_3) and some retained austenite are demonstrated in the bainite. Upon non-isothermal tempering at a heating rate of 5 °C/min, Fe_3C and Cr_7C_3 carbides precipitate as a consequence of retained austenite decomposition.

In the case of martensite (Figure 3-8), no carbides can be seen in martensite, whereas the presence of carbides in tempered martensite is evidence of a large dilatation decrease during non-isothermal tempering depicted in Figure 3-4 (b). The peak related to cementite is seen

after tempering for both specimens, since cementite phase is detectable by XRD, 5% or more cementite exists in tempered steels. These Fe_3C carbides, dissolve upon tempering to form Cr_7C_3 carbides at the same location (Dépinoy et al., 2017).

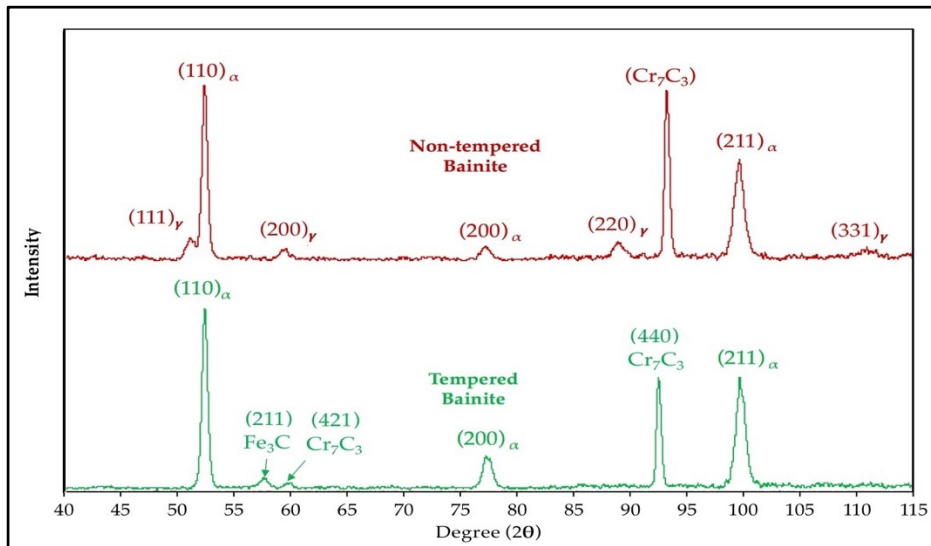


Figure 3-7 XRD spectra of bainite and non-isothermal tempered bainite at heating rate of 5 °C/min.

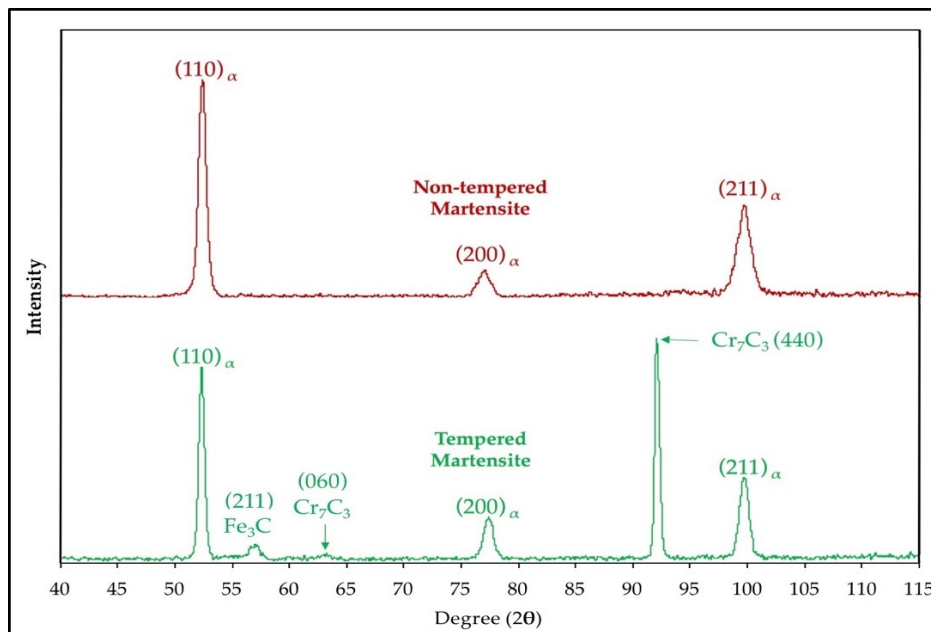


Figure 3-8 XRD spectra of martensite and non-isothermal tempered martensite at heating rate of 5 °C/min.

As discussed earlier, in bainite, the bainitic ferrite contains 0.19 wt.% of carbon. Since there is a small amount of carbon in solid solution, the cementite precipitation during non-isothermal tempering is negligible (Bhadeshia, 2001). By contrast, in supersaturated martensite with 0.29 wt.% of carbon, this phase transformation takes place upon tempering between about 210 °C and 480 °C with a considerable length decrease. Similar observation for cementite precipitation in martensite was reported by Morra et al. (Morra, Böttger et Mittemeijer, 2001). The gradual shift of the transformation temperature to the higher values with increasing the heating rates is due to the time and temperature dependency of carbon diffusion into lattice defects.

It is also worth noting that after completing this non-isothermal tempering and cooling to the ambient temperature, final relative length, calculated by Equation 3.4 dropped by 0.65% in the martensitic sample after tempering, whereas by contrast, it rises by 0.44% in the bainitic specimen.

Analyses of cooling cycles after each non-isothermal tempering are represented in Figure 3-9 to investigate the formation of new phases during cooling. In Figure 3-9 (a), it can be seen that the first derivation of the relative length change is almost constant during cooling. The pattern is similar for the other three cooling cycles. Thus, it can be concluded that no new phase transformation occurred during the fast cooling after non-isothermal tempering.

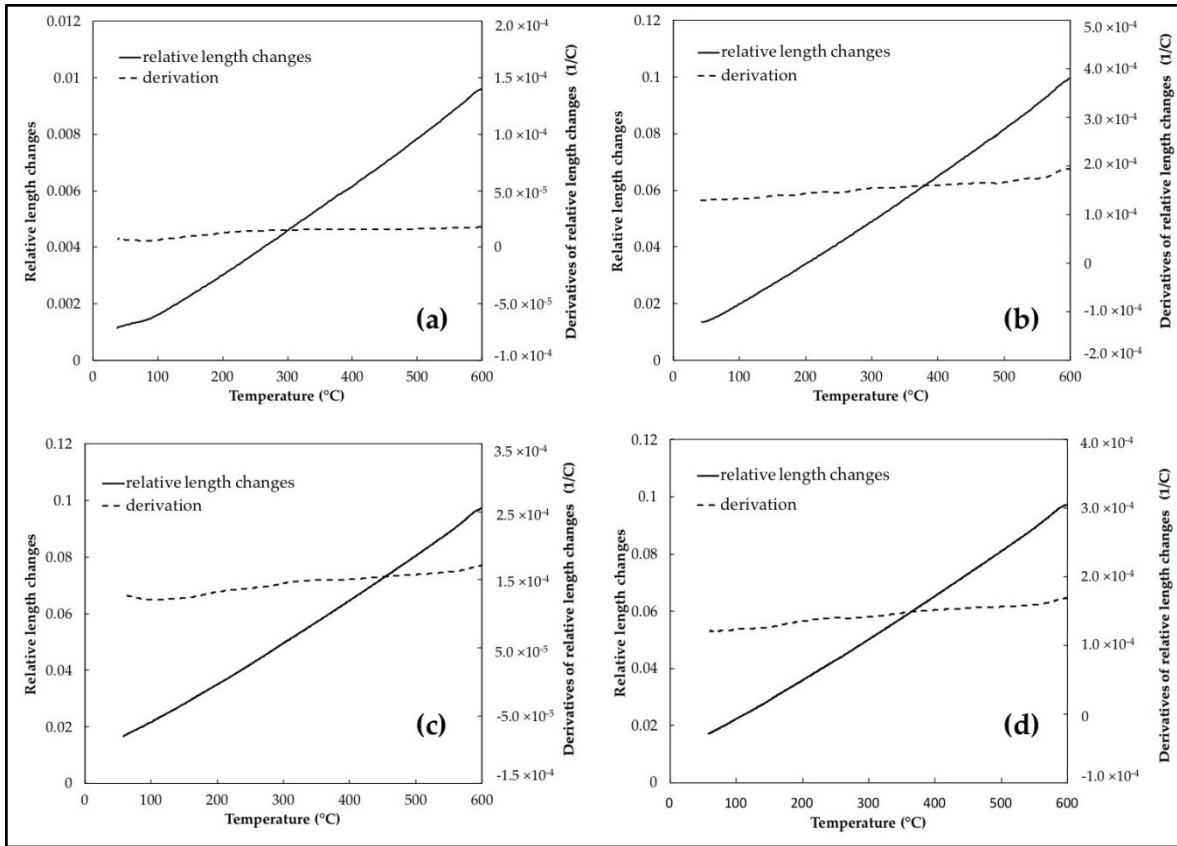


Figure 3-9 Relative length change and its derivation during the cooling cycle (from 600 °C to ambient temperature at a cooling rate of 600 °C/min) after tempering of: (a) The bainitic specimen non-isothermally tempered at a heating rate of 5 °C/min; (b) the bainitic specimen non-isothermally tempered at a heating rate of 30 °C/min; (c) the martensitic specimen non-isothermally tempered at a heating rate of 5 °C/min and (d) the martensitic specimen non-isothermally tempered at a heating rate of 30 °C/min.

3.3.5 Microstructural Evolution during Tempering

In order to study the detailed morphology after tempering, SEM observation was performed for both martensitic and bainitic specimens, before and after non-isothermal tempering. Figure 3-10 (a) shows SEM images of tempered bainite after heating at the rate of 5 °C/min. Examination of the microstructure before tempering revealed the presence of several retained austenite islands with blocky morphologies at the grain boundaries of the bainitic ferrites and are characterized by a smooth surface under SEM (Figure 3-10 (b)). As discussed in Section 3.3, these retained austenite islands decompose in the range of 255 °C to 355 °C and as

reported in Figure 3-10 (c), their smooth surface becomes roughened with the presence of very fine carbides distributed regularly over the surface. According to Yan et al. (Yan et al., 2017), the decomposition of retained austenite may lead to the formation of martensite or lower bainite depending on the applied temperature and holding time during tempering.

In Figure 3-10 (c), the small carbides ordered in parallel bands among bainitic ferrite subunits were observed at the grain boundaries of bainitic ferrite. The axes of these carbides were inclined between 53° and 62° to the growth direction of the bainitic ferrite. It has been reported that the angle between carbides in the lower bainite ferrite inclines at about 60° to the growth direction of ferrite, which is very close to the angles measured in the present investigation (Shimizu, Ko et Nishiyama, 1964). It should also be noted that in agreement with reported results in the literature, the morphology of decomposed retained austenite blocks is very similar to that of lower bainite (Porter, Easterling et Sherif, 2009). On the basis of the above analysis, it can, therefore, reasonably said that the decomposition of retained austenite results in the formation of lower bainite in the investigated steel.

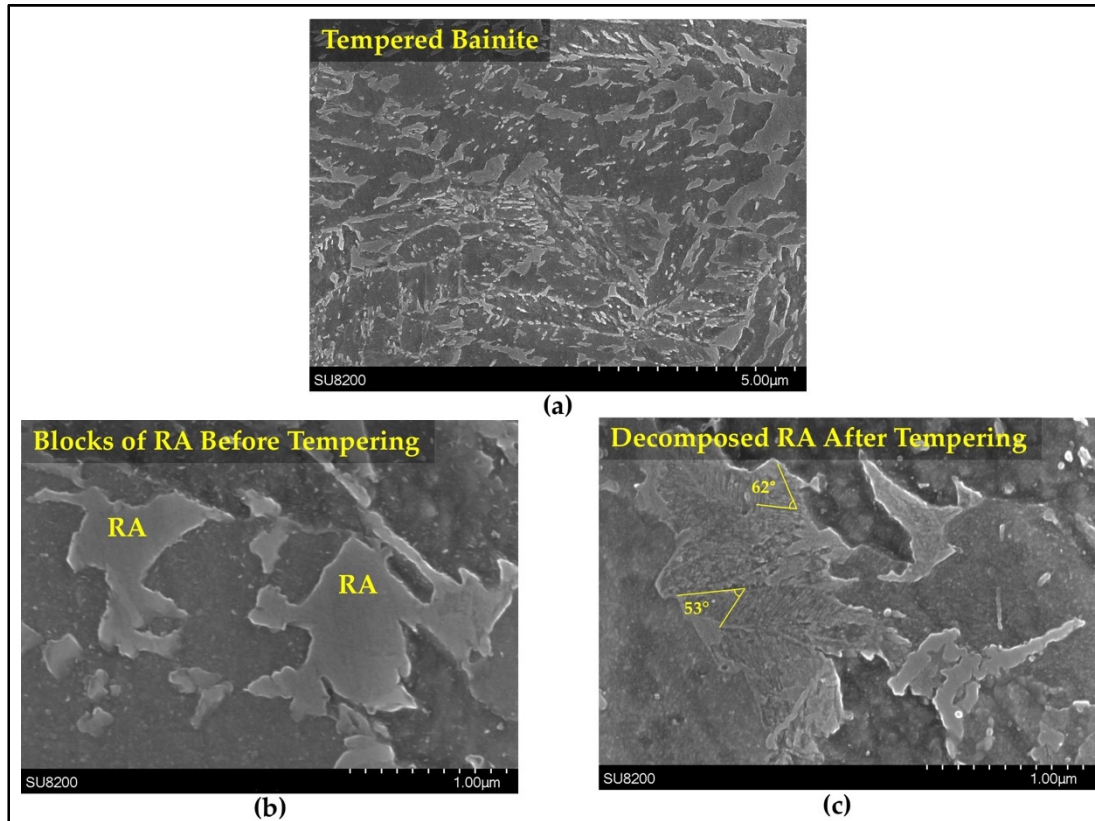


Figure 3-10 SEM images of microstructure evolution in the bainitic sample during non-isothermal tempering at heating rate of 5 °C/min: (a) The microstructure after tempering; (b) blocks of retained austenite (RA) prior to tempering and (c) blocks of decomposed retained austenite after tempering.

The tempered martensitic and bainitic microstructures at heating rates of 30 °C/min are illustrated in Figure 3-11. Figure 3-11 (a) shows that the microstructure of tempered martensite consists in martensite plates with fine needle-like carbides, composed of cementite and chromium carbide, within the plates. Analyses of tempered bainite (Figure 3-11 (b)), shows the presence of coarse rod-shape carbides. This indicates carbide *coarsening* rather than *precipitation* has taken place during non-isothermal tempering of bainite. Since most of carbides have been formed during bainitic transformation; they have, therefore, more time to grow during non-isothermal tempering.

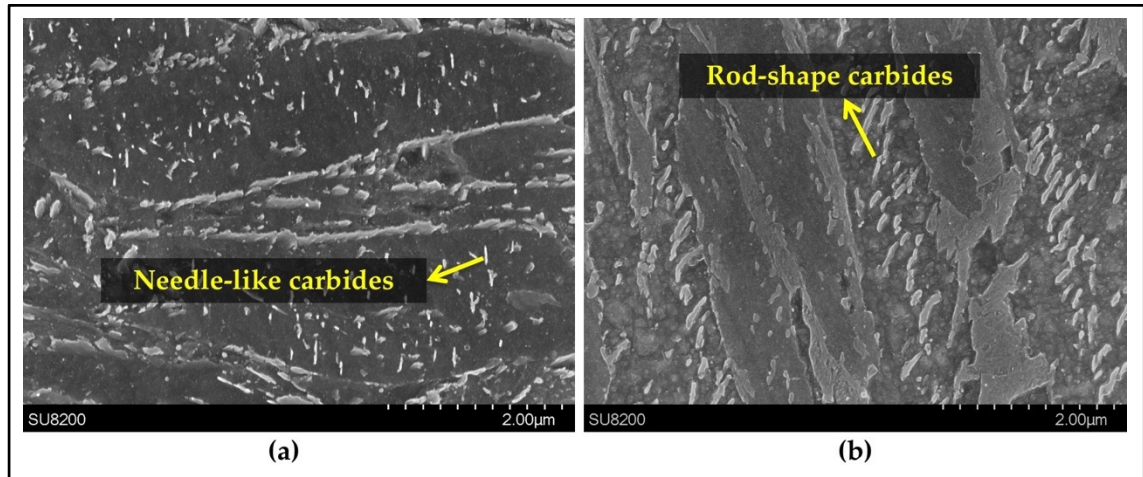


Figure 3-11 SEM images after non-isothermal tempering at heating rate of 30 °C/min: (a) Plates of tempered martensite with fine needle-like carbides within the plate and (b) tempered bainite with coarser rod-shape carbides.

3.4 Conclusions

The non-isothermal tempering behavior of a bainitic microstructure of a medium-carbon high-strength steel was investigated for two different heating rates. A martensitic structure was also used as a reference for comparison purposes. Phase transformations were studied using high-resolution dilatometry and the microstructural features were examined using optical and scanning electron microscopes. The results indicated that tempering effects vary significantly from bainitic to martensitic microstructures helping to draw a clearer picture of the phase transformations in different microstructures. The following conclusions can be drawn from the present study:

- (1) In the bainitic microstructure, retained austenite decomposed to lower bainite associated with volume expansion during tempering in contrast to martensite tempering where great length decrease occurred due to decomposition of medium-carbon martensite to low carbon martensite plus carbides.

(2) Phase transformations during tempering of martensite occurred at slightly higher temperatures than bainite tempering, owing to the auto-tempering effect through bainite formation.

(3) In tempering of the bainitic specimens which contain 23.2% of retained austenite, its decomposition at the heating rate of 5 °C/min caused 3.74% length increase. This percentage decreased steeply to 2.21% when the heating rate increased to 30 °C/min, demonstrating that some amount of retained austenite remained untransformed after non-isothermal tempering at this heating rate, whilst in martensite, the length increase for both heating rates is almost constant indicating completed transformation.

Acknowledgments: The authors are very grateful to Finkl Steel Co. for providing the samples of the present research. The authors would like to appreciate the National Science and Engineering Research Council, Ottawa, ON, Canada for their financial support in the framework of a Collaborative Research and Development project (CRDJP 453683).

CHAPTER 4

RETAINED AUSTENITE DECOMPOSITION AND CARBIDES IDENTIFICATION DURING ISOTHERMAL TEMPERING OF A MEDIUM-CARBON LOW-ALLOY BAINITIC STEEL

S. Hesamodin Talebi ¹, Mohammad Jahazi ¹ and Haikouhi Melkonyan ²

¹ Département de Génie Mécanique, École de Technologie Supérieure, Montréal, QC H3C 1K3, Canada;

² Finkl Steel Inc., 100 McCarthy, Saint-Joseph-de-Sorel, QC J3R 3M8, Canada;

This article has been published in the Journal of Materials, vol. 11 (2018), p.1441.
DOI: 10.3390/ma11081441(Published: 15 August 2018)

Abstract

The effect of isothermal tempering on retained austenite decomposition and carbide precipitation were investigated in a medium-carbon low-alloy bainitic steel. High-resolution dilatometry was used to perform isothermal tempering at 350 °C, 550 °C and 600 °C for different holding times up to 16 h. The decomposition of retained austenite, morphology and composition of carbides were investigated by analyzing the dilatometric curves and were confirmed through scanning and transmission electron microscopy observations. The decomposition behavior of retained austenite varied significantly as a function of the tempering temperature with a full decomposition observed at 600 °C. It was also found that by increasing the tempering temperature from 550 °C to 600 °C, carbides precipitate approximately twice as fast, and evolve from M_3C type to Cr_7C_3 and $Cr_{23}C_6$ after 16 h of tempering at 600 °C.

4.1 Introduction

Medium-carbon, low-alloy steels containing chromium and nickel are used as mold material for the production of plastic components employed in transportation industries (Firrao et al.,

2007; Firrao et al., 2013; Mouritz, 2012). Following ingot casting, these steels undergo open die forging and quench and temper operations to achieve the required sizes and mechanical properties, respectively. In recent years, with the growing industrial demand for ever larger parts, the forged blocks have significantly increased in size. Therefore, during the quench process, significant temperature gradients are produced that result in a variety of microstructures, such as martensite, bainite and retained austenite through the thickness of the large-size block (Chentouf et al., 2014; Loucif et al., 2018). The hard martensitic phase is generally located near the surface region with the proportions of bainite and retained austenite increasing with the thickness (Talebi et al., 2017). Such heterogeneity in the microstructure translates into variable mechanical properties from one location to another of the block and could impact the machinability and service durability of the mold.

The objective of the tempering process is to reduce or eliminate the undesirable retained austenite and improve the ductility of the material by decreasing the carbon supersaturation in the martensitic and bainitic constituents through carbide precipitation (Lyassami et al., 2018; Talebi et al., 2017). Carbon segregation, precipitation of transition carbides, retained austenite decomposition, carbide precipitation and carbide coarsening are the main microstructural changes that take place during the tempering process (Morra, Böttger et Mittemeijer, 2001; Olson et Cohen, 1983; Speich et Leslie, 1972; Taylor et al., 1989).

It is known that during cooling of austenite and formation of bainite, the reaction stops when the carbon content of retained austenite is equal to the composition specified by the T_0 curve, instead of the equilibrium A_3 curve (Bhadeshia, 2001). Therefore, the mixed microstructure composed of carbon-enriched retained austenite and bainite is not stable from a thermodynamic point of view (Bhadeshia, 2001). Accordingly, keeping this microstructure at an elevated temperature for adequate time should result in the decomposition of the retained austenite. The product of retained austenite decomposition, depending on steel composition, can be ferrite and carbides, martensite or bainite, which affect the mechanical properties (Mittemeher et al., 1988; Yan et al., 2017). Therefore, the determination of the kinetics of retained austenite decomposition is of significant practical as well as theoretical importance.

In addition to retained austenite decomposition, the type and size of carbides that precipitate during tempering affect mechanical properties and therefore need to be engineered during the tempering process (Parameswaran, Vijayalakshmi et Raghunathan, 2002; Cheng et al., 1988; Bhadeshia, 1980). Five types of carbides, M_3C , M_2C , M_7C_3 , $M_{23}C_6$ and M_6C , have the potential to precipitate in medium carbon low alloy steels, based on tempering time and temperature (Dépinoy et al., 2017; Hou, Li et Wu, 2012; Mitchell et Ball, 2001; Taneike, Sawada et Abe, 2004). Among them, $M_{23}C_6$ is the equilibrium carbide, M_3C is the stable carbide, M_2C and M_7C_3 are metastable carbides (Dépinoy et al., 2017; Jayan, Khan et Hussain, 2003; Mitchell et Ball, 2001; Thomson et Bhadeshia, 1994).

While tempering of quenched steels has been extensively studied; however, little data is available on isothermal tempering of low-alloy bainitic mold steels, particularly, on the determination of the tempering temperature required for complete retained austenite decomposition, and identification of the types of carbides that can form during tempering of these steels. The present work has been defined in this framework and the objective is to investigate the influence of tempering holding time and temperature on carbon-enriched retained austenite decomposition and the formation of carbides, using a combination of high resolution dilatometry, and scanning and transmission electron microscopies.

4.2 Materials and Methods

The chemical composition of the studied steel is provided in Table 4-1.

Table 4-1 Chemical composition of the investigated steel (wt.%).

C	V	Mn	Si	Ni	Cr	Mo	Cu
0.35	0.15	0.99	0.41	0.50	1.86	0.53	0.16

The original material was an as-forged slab with initial dimensions of 6000 mm × 1200 mm × 800 mm, provided by Finkl Steel Inc. (Sorel, QC, Canada). Initially, a 127 mm diameter

and 177 mm length ‘carrot’ was extracted from a region about 200 mm below the surface (quarter of the thickness). Cylindrical samples of 10 mm length and 4 mm diameter were machined from the ‘carrot’ for dilatometry experiments. All the heat treatment cycles were performed using a high-resolution TA DIL 805A/D dilatometer (TA instruments, New Castle, DE, USA). Prior to the tempering experiments, the bainitic specimens were austenitized by heating them up to 870 °C, held for 10 min for homogenization and then cooled to room temperature with a cooling rate of 4.8 °C/min which produced a microstructure composed of bainite and about 23% of retained austenite. Figure 4-1 shows the primary bainitic microstructure before isothermal tempering. Examination of the microstructure revealed the presence of needle-like carbides, thin films, and blocks of retained austenite at the grain boundaries of the ferritic bainite which are characterized by a smooth surface under SEM (Scanning Electron Microscope). Chemical analysis of the carbides before tempering indicated that they are very rich in Fe with nearly no presence of Cr.

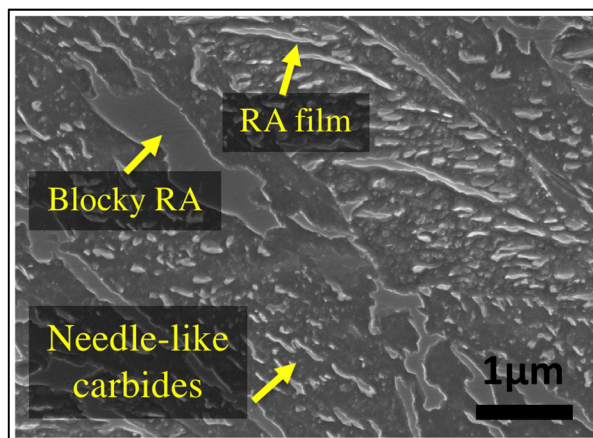


Figure 4-1 Primary microstructure of bainite with retained austenite before tempering.

Isothermal tempering at three temperatures of 350 °C, 550 °C and 600 °C with different holding times up to 16 h were performed immediately after cooling. Samples were heated with a heating rate of 600 °C/min up to isothermal tempering temperature. The fast heating rate was used in order to avoid any effect of heating rate on microstructure change during heating. The tests were performed under vacuum to avoid any oxidation and decarburization.

To study the microstructure, after dilatometry tests, samples were cut, using very thin diamond blades, in the longitudinal direction. They were then prepared through conventional polishing procedures and etched with Vilella solution. Retained austenite measurement was carried out according to ASTM E975 using a Bruker Discover D8-2D diffractometer (Bruker, Madison, WI, USA) with Co K α radiation in standard θ - 2θ mode. A Hitachi-SU8230 Field Emission Gun SEM (FEG-SEM) (Hitachi, Tokyo, Japan) was used to study the microstructures. TEM observations were made by a JEOL JEM-2100F transmission electron microscope (JEOL, Tokyo, Japan) equipped with Selected Area Electron Diffraction Analysis (SAED) operated at 200 kV acceleration voltage on carbon extraction replicas. Average Rockwell C hardness of each sample was measured from 121 tests under loading conditions of 2 kg for 10 s

4.3 Results and Discussion

4.3.1 Retained austenite decomposition

Retained austenite decomposition should be accompanied by a length increase of the sample (Cheng et al., 1988). Curves in Figure 4-2(a), (b) and (c) show the strain changes of dilatation curves versus tempering time for 16 h of isothermal tempering for a bainitic specimen containing 23% of retained austenite at 350 °C, 550 °C and 600 °C, respectively.

For instance, it can be seen in Figure 4-2 (a) that by tempering at 350 °C, strain increased sharply and reached a maximum amount of 0.20% after 0.79h, then slowly decreased without reaching a plateau even after 16h. Podder et al and Yan et al. (Saha Podder et Bhadeshia, 2010; Yan et al., 2017) observed similar behavior in a bainitic structure and related it to the start of the decomposition of retained austenite. Since 350 °C is the lowest temperature for retained austenite decomposition (Talebi et al., 2017), the maximum amount of increase due to retained austenite decomposition is about 0.20%.

However, tempering at higher temperature causes carbide precipitation, which is characterized with a length reduction. This is illustrated in Figure 4-2(b), where at 550 °C a

0.13% of length increase is observed during the first 0.09 h of tempering and after that, the specimen's length decreased until 11.4 h of tempering when it reached its initial length before tempering. During tempering at 600 °C, 0.02% more length increase occurred in comparison with 550 °C, which was followed by around 0.03% length decline until 4.7 h of tempering; afterwards, remarkable length increase was observed (Figure 4-2 (c)). Therefore, the samples tempered at 600 °C and 550 °C show only an increase of 0.15% and 0.13%, respectively. It should be noted that the higher expansion observed during the early stages of tempering at 600 °C indicates that a higher amount of retained austenite has been decomposed at this temperature compared to 550 °C.

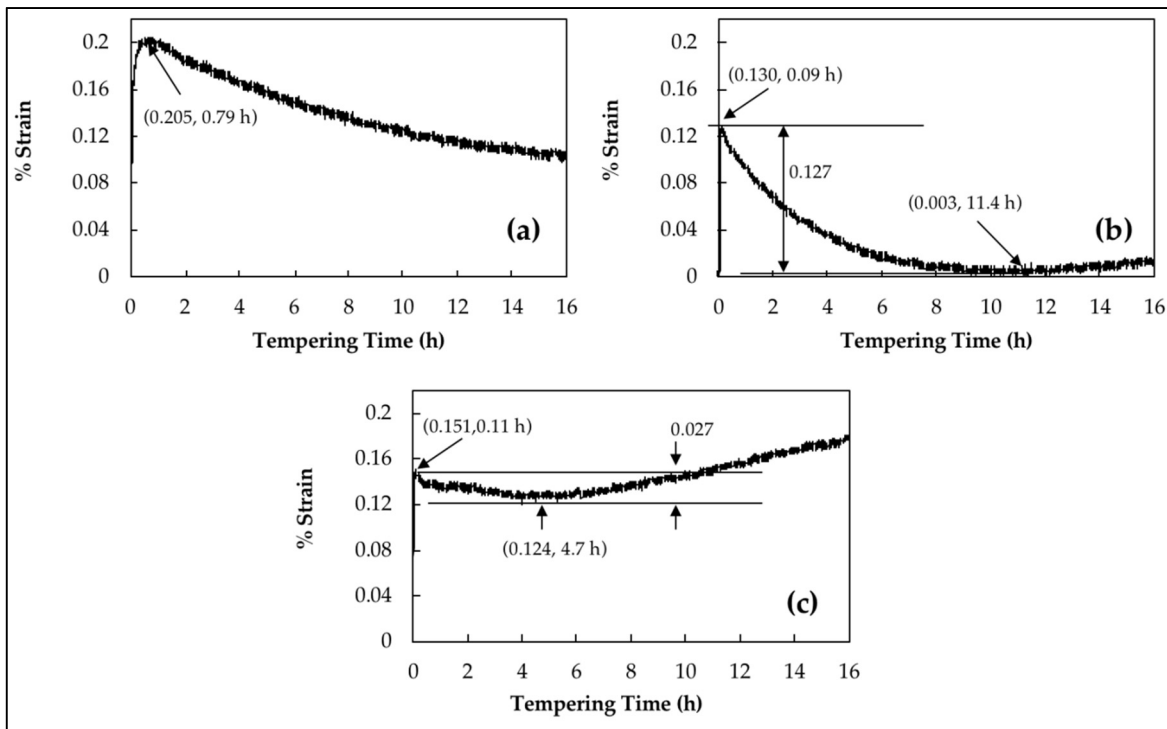


Figure 4-2 Dilatometry curves during isothermal tempering for 16 h at (a) 350 °C, (b) 550 °C, and (c) 600 °C.

The possible presence of retained austenite in the microstructure was investigated using X-ray diffraction (XRD). However, no retained austenite peak was detected. Considering that the minimum detection limit by XRD is 5%, it can be said that the amount of retained

austenite in the tempered microstructure is less than 5%. Subsequently, high-resolution dilatometry, which can reveal the presence of retained austenite at much lower levels and its transformation during the tempering cycle was conducted (Saha Podder et Bhadeshia, 2010; Morra, Böttger et Mittemeijer, 2001).

Retained austenite which remains undecomposed during tempering can be transformed to fresh martensite during cooling to room temperature (Yan et al., 2017). To investigate any possible martensitic transformation during cooling of the investigated steel, samples were cooled with a cooling rate of 600 °C/min. Figure 4-3(a) and (b) illustrate dilatometry curves of cooling after 16 h of tempering at 550 °C and 600 °C, respectively. In Figure 4-3 (a), a transformation point can be seen that starts at 277 °C and finishes at 192 °C. These two points are associated with martensite start (M_s) and finish (M_f) temperatures. Similar martensitic transformations were observed after tempering at 550 °C for 1 h, 4 h, 8 h and 12 h with M_s values of 228 °C, 256 °C, 260 °C and 272 °C, respectively. However, examination of the dilatometry curve at 600 °C, reported in Figure 4-3(b), did not reveal any length changes related to martensitic transformation, indicating that there is very low or no more retained austenite to be transformed into martensite. Therefore, it can be said that isothermal tempering of 16 h at 600 °C has decomposed any detectable retained austenite. The decomposition is characterized on the dilatometry curve by a 0.15% increase in the strain.

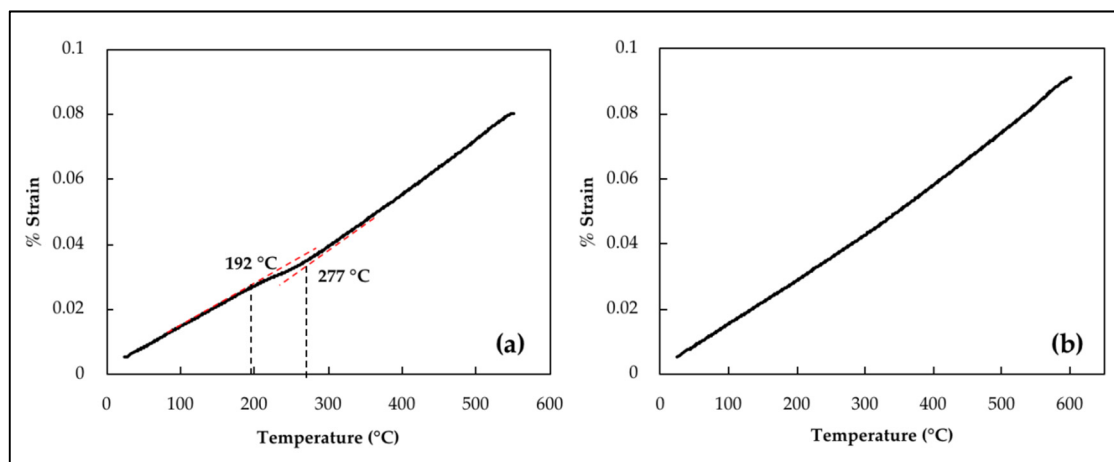


Figure 4-3 dilatometry curves of cooling cycle with cooling rate of 600 °C/min after isothermal tempering for 16 h at (a) 550 °C, and (b) 600 °C.

The carbon content of retained austenite before tempering was determined by XRD from lattice parameter measurements. Figure 4-4 shows the (111) peak of retained austenite. The lattice parameter ($a_0 \gamma$) measured for this austenite is 0.35801nm. The carbon content of the retained austenite was estimated to be 0.24 wt.% based on the following equation (Ridley, Stuart et Zwell, 1969; Ruhl et Cohen, 1969).

$$a_0 \gamma = 3.572 + 0.033(\text{wt. \% C}) \quad (4.1)$$

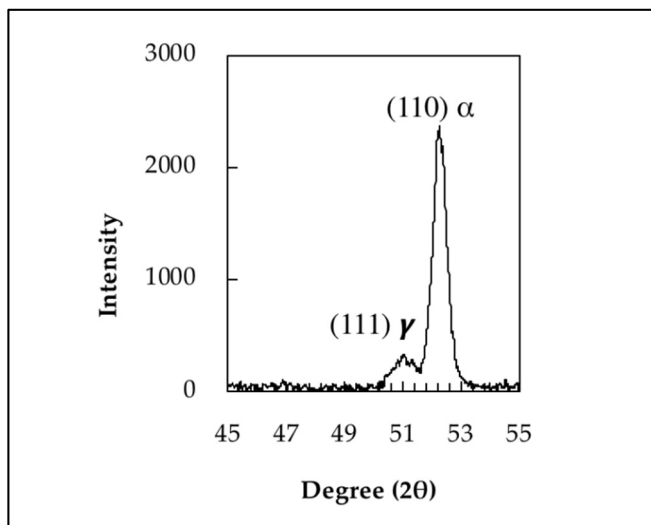


Figure 4-4 XRD (111) peak of retained austenite.

Based on the M_s temperatures determined by the slope change of the cooling curves and using the following equation (Wang et Van Der Zwaag, 2001), the carbon content of retained austenite was calculated after different holding times at 550 °C and the results are reported in Figure 4-5:

$$M_s (K) = 273 + 545.8 \cdot e^{-1.362w_c} \quad (4.2)$$

Where, w_c , represents the weight percentage of carbon in austenite.

It can be seen from Figure 4-5 that the carbon content of retained austenite which is 0.24 wt.% before tempering becomes 0.64 wt.% after 1 h of tempering at 550 °C due to the decomposition of retained austenite. This amount continuously drops during tempering until

reaching 0.50 wt.% after 16 h of tempering. The above results agree with the findings by Bhadeshia (Bhadeshia, 2001), who reported that austenite to bainite transformation continues until the amount of carbon reaches the amount defined by the T_0 curve (i.e. retained austenite is expected to become enriched in carbon with the tempering time as long as the decomposition continues).

The fact that the carbon content of retained austenite has been reduced during isothermal tempering demonstrates that the decomposition of retained austenite did not occur during the entire tempering process and ceased, or significantly slowed down, during the first hour of isothermal tempering at 550 °C, where carbon content of retained austenite dropped from 0.64% after 1 h to 0.56% after 4 h.

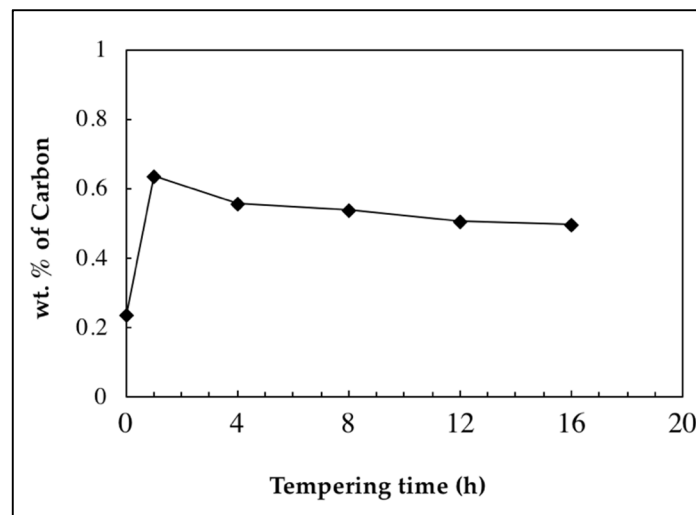


Figure 4-5 Change in carbon content of retained austenite during tempering at 550 °C.

4.3.2 Product of retained austenite decomposition

During tempering, retained austenite transforms to lower bainite. Figure 4-6(a) shows that at 350 °C there are still many untransformed islands of retained austenite, indicating that this temperature is not high enough for its complete transformation. In contrast, as shown in Figure 4-6(b), after 16 h of tempering at 550 °C, fresh martensite can be seen, instead of

decomposed austenite, which confirms martensite formation in the microstructure during the cooling cycle.

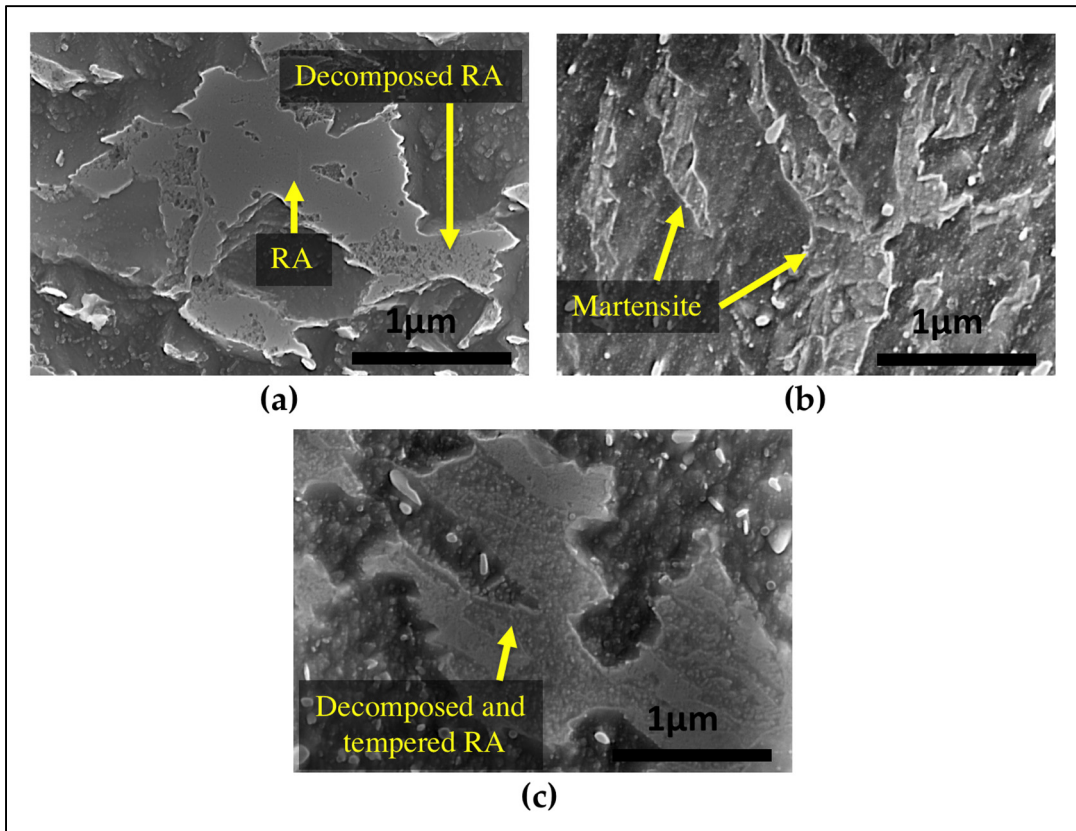


Figure 4-6 SEM images of (a) blocks of partially decomposed retained austenite after 16 h of tempering at 350 °C, (b) fresh martensite formed during cooling after 16 h of tempering at 550 °C, and (c) fully decomposed retained austenite and tempered microstructure blocks after 16 h of tempering at 600 °C.

The final product of retained austenite decomposition includes precipitation of new M_3C carbides. During tempering at 600 °C, these new carbides rapidly spheroidize (Dépinoy et al., 2017) and as shown in Figure 4-6(c), the product of tempered retained austenite includes small spherical-shape carbides inside the previous blocky type retained austenite.

4.3.3 Carbides precipitation and hardness evolution

Carbide precipitation during tempering is characterized by a length reduction in the dilatometry diagram (Morra, Böttger et Mittemeijer, 2001; Speich et Leslie, 1972). The

obtained results in the present investigation are in agreement with the published literature and as shown in Figure 4-2, a reduction in length is observed for the three samples. Further tempering causes carbide coarsening, which is accompanied with a length increase as is shown in Figure 4-2(b) and (c). The presence of a negative strain after retained austenite decomposition, as observed in Figure 4-2(a) demonstrated that when tempering at 350 °C, the precipitation of carbides did not finish even after 16 h. Carbon trapping in lower energy sites, such as dislocations has been reported as the main source for the observed slow length reduction during tempering (Garcia-Mateo et al., 2004; Kalish et Cohen, 1970).

In order to better illustrate the impact of the tempering process on the evolution of mechanical properties, Figure 4-7 shows hardness evolution as a function of different tempering times and temperatures. In the case of tempering at 350 °C, as shown in Figure 4-7, minor variations (between 42HRC to 46HRC) were observed by increasing the time. This fluctuation is probably due to the partial decomposition of retained austenite into fresh bainite and its tempering during holding.

During tempering at 550 °C, carbides precipitation caused a 0.127% decrease in length and end after 11.4 h of tempering (Figure 4-2(b)). This behavior correlates well with hardness evolution, which increased up to 8 h of tempering at 550 °C and reached the high value of 48HRC. Analysis of the dilatometry curves indicated that after 11.4 h of tempering, carbide coarsening characterized with a positive strain value is the dominant mechanism which causes a marginal drop in hardness from 48HRC to 46.5HRC.

Carbides precipitation during tempering at 600 °C ended after 4.7 h tempering with a 0.027% length reduction observed in the dilatometry curves. The lower length reduction compared to 550 °C is probably due to more intense carbide coarsening kinetics (characterized with higher length increase) occurring simultaneously with carbide precipitation during tempering at 600 °C. Comparison of hardness values between the two tempering temperatures of 550 °C and 600 °C, demonstrates that 50 °C increase in tempering temperature leads to a significant reduction in the time required for carbide precipitation and modification of the hardness

levels. As shown in Figure 4-7, for the sample tempered 8 h at 600 °C, carbide coarsening drops the hardness to 40HRC and further tempering up to 16 h decreases the hardness to 36HRC. Accordingly, hardness results are consistent with dilatometric curves and the sequence of carbide precipitation and coarsening show that carbide coarsening occurs after 4.7 h of tempering at 600 °C (Figure 4-2(c)).

in tempering temperature leads to a significant reduction in the time required for carbide precipitation and modification of the hardness levels. For example, for the sample tempered 8 h at 600 °C, hardness drops to 40HRC and further tempering up to 16h, decreases the hardness to 36HRC. Accordingly, hardness results are consistent with dilatometric curves, which show that carbide coarsening occurs after 4.7 h of tempering at 600 °C

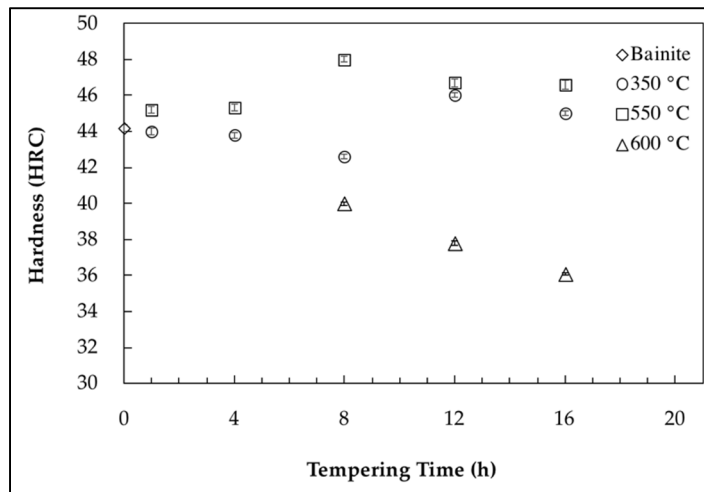


Figure 4-7 Bainite hardness as a function of tempering time for tempering temperatures of 350 °C, 550 °C and 600 °C.

4.3.4 Characterization and identification of carbides

SEM analysis was performed before and after tempering to confirm and validate the dilatometry results. Figure 4-8(a) illustrates that tempering at 350 °C leads only to partial changes in the microstructure. Similar to the primary bainite microstructure (Figure 4-1),

needle-like carbides can still be seen after 16 h of tempering at this temperature, and there is no obvious change in the shape of carbides and bainite.

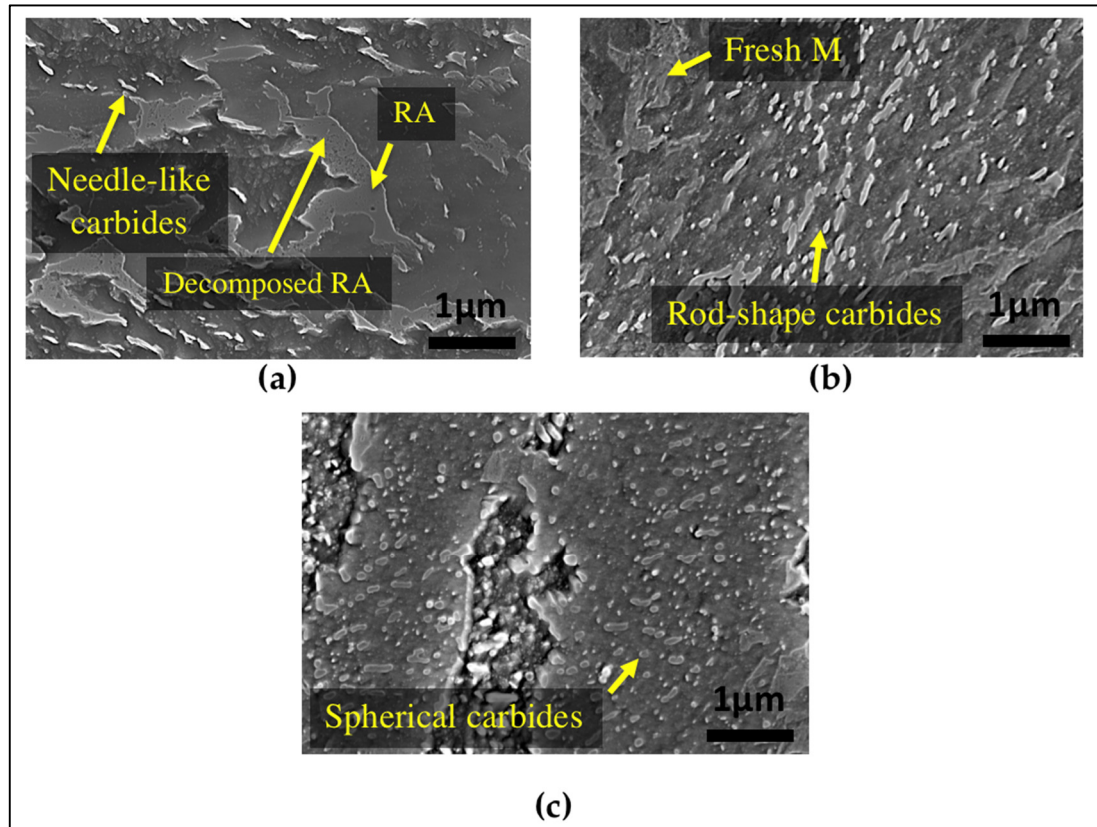
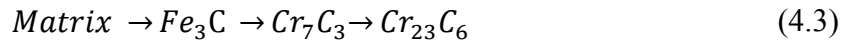


Figure 4-8 SEM images bainitic specimens after tempering for 16 h at (a) 350 °C, (b) 550 °C, and (c) 600 °C.

The microstructure of the sample tempered after 16 h at 550 °C is shown in Figure 4-8(b), where a severely tempered bainitic microstructure can be observed. In this specimen, needle-like carbides within the bainite sheaves are transformed to coarser rod-shape carbides. Fresh martensite can also be observed, whose presence is the result of retained austenite transformation to martensite during cooling after tempering. In comparison with tempering at 550 °C, increasing the temperature to 600 °C with the same tempering time led to major morphological changes in the bainite (Figure 4-8(c)). Although still some rod-shape carbides can be seen in the microstructure, the morphology consists of globular shape carbides with no needle-like carbide.

During tempering of bainitic steels containing chromium at temperatures higher than 500 °C, Cr_7C_3 and $Cr_{23}C_6$ chromium carbides are frequently observed, which form according to the following sequence (Bhadeshia et Honeycombe, 2011):



M_3C carbides, mostly rich in Fe but also with Cr and Mo, exist in the matrix and also precipitate due to retained austenite decomposition. These M_3C carbides dissolve and Cr_7C_3 and $Cr_{23}C_6$ carbides form (Dépinoy et al., 2017). $Cr_{23}C_6$ is the equilibrium carbide and a plateau is observed in the dilatometry curves after precipitation of this carbide. However, in order to determine the nature and morphology of carbides after tempering of the investigated steel, a TEM study was carried out. To this end, two samples were selected: One from the early stages of tempering, after 1 h at 550 °C, and the other, after 16 h of tempering at 600 °C in the middle of the carbides coarsening stage; results are reported in Figure 4-9.

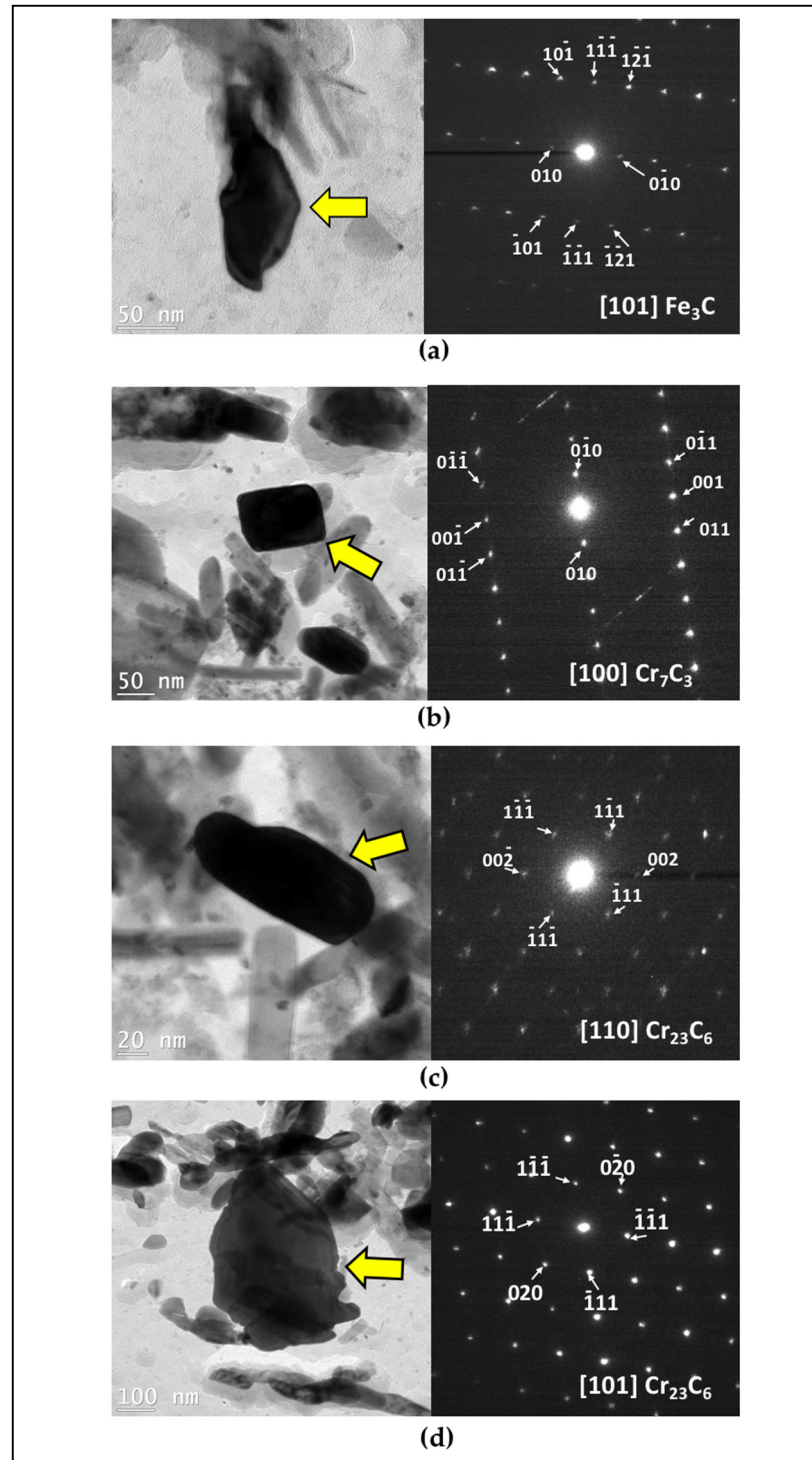


Figure 4-9 Bright-field TEM image and corresponding selected area electron diffraction (SAED) pattern of (a) Fe_3C carbide after 1 h of tempering at 550 °C, (b) Cr_7C_3 carbide after 16 h of tempering at 600 °C, (c) and (d) Cr_{23}C_6 carbides after 16 h of tempering at 600 °C.

As can be seen in Figure 4-9(a), after 1 h of tempering at 550 °C, many carbides with various sizes are present in the microstructure. EDS (Energy-dispersive X-ray spectroscopy) analysis of the carbides in the carbon replica, revealed that they are very rich in Fe with nearly no presence of Cr. Hence, there is no chromium carbide formed during the first hour of tempering or they are very small to be extracted with carbon replicas. Figure 4-9(a) shows an Fe_3C carbide with its related selected area electron diffraction (SAED) pattern at this tempering condition. No specific orientation between carbides and matrix was revealed in this study since all the TEM investigations were made on carbon extraction replicas.

By increasing the time and temperature of tempering to 16 h at 600 °C, carbides tend to be richer in chromium. The carbide pointed by an arrow in Figure 4-9(b) is a Cr_7C_3 carbide based on SAED pattern, with rhombus-shape, orthorhombic crystal system and an equivalent diameter of 98nm. As can be seen in Figure 4-9(c), the other type of carbide detected by TEM and SAED is Cr_{23}C_6 with a cubic crystal system, which has a rod-like shape with an equivalent diameter of 95 nm; however, the coarser globular shape of Cr_{23}C_6 with an equivalent diameter of 404 nm can be observed as well. Therefore, the rod-like and spherical carbides that can be seen in SEM image of Figure 4-8(c) can be considered as Cr_{23}C_6 carbides.

Generally, carbides can be classified into four types according to their shape: needle-like, rod-like, lenticular and rhombus or globular. Table 4-2 summarizes the morphology, size and crystal structure of carbides that were identified in the investigated steel. It is interesting to note, while the obtained results are consistent with the observations made by several authors on Cr-Mo steels (Andr n, Cai et Svensson, 1995; D pinoy et al., 2017; Pelletier, 1981); in our study, no molybdenum carbide was identified in the material even after 16 h of tempering at 600 °C.

Table 4-2 Crystal structure, morphology and size of identified carbides in the tempered medium-carbon low-alloy bainite.

Carbide	Tempering treatment	Crystal system	morphology	Equivalent diameter
Fe ₃ C	1 h at 550 °C	Orthorhombic a= 5.092Å, b= 6.741Å, c= 4.527Å	lenticular	-
Cr ₇ C ₃	16 h at 600 °C	Orthorhombic a= 7.01Å, b= 12.142Å, c= 4.526Å	rhombus-shape	98nm
Cr ₂₃ C ₆	16 h at 600 °C	Cubic a= 10.65Å	rod-like globular	95nm 404nm

4.4 Conclusions

Retained austenite decomposition and carbides precipitation were investigated during isothermal tempering at 350 °C, 550 °C and 600 °C in a medium-carbon low-alloy bainitic steel. The following conclusions can be derived from the present study:

- (1) Retained austenite decomposition starts at 350 °C but cannot be fully decomposed at this temperature nor at 550 °C. The final product of retained austenite decomposition depends on the tempering temperature. Undecomposed retained austenite remains in the microstructure during cooling from 350 °C, which requires further tempering at higher temperatures. In the case of 550 °C, fresh martensite forms from the undecomposed retained austenite during cooling. However, rising the tempering temperature to 600 °C led to a full decomposition of retained austenite during isothermal tempering.
- (2) Dilatometry analyses of isothermal tempering curves at 550 °C showed that the decomposition of retained austenite only occurred during the first hour of tempering.

Chromium carbide precipitation accompanied with hardening occurred at about 11.4 h of tempering at 550 °C. This precipitation time dropped to 4.7 h by increasing the temperature to 600 °C.

- (3) No chromium carbide precipitated during the first hour of tempering at 550 °C. The Fe rich carbides were transformed to rhombus-shape Cr_7C_3 , as well as rod-shape and globular Cr_{23}C_6 precipitated from the matrix during tempering at 600 °C, but no molybdenum carbide was observed.

Acknowledgments: The authors would like to thank Dr. Mohammad Saadati and Dr. Hadi Ghasemi-Nanesa for helpful discussions and their assistance during the experiments. The authors would like to acknowledge Finkl Steel Co. for providing the samples of this study. The authors are also grateful to the National Science and Engineering Research Council Canada (NSERC) for their financial support in the framework of a Collaborative Research and Development project (CRDJP 453683).

CHAPTER 5

Optimization of Industrial Tempering Heat Treatment Process

5.1 Introduction

In the previous chapters, different microstructural changes occurring during tempering of bainite and martensite were studied for a medium-carbon low-alloy steel. In this chapter, the above findings will be used to analyze the tempering process of a large-size slab and propose a modified tempering cycle which may result in significant reduction in processing times.

A typical industrial tempering process for a large-size slab of medium-carbon low-alloy steel can be seen in the Figure 5-1. Two tempering cycles, the first for 42 h at 550 °C and the second for 42 h at 600 °C, are generally used to achieve a final hardness between 34HRC to 38HRC.

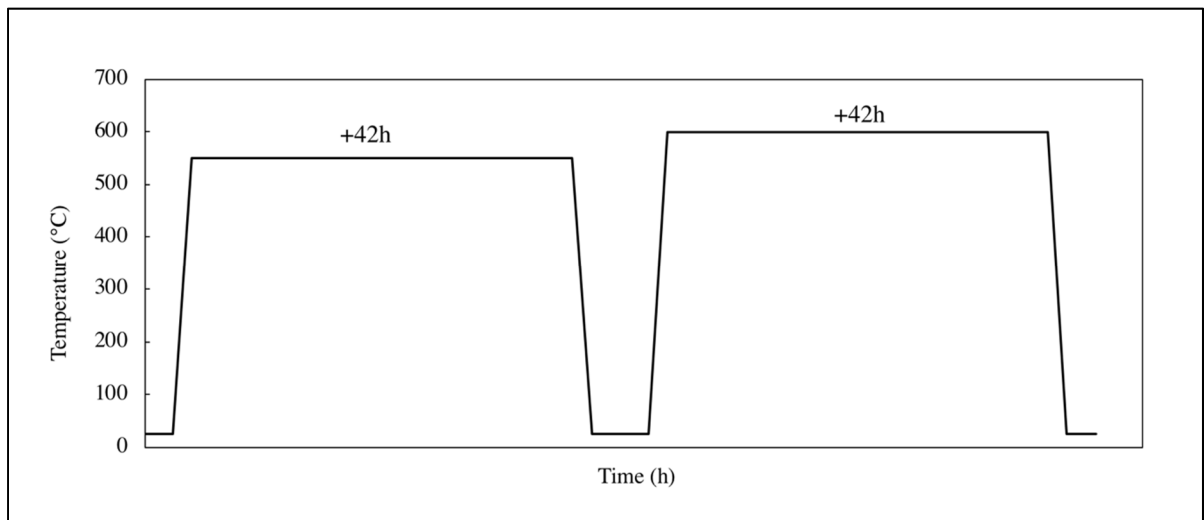


Figure 5-1 Schematic of double tempering process for a medium-carbon low-alloy steel.

5.2 Tempering temperature

As it is shown in Figure 5-1, two long-time tempering cycles are applied to achieve the desired hardness. The first and second tempering cycles are at 550 °C and 600 °C, respectively. As mentioned in the literature review chapter, the reasons for the second tempering are:

- 1- Temper the fresh martensite or bainite produced as results of retained austenite transformations that occur during the first temper.
- 2- Decompose the remnants of the retained austenite that did not transform during the first temper.

Results in chapter 4 showed that by tempering at 550 °C for the studied steel, fresh martensite forms during the cooling cycle of the first temper, hence, another tempering is required to temper the fresh martensite. However, the results of chapter 4 showed that tempering at 600 °C led to a complete decomposition of retained austenite during tempering and no fresh martensite exists at the end of the first tempering. Consequently, by tempering at 600 °C instead of 550 °C, there is no need for double tempering and tempering process can be reduced to one cycle.

5.3 Tempering time

Next step is to find the appropriate tempering time at 600 °C to reach the target hardness range of 34HRC to 38HRC.

Examination of Figure 5-1 shows that the industrial tempering cycle for a large-size slab can be divided into a non-isothermal step and an isothermal one. Therefore, in order to find the appropriate tempering time, both parts should be investigated separately. In the following sections, the effects of each tempering step on the hardness is investigated.

5.3.1 Non-isothermal tempering time of a large-size slab

In the case of large-size slabs, non-isothermal tempering step has a very slow heating rate. After researchers in the CM2P group showed that during tempering, temperature at the surface of a large-size slab with dimensions of 3000 mm × 1500 mm × 1000 mm takes approximately 20 hours from ambient temperature to reach 600 °C. Hence, non-isothermal tempering plays an important role in the tempering process and cannot be neglected.

In this section, to study the effect of non-isothermal tempering on the hardness of a large-size slab, the real cycle was experimentally simulated by dilatometry machine. The input data of this test came from temperature measurements of the surface of a large-size slab with the dimensions given above carried out by other researchers within the CM2P research group. Figure 5-2 shows the real non-isothermal tempering cycle simulated by dilatometry machine.

It should be mentioned that optimization of the tempering process is based on the surface hardness, because it is the one measures in industry for evaluating the tempering efficiency. Hence, specimens with martensitic microstructure were used for tempering tests.

On the base of the above analysis, non-isothermal tests were carried out from room temperature to 600 °C for 21.6 hours. The heating rate was adjusted so that to simulate the one obtained from the industrial heating conditions. Once reaching 600 °C, the test was stopped, and the sample air cooled to room temperature. A Rockwell C hardness map composed of 25 measurements was then obtained (2 kg load, 10 seconds). The results indicated a HRC value of 37.4 after 21.6 h of non-isothermal tempering.

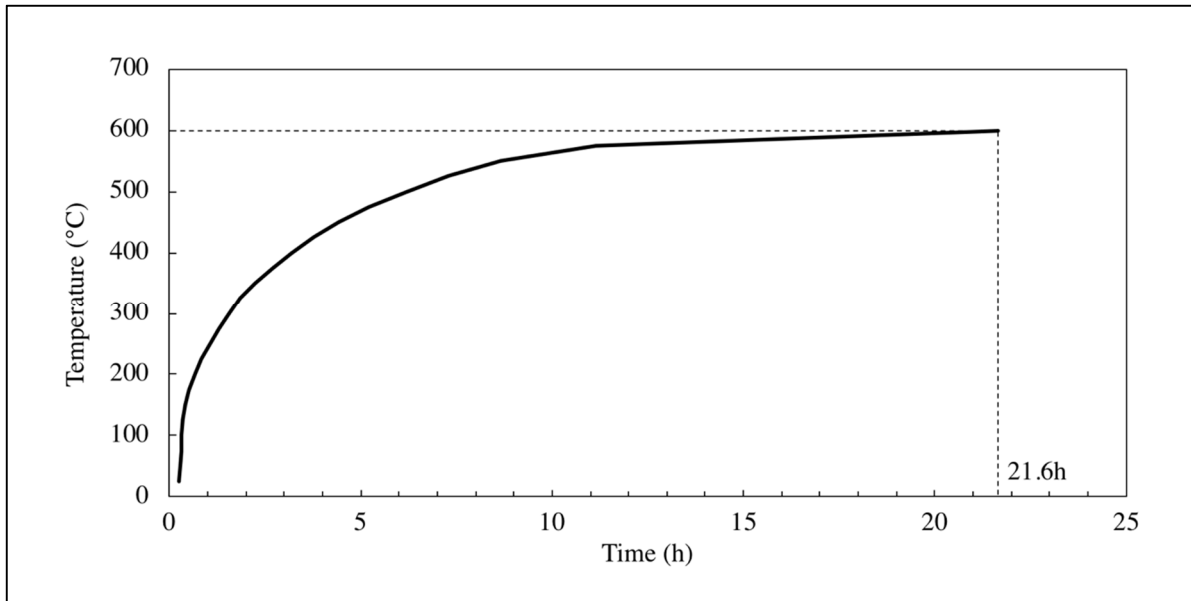


Figure 5-2 Real temperature versus time curve during non-isothermal tempering of a large-size slab.

5.3.2 Isothermal tempering time of a large-size slab

As shown in Figure 5-1, following heating (non-isothermal tempering) to the target temperature, isothermal tempering for 42 hours in each cycle for reaching the desired hardness occurs. Before starting the isothermal tempering at 600 °C, hardness is 37.4HRC. Hence, an isothermal tempering should be designed to decrease this hardness to 36HRC (middle of the acceptable harness range). For this purpose, the following steps were taken to design the isothermal tempering at 600 °C.

- 1- Find an isothermal tempering cycle at 600 °C leading to a hardness of 36HRC.
- 2- Find an isothermal tempering cycle at 600 °C leading to a hardness of 37.4HRC which is the hardness after non-isothermal tempering part.
- 3- The difference of time between isothermal tempering cycles in steps one and two is the required tempering time at 600 °C to decrease the hardness from 37.4HRC to

36HRC and would be the appropriate time for isothermal tempering of a large-size slab.

In order to find these tempering cycles, many isothermal tempering cycles at 600 °C for different holding times were performed. The results are illustrated in Table 5-1, which show that the hardness of the steel after 16 h and 30 h of isothermal tempering at 600 °C becomes 37.4HRC and 36.0HRC, respectively.

Table 5-1 Hardness changes during isothermal tempering with different holding times at 600 °C

Sample	Time (h)	Hardness (HRC)
Martensite before temper	-	53.9 ± 0.1
Temper at 600 °C	4	41.4 ± 0.2
Temper at 600 °C	6	40.4 ± 0.1
Temper at 600 °C	10	39.2 ± 0.1
Temper at 600 °C	16	37.4 ± 0.1
Temper at 600 °C	30	36.0 ± 0.1

Consequently, 14 hours (30-16 hours) of tempering at 600 °C is required to decrease the hardness from 37.4HRC, the hardness after non-isothermal tempering part, to 36HRC, the final required hardness.

5.4 Proposed tempering cycle

Based on the findings of this research, a new tempering cycle has been designed for a large-size slab of the studied steel and shown in Figure 5-3. It consists of 21.6 h of non-isothermal tempering up to 600 °C following by 14 h of isothermal tempering at 600 °C for a total tempering time of 35.6 h.

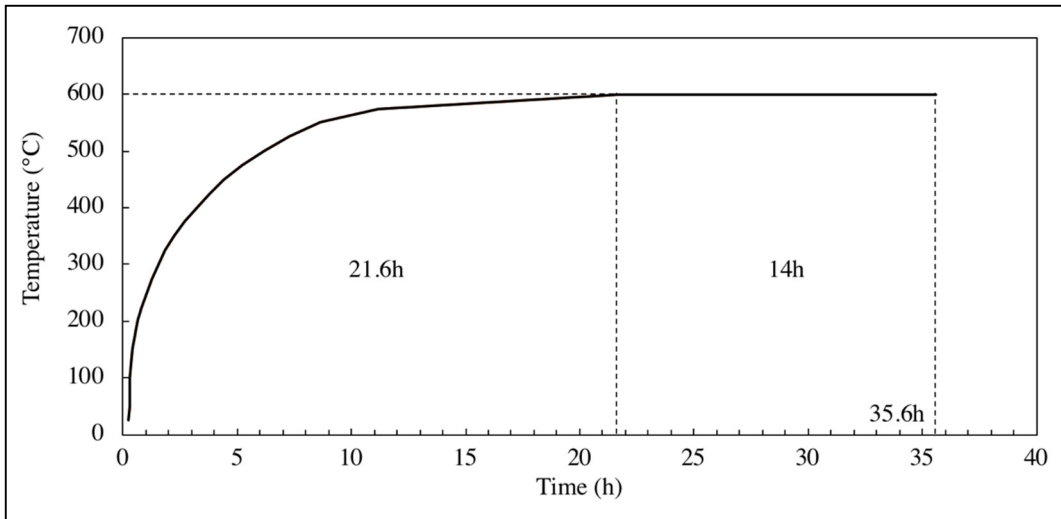


Figure 5-3 Proposed tempering cycle for a large-size slab.

In conclusion, for a large-size slab instead of double tempering process (Figure 5-1), which consists tempering for 42 h at 550 °C plus 42 h at 600 °C, one cycle of tempering for 35.6 h at 600 °C (Figure 5-3) is proposed to achieve the required hardness in the surface.

CONCLUSIONS

Different stages and phase transformations during tempering of a medium-carbon low-alloy steel were investigated in this research by experimentally simulating the industrial tempering conditions and at the end, industrial tempering process has been optimized. The significant contributions of this research are:

- 1- Phase transformations during bainite tempering are remarkably different from phase transformations of martensite tempering. Carbon segregation and transition carbide precipitation were not observed during bainite tempering because of auto-tempering effect and lower amount of carbon in the supersaturated bainitic ferrite in comparison with martensite.
- 2- The retained austenite in bainitic specimens decomposed to lower bainite during non-isothermal tempering which led to a length increase in dilatometry experiments. In contrast when the starting microstructure was martensite, a length decrease was observed due to decomposition of medium carbon martensite to low carbon martensite plus carbides.
- 3- The final product of tempering of retained austenite is temperature dependent. By tempering at 550 °C, partial decomposition of retained austenite occurred and the residue amount of retained austenite transformed to martensite during cooling after tempering. Tempering at 600 °C caused full decomposition of retained austenite to lower bainite and the final product became tempered lower bainite.
- 4- After one hour of tempering at 550 °C and during early stages of tempering, mostly iron rich carbides were detected. However, after 16 h of tempering at 600 °C, two types of chromium carbides, Cr_7C_3 and Cr_{23}C_6 , were observed.

- 5- Based on the findings of this research, instead of two tempering cycles at 550 °C and 600 °C in large-size slabs, one tempering cycle for 35.6 h at 600 °C is proposed to achieve the desired hardness in the surface.

RECOMMENDATIONS

This research has mostly focused on different phase transformations during tempering of bainitic medium-carbon low-alloy steels. The following researches are recommended to improve the knowledge of bainite tempering.

1- Study different types of alloying carbides and their kinetics of growth as a function of tempering time and temperature in bainitic steels. Then, analyse the effects of these alloying carbides on mechanical properties.

2- In this research, the effects of time and temperature on retained austenite decomposition were investigated. However, alloying elements also play an important role in the stability of retained austenite. Therefore, the effect of alloying elements on the mechanism of retained austenite decomposition during tempering and retained austenite transformation during cooling after tempering needs to be investigated.

3- Phase transformations occurrence and their temperature range during tempering have been determined in this study. Further numerical study of kinetics of phase transformation during tempering of a bainitic steel is recommended.

LIST OF BIBLIOGRAPHICAL REFERENCES

- A.M. Bayer, T. V. a. L. R. W. (1990). ASM Handbook, ASM International, 1, 757–779.
- Andrén, Hans-Olof, Guangjun Cai and Lars-Erik Svensson. (1995). Microstructure of heat resistant chromium steel weld metals. *Applied Surface Science*, 87-88, 200-206.
- Bain, E. C., and Paxton, H. W. (1966). Alloying elements in steel. American Society For Metals, Metals Park, Ohio.
- Baker, R., and Nutting, J. (1959). The tempering of a Cr-Mo-V-W and a Mo-V steel. *Iron and Steel Institute Special Report*, 64, 1-22.
- Bhadeshia, H. (1980). The lower bainite transformation and the significance of carbide precipitation. *Acta metallurgica*, 28(8), 1103-1114.
- Bhadeshia, H. (1981). A rationalisation of shear transformations in steels. *Acta metallurgica*, 29(6), 1117-1130.
- Bhadeshia, H. K. D. H. (2001). *Bainite in Steels: Transformations, Microstructure and Properties* (2nd edition). IOM Communications.
- Bhadeshia, H., Honeycombe, R. (2011). *Steels: Microstructure and Properties*. Elsevier Science.
- Biss, V., and R. L. Cryderman. (1971). Martensite and retained austenite in hot-rolled, low-carbon bainitic steels. *Metallurgical and Materials Transactions B*, 2, 2267-2276.
- Caballero, F. G., M. K. Miller, C. Garcia-Mateo, C. Capdevila and S. S. Babu. (2008). Redistribution of alloying elements during tempering of a nanocrystalline steel. *Acta Materialia*, 56, 188-199.
- Caballero, F. G., M. K. Miller, S. S. Babu and C. Garcia-Mateo. (2007). Atomic scale observations of bainite transformation in a high carbon high silicon steel. *Acta Materialia*, 55, 381-390.
- Cheng, L., Brakman, C. M., Korevaar, B. M., and Mittemeijer, E. J. (1988). The tempering of iron- carbon martensite; dilatometric and calorimetric analysis. *Metallurgical Transactions A*, 19(10), 2415-2426.

- Chentouf, S. M., Jahazi, M., Lapierre-Boire, L.-P., and Godin, S. (2014). Characteristics of Austenite Transformation During Post Forge Cooling of Large-Size High Strength Steel Ingots. *Metallography, Microstructure, and Analysis*, 3(4), 281-297.
- Davenport, E., Bain, E., Paxton, H. W., and Westbrook, J. (1930). Transformation of Austenite at Constant Subcritical Temperatures.
- Davis, J. R. (1994). Surface Engineering of Carbon and Alloy Steels. ASM International, *Metals Handbook. Tenth Edition.*, 5, 701-740.
- Demeri, M. Y. (2001). High Strength and Stainless Steels for Automotive Applications, Innovations in Processing and Manufacturing of Sheet Materials. *TMS Proceedings*, 83-95.
- Dépinoy, S., Toffolon-Masclét, C., Urvoy, S., Roubaud, J., Marini, B., Roch, F., Gourgues-Lorenzon, A.-F. (2017). Carbide Precipitation in 2.25 Cr-1 Mo Bainitic Steel: Effect of Heating and Isothermal Tempering Conditions. *Metallurgical and Materials Transactions A*, 48(5), 2164-2178.
- Dhua, S. K., Ray, A., and Sarma, D. S. (2001). Effect of tempering temperatures on the mechanical properties and microstructures of HSLA-100 type copper-bearing steels. *Materials Science and Engineering: A*, 318(1), 197-210.
- Firrao, D., Gerosa, R., Ghidini, A., Matteis, P., Mortarino, G., Pinasco, M. R., Stagno, E. (2007). Relation between fatigue crack initiation and propagation, toughness and microstructure in large steel blooms for automotive plastic molds. *International Journal of Fatigue*, 29(9), 1880-1884.
- Firrao, D., Matteis, P., Russo Spina, P., and Gerosa, R. (2013). Influence of the microstructure on fatigue and fracture toughness properties of large heat-treated mold steels. *Materials Science and Engineering: A*, 559, 371-383.
- Fonstein, N. (2015). *Advanced High Strength Sheet Steels: Physical Metallurgy, Design, Processing, and Properties*. Springer International Publishing.
- Garcia-Mateo, C., Peet, M., Caballero, F., and Bhadeshia, H. (2004). Tempering of hard mixture of bainitic ferrite and austenite. *Materials Science and Technology*, 20(7), 814-818.
- Ghasemi Nanesa, Hadi, and Mohammad Jahazi. (2015). Alternative phase transformation path in cryogenically treated AISI D2 tool steel. *Materials Science and Engineering: A*, 634, 32-36.

- Gojić, M., M. Sućeska and M. Rajić. (2004). Thermal analysis of low alloy Cr-Mo steel. *Journal of Thermal Analysis and Calorimetry*, 75(3), 947-956.
- Greenwood, G. (1956). The growth of dispersed precipitates in solutions. *Acta metallurgica*, 4(3), 243-248.
- Handbook, M. (1990). *Properties and Selection: "Classification and Designation of Carbon and Low Alloy Steels"*: ASM International, Materials Park, Ohio, USA.
- Hashmi, S. (2014). *Comprehensive materials processing*.
- Honeycombe, R. W. K., and Mehl, R. F. (1976). Transformation from austenite in alloy steels. *Metallurgical Transactions A*, 7(7), 915-936.
- Hou, T. P., Li, Y., and Wu, K. M. (2012). Effect of high magnetic field on alloy carbide precipitation in an Fe-C-Mo alloy. *Journal of Alloys and Compounds*, 527, 240-246.
- Huang, B., Yang, J., Yen, H., Hsu, C., Huang, C., and Mohrbacher, H. (2014). Secondary hardened bainite. *Materials Science and Technology*, 30(9), 1014-1023.
- Inoue, A., and Masumoto, T. (1980). Carbide reactions ($M_3C \rightarrow M_7C_3 \rightarrow M_{23}C_6 \rightarrow M_6C$) during tempering of rapidly solidified high carbon Cr-W and Cr-Mo steels. *Metallurgical Transactions A*, 11(5), 739-747.
- Irvine, K., and Pickering, F. (1957). Low carbon bainitic steels. *The Journal of the Iron and Steel Institute*, 187, 292-309.
- Jack, KH. (1951). Structural transformations in the tempering of high-carbon martensitic steels. *The Journal of the Iron and Steel Institute*, 169, 26-36.
- Janjusevic, Z., Gulisija, Z., Mihailovic, M., and Pataric, A. (2009). The investigation of applicability of the Hollomon-Jaffe equation on tempering the HSLA steel. *Chemical Industry and Chemical Engineering Quarterly/CICEQ*, 15(3), 131-136.
- Jayan, V., Khan, M. Y., and Hussain, M. (2003). X-ray investigation of solid solution partitioning in 2.25Cr-1Mo steel after extended elevated temperature service in power station. *Materials Science and Technology*, 19(11), 1546-1552.
- Jung, Minsu, Seok-Jae Lee and Young-Kook Lee. (2009). Microstructural and dilatational changes during tempering and tempering kinetics in martensitic medium-carbon steel. *Metallurgical and materials transactions A*, 40(3), 551-559.

- Kalish, D., and Cohen, M. (1970). Structural changes and strengthening in the strain tempering of martensite. *Materials Science and Engineering*, 6(3), 156-166.
- Kang, M. K., Y. L. Ai, M. X. Zhang, Y. Q. Yang, M. Zhu and Y. Chen. (2009). Carbon content of bainite ferrite in 40CrMnSiMoV steel. *Materials Chemistry and Physics*, 118(2), 438-441.
- Krauss, G. (1999). Martensite in steel: strength and structure. *Materials Science and Engineering: A*, 273, 40-57.
- Krauss, George. (2017). Tempering of Lath Martensite in Low and Medium Carbon Steels: Assessment and Challenges. *steel research international*, 88(10), 1700038.
- Leiva, J. A. V., E. V. Morales, E. Villar-Cociña, C. A. Donis and Ivani de S. Bott. (2009). Kinetic parameters during the tempering of low-alloy steel through the non-isothermal dilatometry. *Journal of Materials Science*, 45(2), 418.
- Liu, Dongsheng, Guodong Wang, Xianghua Liu and Dewen Zhao. (1998). Effect of Cooling Rates and Compressive Deformation of Austenite on Bainitic Transformation and Microstructure for Plastic Die AISI P20 Steel. *ISIJ International*, 38(5), 482-488.
- Liu, Fenggang, Xin Lin, Menghua Song, Haiou Yang, Kan Song, Pengfei Guo and Weidong Huang. (2016). Effect of tempering temperature on microstructure and mechanical properties of laser solid formed 300M steel. *Journal of Alloys and Compounds*, 689, 225-232.
- Loucif, A., Ben Fredj, E., Harris, N., Shahriari, D., Jahazi, M., and Lapierre-Boire, L.-P. (2018). Evolution of A-Type Macrosegregation in Large Size Steel Ingot After Multistep Forging and Heat Treatment. *Metallurgical and Materials Transactions B*, 49(3), 1046-1055.
- Lyassami, M., Shahriari, D., Ben Fredj, E., Morin, J.-B., and Jahazi, M. (2018). Numerical Simulation of Water Quenching of Large Size Steel Forgings: Effects of Macrosegregation and Grain Size on Phase Distribution. *Journal of Manufacturing and Materials Processing*, 2(2), 34.
- Miller, M. K., P. A. Beaven and G. D. W. Smith. (1981). A study of the early stages of tempering of iron-carbon martensites by atom probe field ion microscopy. *Metallurgical Transactions A*, 12(7), 1197-1204.

- Mitchell, D. R. G., and Ball, C. J. (2001). A quantitative X-ray diffraction and analytical electron microscopy study of service-exposed 2.25Cr–1Mo steels. *Materials Characterization*, 47(1), 17-26.
- Mittemeher, E. J., Cheng, L., van der Schaaf, P. J., Brakman, C. M., and Korevaar, B. M. (1988). Analysis of nonisothermal transformation kinetics; tempering of iron-carbon and iron-nitrogen martensites. *Metallurgical Transactions A*, 19(4), 925-932.
- Morra, P. V., Böttger, A. J., and Mittemeijer, E. J. (2001). Decomposition of Iron-based Martensite. A kinetic analysis by means of differential scanning calorimetry and dilatometry. *Journal of Thermal Analysis and Calorimetry*, 64(3), 905-914.
- Mouritz, A. P. (2012). *Introduction to Aerospace Materials*. Elsevier Science.
- Nagakura, S., Y. Hirotsu, M. Kusunoki, T. Suzuki and Y. Nakamura. (1983). Crystallographic Study of the Tempering of Martensitic Carbon Steel by Electron Microscopy and Diffraction. *Metallurgical Transactions A*, 14(5), 1025-1031.
- Nahamin Pardazan Asia, (2014), <http://en.metsofts.ir>.
- Nakamura, Yoshio, and Sigemaro Nagakura. (1986). Structure of iron-carbon martensite in the transition state from the first to the third stage of tempering studied by electron microscopy and diffraction. *Transactions of the Japan institute of metals*, vol. 27(11), 842-848.
- Nam, W. J. (1999). Effect of initial microstructure on the coarsening behavior of cementite particles. *ISIJ international*, 39(11), 1181-1187.
- Naraghi, R., Selleby, M., and Ågren, J. (2014). Thermodynamics of stable and metastable structures in Fe–C system. *Calphad*, 46, 148-158.
- Olson, G. B., and Cohen, M. (1983). Early Stages of Aging and Tempering of Ferrous Martensites. *Metallurgical Transactions A*, 14(5), 1057-1065.
- Parameswaran, P., Vijayalakshmi, M., and Raghunathan, V. S. (2002). The Influence of Prior Microstructure on Tempering Stages in 2.25Cr-1Mo Steel High Temperature Materials and Processes, 21, 251.
- Peet, Mathew J., Sudarsanam Suresh Babu, Mike K. Miller and H. K. D. H. Bhadeshia. (2017). Tempering of Low-Temperature Bainite. *Metallurgical and Materials Transactions A*, 48(7), 3410-3418.

- Pelletier, M. (1981). Study of structural transformations occurring in low carbon chromium-molybdenum ferritic steels: influence of small additions of vanadium and niobium.
- Philip, T. V., and Mccaffrey, T. J. (1990). Ultrahigh-strength steels, Properties and Selection. ASM International, Metals Handbook. Tenth Edition, 1, 430-448.
- Podder, A. S. (2011). Tempering of a mixture of bainite and retained austenite.
- Porter, D. A., and Easterling, K. E. (1992). Phase Transformations in Metals and Alloys, Third Edition (Revised Reprint). Taylor and Francis.
- Primig, S., and H. Leitner. (2011). Separation of overlapping retained austenite decomposition and cementite precipitation reactions during tempering of martensitic steel by means of thermal analysis. *Thermochimica Acta*, 526(1), 111-117.
- R.A. Mesquita, R. S. a. C. S. G. (2014). Heat Treating of Mold Steels and Corrosion-Resistant Tool Steels. Heat Treating of Irons and Steels, ASM Handbook, ASM International, 4, 358–362.
- Ridley, N, H Stuart and L Zwell. (1969). Lattice parameters of Fe-C austenites at room temperature. *Trans Met Soc Aime*, 245(8), 1834-1836.
- Roberts, G. A., Kennedy, R., and Krauss, G. (1998). Tool steels. ASM international.
- Rodrigues, P. C. M., E. V. Pereloma and D. B. Santos. (2000). Mechanical properties of an HSLA bainitic steel subjected to controlled rolling with accelerated cooling. *Materials Science and Engineering: A*, 283, 136-143.
- Ruhl, Robert C, and Morris Cohen. (1969). Splat Quenching of Iron-Nickel-Boron Alloys. *TRANS MET SOC AIME*, 245(2), 253-257.
- Saha Podder, A., and Bhadeshia, H. K. D. H. (2010). Thermal stability of austenite retained in bainitic steels. *Materials Science and Engineering: A*, 527(7), 2121-2128.
- Saha, D. C., Nayak, S. S., Biro, E., Gerlich, A. P., and Zhou, Y. (2014). Mechanism of secondary hardening in rapid tempering of dual-phase steel. *Metallurgical and Materials Transactions A*, 45(13), 6153-6162.
- Sandvik, B. (1982). The bainite reaction in Fe-Si-C alloys: the primary stage. *Metallurgical Transactions A*, 13(5), 777-787.

- Shimizu, Ken'ichi, Tyuki Ko and Zenji Nishiyama. (1964). Transmission Electron Microscope Observation of the Bainite of Carbon Steel. Transactions of the Japan Institute of Metals, 5(4), 225-230.
- Sinha, A. K. (1989). Ferrous physical metallurgy.
- Smallman, R. E., and Ngan, A. (2011). Physical metallurgy and advanced materials. Butterworth-Heinemann.
- Speich, G. R., and Leslie, W. C. (1972). Tempering of steel. Metallurgical Transactions, 3(5), 1043-1054
- Swallow, E., and Bhadeshia, H. (1996). High resolution observations of displacements caused by bainitic transformation. Materials Science and Technology, 12(2), 121-125.
- Takahashi, M., and Bhadeshia, H. (1990). Model for transition from upper to lower bainite. Materials Science and Technology, 6(7), 592-603.
- Talebi, S., Ghasemi-Nanesa, H., Jahazi, M., and Melkonyan, H. (2017). In Situ Study of Phase Transformations during Non-Isothermal Tempering of Bainitic and Martensitic Microstructures. Metals, 7(9), 346.
- Taneike, M., Sawada, K., and Abe, F. (2004). Effect of carbon concentration on precipitation behavior of M₂₃C₆ carbides and MX carbonitrides in martensitic 9Cr steel during heat treatment. Metallurgical and Materials Transactions A, 35(4), 1255-1262.
- Taylor, K. A., Olson, G. B., Cohen, M., and Sande, J. B. V. (1989). Carbide precipitation during stage I tempering of Fe-Ni-C martensites. Metallurgical Transactions A, 20(12), 2749-2765.
- Thelning, K. (1975). Nitriding, Steel and its heat treatment: Bofors Handbook: Boston, MA: Butterworths.
- Thomson, R. C., and Bhadeshia, H. K. D. H. (1994). Changes in chemical composition of carbides in 2.25Cr-1Mo power plant steel. Materials Science and Technology, 10(3), 193-204.
- Totten, G. E., and Howes, M. A. H. (1997). Steel Heat Treatment Handbook. Taylor and Francis.
- Totten, G. E., Funatani, K., and Xie, L. (2004). Handbook of metallurgical process design. CRC press.

- Wang, J., and Van Der Zwaag, S. (2001). Stabilization mechanisms of retained austenite in transformation-induced plasticity steel. *Metallurgical and Materials Transactions A*, 32(6), 1527-1539.
- Woodhead, J., and Quarrell, A. G. (1965). The role of carbides in low-alloy creep-resisting steels. 39 P. Climax Molybdenum Company Ltd., 2 Cavendish Place, London W1, England.
- Wu, R. M., Y. F. Zheng, X. C. Wu and X. C. Li. (2017). Effect of titanium on the microstructure and hardness uniformity of non-quenched and tempered prehardened steel for large-section plastic mould. *Ironmaking and Steelmaking*, 44(1),17-22.
- Yan, G., Han, L., Li, C., Luo, X., and Gu, J. (2017). Characteristic of retained austenite decomposition during tempering and its effect on impact toughness in SA508 Gr.3 steel. *Journal of Nuclear Materials*, 483, 167-175.

